MAGNETIC RESONANCE AND INFRA-RED STUDIES OF INSULIN AND ITS INTERACTION WITH PHOSPHOLIPID

by

Traugott Peter Fischer

dipl.sc.nat. Swiss Federal Institute of Technology, 1987

THESIS SUBMITTED IN PARTIAL FULFILLMENT OF

THE REQUIREMENTS FOR THE DEGREE OF

MASTER OF SCIENCE

in the department

of

Chemistry

SIMON FRASER UNIVERSITY

August 1992

APPROVAL

Name: Traugott Peter Fischer

Degree: Master of Science

Title of Thesis: Magnetic Resonance and Infra-red Studies of Insulin and its Interaction with Phospholipid

Examining Committee:

Chair: Dr. D. Sutton

Dr. R.J. Cushley, (Professor)
Senior Supervisor

Dr. B.M. Pinto, (Associate Professor)
Committee Member

Dr. W.R. Richards, (Professor)
Committee Member

Dr. S. Wolfe, (Professor)
Internal Examiner

Date Approved: Aug. 7, 1992

PARTIAL COPYRIGHT LICENSE

I hereby grant to Simon Fraser University the right to lend my thesis, project or extended essay (the title of which is shown below) to users of the Simon Fraser University Library, and to make partial or single copies only for such users or in response to a request from the library of any other university, or other educational institution, on its own behalf or for one of its users. I further agree that permission for multiple copying of this work for scholarly purposes may be granted by me or the Dean of Graduate Studies. It is understood that copying or publication of this work for financial gain shall not be allowed without my written permission.

Title of Thesis/Project/Extended Essay:

Magnetic Resonance and Infra-red Studies of Insulin and its Interaction with Phospholipid

Author: _____
(signature)

Traugott Peter Fischer
(name)

12 August 1992
(date)

ABSTRACT

Insulin is a peptide hormone with a molecular weight of 5,700, consisting of an A-chain of 21 amino acids and a B-chain of 30 amino acids. An answer was sought to the question whether conformational studies of insulin bound to membranes by means of FTIR and 2D ^1H NMR would be feasible. In aqueous solution at pH 2-3 the peptide associates to dimers in millimolar concentrations, and it is insoluble from pH 3.8 to pH 7.5. Investigations of structural properties of the peptide in solution by NMR- and FTIR spectroscopy have to take into account the solution properties of the peptide. The interaction of insulin with phospholipid bilayers was studied extensively. Experiments included a solubilization test of insulin with egg yolk phosphatidylcholine (egg PC) unilamellar vesicles in phosphate buffer at neutral pH, fluorescence emission spectroscopy, and quantitation of insulin bound to vesicles after removal of free insulin. These result were inconclusive.

Two-dimensional proton (2-D ^1H) NMR spectra of insulin in D_2O at pH 3 and in d_6-DMSO were recorded on a Bruker WM 400 spectrometer in order to investigate the feasibility of this method for structural studies of the peptide.

After the work had commenced, a study of insulin was published (Kline and Justice, (1990) Biochemistry, 29, 2906). From my data and those of Kline and Justice it was established that insulin can only be investigated in aqueous solution by 2-D ^1H NMR after the addition of organic solvent and only at high field (≥500 MHz). Because of this, only FTIR spectroscopy appeared suited for an investigation of the peptide bound to phospholipid membranes.

FTIR spectra of insulin in D_2O at pH 3 were analyzed by deconvolution and bandshape fitting, and the secondary structure of the peptide was quantitated from the fitted band intensities. A comparison of secondary structure determined from FTIR data with that determined from X-ray crystallographic data showed good agreement.

ACKNOWLEDGEMENTS

I wish to express my sincere thanks to my senior supervisor, Dr. R.J. Cushley, for his guidance, encouragement and support during the course of this work. I would also like to thank Dr. W.R. Richards and Dr. B.M. Pinto for their time spent as members of the supervisory committee.

I would like to extend my appreciation to past and present members of the research group for their assistance, advice, and many helpful discussions: Dr. W.D. Treleaven, Dr. S. Arumugam, Mrs Jenny Lum, and especially Mr. Patrick Chin for running and photographing SDS gels and processing of FTIR data.

I wish to thank Dr. A. Tracey for his advice and many helpful discussions concerning the WM-400 NMR spectrometer.

I would like to thank my mother for her support during my studies.

Finally, I am indebted to my co-worker at Mepha Pharma Ltd., Switzerland, Miss Andrea Hugentobler. Her valuable collaboration at the company, together with her untiring encouragement and organizing skills made the accomplishment of this work feasible.

TABLE OF CONTENTS

LIST OF TABLES

LIST OF FIGURES

1. INTRODUCTION

1.1. INSULIN

Insulin, a peptide hormone with a molecular weight of 5,700 Da, consists of an A-chain of 21 amino acids and a B-chain of 30 amino acids. The two chains are linked by interchain disulfide bridges between Cys A7-Cys B7, and Cys A20-Cys B19, respectively (Hiroyuki, 1971).

Preproinsulin, synthesized in the islet β-cells of the pancreas, contains 81 amino acids and a signal peptide of 24 amino acids. After processing of the prepeptide in the lumen of the rough endoplasmic reticulum and the Golgi apparatus, insulin is stored as a crystalline hexamer in secretory granules of the pancreas. The hexamer is composed of three dimers coordinated around two Zn^{2+} ions (Steiner et al., 1970, 1978; Cheshnovsky et al., 1983).

Upon release from the pancreas, insulin is diluted to approximately 10^{-10} M, a concentration, where the monomeric form is prevalent (Cheshnovsky et al., 1983). The monomer finally binds to the insulin receptor on the membranes of liver, muscle and adipose cells (Pessin et al., 1985; Jacobs, 1985; Heidenreich & Olefsky, 1985). Upon binding of the hormone, the receptor - a tyrosinekinase - induces

activation of glycogensynthase and/or acetyl-CoA-carboxylase (lipogenesis).

The sequences of mammalian insulins differ only slightly. Ala A8 and Val A10 in bovine insulin are replaced by Thr A8 and Ile A10 in human and porcine insulin, respectively, Ala B30 in bovine and porcine insulin by Thr B30 in human insulin. The primary structure of insulin A- and B-chains from different species is given in Figures 1.1 and 1.2 (page 3).

Figure 1.1:

Insulin A-Chains

```
Man  H-Gly-Ile-Val-Glu-Gln-Cys-Cys-Thr-Ser-Ile-Cys-Ser-Leu-Tyr-Gln-Leu-Glu-Asn-Tyr-
         Cys-Asn-OH

Pig      --- --- --- --- --- --- --- --- --- --- --- --- --- --- --- --- --- --- ---
         --- ---

Cow      --- --- --- --- --- --- --- Ala --- Val --- --- --- --- --- --- --- --- ---
         --- ---
```

Figure 1.2:

Insulin B-Chains

```
Man  H-Phe-Val-Asn-Gln-His-Leu-Cys-Gly-Ser-His-Leu-Val-Glu-Ala-Leu-Tyr-Leu-Val-Cys-
         Gly-Glu-Arg-Gly-Phe-Phe-Tyr-Thr-Pro-Lys-Thr-OH

Pig      --- --- --- --- --- --- --- --- --- --- --- --- --- --- --- --- --- --- ---
         --- --- --- --- --- --- --- --- --- --- Ala-OH

Cow      --- --- --- --- --- --- --- --- --- --- --- --- --- --- --- --- --- --- ---
         --- --- --- --- --- --- --- --- --- --- Ala-OH
```

(From The Handbook of Biochemistry, 2nd edition, Sober H.A., ed., The Chemical Rubber Co., 1970)

The single crystal X-ray structure of insulin was first reported in 1969 (Adams et al., 1969). According to these data, the insulin monomer contains two short stretches of near helical conformation between the residues A2 to A6 and A13 to A19. An intrachain disulfide bridge links Cys A6 and Cys A11. In the central part of the B-chain, there are three turns of α-helix with 3.6 residues per turn. The interchain disulfide bonds, Cys B7-Cys A7 and Cys B19-Cys A20, are at the end of the helix and provide a rigid backbone.

More recent X-ray diffraction studies provide a more detailed insight into the secondary and tertiary structure of insulin dimers in Zn-hexamers (Dodson et al., 1979). According to these data, residues A1 to A7 form an α-helix. The intrachain disulfide bridge between Cys A6 and Cys A11 induces a sharp turn that is followed by an extended structure from Ser A9 to Ser A12. Residues A13 to A20 form a helical segment close to a 3_{10}-helix with 3.0 residues per turn, which runs parallel to the α-helix.

The B-chain is extended from residue B1 to B8 and B24 to B30, respectively, with an α-helical part from B9 to B19 and a sharp turn from B20 to B23.

The two chains are linked by the two interchain disulfide bonds mentioned above, by H-bonds between A6 and

B5, A11 and B4, A19 and B25, and a charge interaction between Glu A4 and Lys B29, respectively.

In the insulin dimer, the sequences B23 to B28 of the monomers form an antiparallel β-sheet (Dodson et al., 1979). A model of the tertiary structure of insulin is given in Fig. 1.3.

Figure 1.3: The Tertiary Structure of Insulin (adapted from Kline & Justice, 1990).

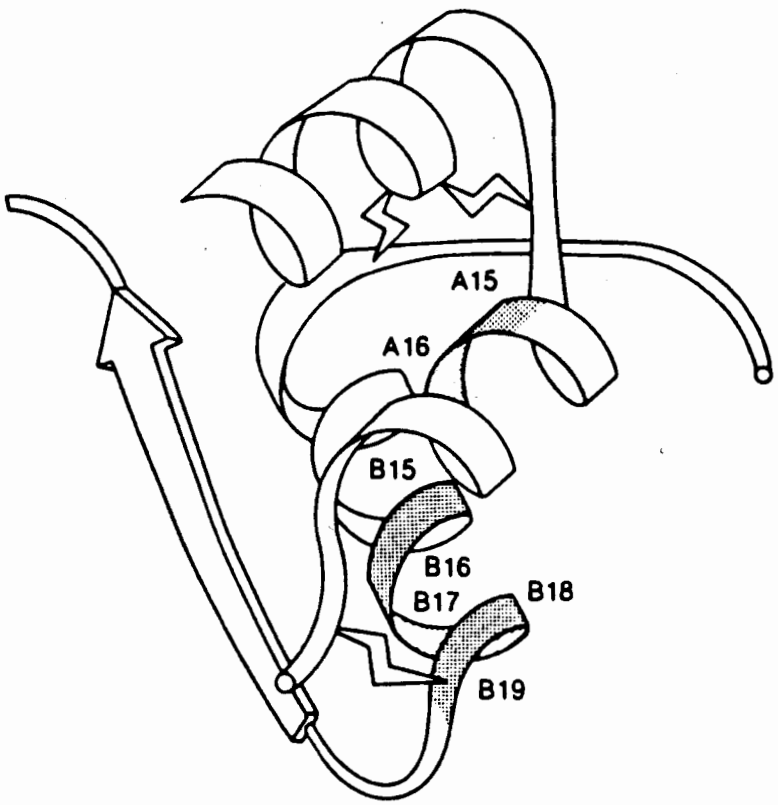

In solution and at concentrations higher than the physiological concentration, insulin shows a complex association behavior. The most accepted model of its association is

$$\text{monomer} \rightleftharpoons \text{dimer} \rightleftharpoons \text{tetramer} \rightleftharpoons \text{hexamer}$$

(Fredericq & Neurath, 1950; Jeffrey & Coates, 1965, 1966; Pekar & Frank, 1972; Lord et al., 1973; Goldman & Carpenter, 1974). At pH 2 to 3, the prevalent form of insulin is its dimer. In concentrations greater than the physiological concentration, insulin is insoluble between pH 3.8 and pH 7.5 (Cheshnovsky et al., 1983). In Table 1.1, the reported association constants of insulin are listed:

Table 1.1: Association Constants of Insulin.

pH	K_{12}	K_{24}	K_{46}	K_{26}	Ref.
2.0	1.25×10^4	7.8×10^2	6.7×10^2		1
8.0	2.22×10^5	40	220		2
7.0	1.40×10^5			4×10^8	3
2.0	4.00×10^4				4
7.0	7.50×10^5	5.0×10^3	45		5

1 Jeffrey & Coates, 1965, 1966
2 Goldman & Carpenter, 1974
3 Pekar & Frank, 1972
4 Lord et al., 1973
5 Pocker & Biswas, 1981

It was suggested that the insulin monomer binds to lipid bilayers (Oomen & Kaplan, 1987). Binding of the peptide to membranes would change the membrane fluidity and

facilitate subsequent interaction with the insulin receptors (Farias, 1987).

Association of a peptide with a lipid membrane may involve an amphipathic α-helical secondary structure (DeLisi & Berzovsky, 1985), where the hydrophobicity of the residues alternates with a frequency of 3.6 residues per turn (Eisenberg et al., 1984), forming a polar and a nonpolar face oriented along the helix axis (Segrest et al., 1974; Segrest et al., 1990). But what is of importance is not necessarily the native secondary structure of a peptide but the ability to form an α-helical structure which is induced and stabilized by the amphipathic environment in a lipid/water interface (DeLisi & Berzovsky, 1985). A specific distribution of charged residues along the polar face is characteristic for amphipathic α-helices with negatively charged amino acids in a narrow longitudinal zone in the center of the polar face and positively charged residues along interfacial edges between polar and nonpolar faces (Segrest & Feldmann, 1974). However, association of a peptide with a lipid membrane does not only involve amphipathic α-helices. An alternating hydrophobicity of 3.0 residues in a peptide segment results in a 3_{10}-helical, an alternating hydrophobicity of 4.4 residues in a π-helical, and of 2.2 residues in a β-sheet structure, respectively, upon binding to a lipid bilayer. A peptide segment of

nonpolar amino acids can be inserted into a membrane, forming a transmembrane helix. The strength of binding depends on the distribution of positive and negative charges in the peptide segment and on the composition of the bilayer.

In the helical segment B9-B19 of insulin, the polar residues Glu B13, Tyr B16, and Cys B19 lie on one side of the helix (Blundell et al., 1972). This segment may thus have a potential to associate with lipid bilayers. The segment A4-A17 of insulin cannot be induced to form an α-helix because of the constraints of the disulfide bond between A6 and A11, but it is already stabilized in an amphipathic secondary structure (DeLisi & Berzovsky, 1985). Hence, it may also be involved in binding to a membrane surface. Residues A4-A7 form one turn of an α-helix followed by an extended structure from A9-A12. Residues A13-A17 form a helical segment which is close to a 3_{10}-helix.

X-ray diffraction is a well established method for the investigation of protein structures. Since crystals are investigated by this method, it is likely that the crystal structure of a protein may slightly deviate from its conformation in an aqueous, physiological environment, because techniques of crystallizing proteins often have to

use high salt concentrations. In the past few years, Fourier Transform Infrared (FTIR) and Nuclear Magnetic Resonance (NMR) methods have been developed to investigate conformational properties of peptides and proteins in solution. By means of FTIR spectroscopy, structural elements like extended structures, β-structures, helices, turns and random conformation can be quantitatively assigned to proteins (Ferraro & Basile, 1978; Byler & Susi, 1986; Surewicz et al., 1987a, 1987b; Surewicz & Mantsch, 1988). With multidimensional NMR techniques, structural elements of certain peptides or proteins can be sequence-specifically assigned, thus allowing the investigation of the secondary and tertiary structure of a peptide or protein in solution (Wüthrich, 1986; Ernst et al., 1987).

The solution properties of a peptide may be a limiting factor for both methods. Peptides may not be readily soluble in aqueous solutions at certain pH-values, temperatures and salt concentrations. They may also tend to aggregate. Another limiting factor for NMR studies is the size of a peptide or protein. A spectrum easily becomes uninterpretable by too many or overlapping resonances. To some extent, this problem may be circumvented by 3-D NMR techniques (Oschkinat et al., 1988; Szalma & Pelczer, 1988;

Oschkinat et al., 1989) and/or isotopic labelling (LeMaster & Richards, 1988; Fesik, 1988; Westler et al., 1988; Torchia et al., 1988; Lowry et al., 1988).

1.2. EGG YOLK PHOSPHATIDYLCHOLINE

Phosphatidylcholine belongs to the class of phosphoglycerides, the most abundant membrane lipids. Phosphoglycerides consist of a backbone of sn-glycerol 3-phosphate with acyl groups bound to C1 and C2. Esterification of the phosphate group with choline yields phosphatidylcholine. Its structure is given in Figure 1.4.

Figure 1.4: The Structure of Phosphatidylcholine (adapted from D. Rawn, 1983).

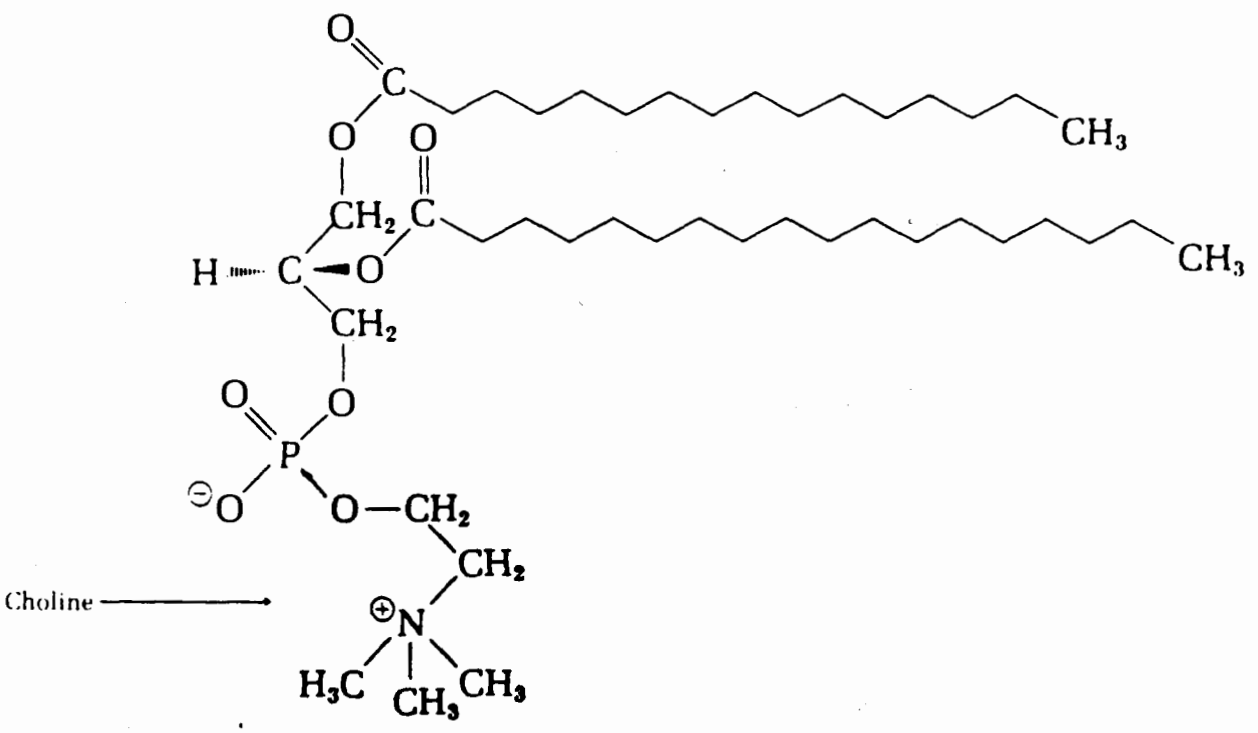

The fatty acid composition of egg yolk phosphatidylcholine is summarized in Table 1.2.

Table 1.2: Fatty Acid Composition of Egg Yolk Phosphatidylcholine (adapted from Forrest, 1977).

Palmitic Acid	(16:0)	42.7 %
Palmitoleic Acid	(16:1)	1.6 %
Stearic Acid	(18:0)	16.9 %
Oleic Acid	(18:1)	27.7 %
Linoleic Acid	(18:2)	11.0 %

Based on this composition, an average molecular weight of M_w = 764 can be calculated for egg PC.

Phospholipids spontaneously form multiple lipid bilayers in an aqueous environment with the polar head groups exposed to the aqueous phase and the hydrocarbon tails buried in the hydrophobic interior of the bilayer. The driving force for the formation of bilayers is the hydrophobic effect. The head groups of the lipids lie at roughly right angles to the plane of the bilayer surface, thus providing it with an ionic coat. Upon sonication, the multilamellar structure breaks up and unilamellar vesicles are formed.

The aim of this work was to investigate whether studies of structural elements of human or porcine insulin

in solution by means of FTIR and 2-D ^{1}H-NMR were feasible, and, if so, to compare them with published structures from X-ray diffraction studies. The solution properties of the peptide had to be taken into account, i.e. dimer formation and insolubility in millimolar concentrations from pH 3.8 to pH 7.5. For this reason, 2-D ^{1}H NMR spectra were recorded of the peptide both in D_2O at pD = 3.4 and in d_6-DMSO. When this work was in progress, the complete sequence-specific 2-D ^{1}H NMR assignments for human insulin were published by other researchers (Kline & Justice, 1990). Our results were then compared to theirs.

The question had to be answered if conformational changes of insulin upon binding to phospholipid bilayers could be examined by means of FTIR and 2-D ^{1}H NMR and, if so, at what molar ratio lipid:peptide. In order to investigate the interaction of monomeric insulin with phospholipid bilayers, conditions would have to be found at which the prevailing form of the peptide is its monomer. But since addition of organic solvents would destabilize phospholipid bilayers, this option had to be excluded. Recently, a 2-D ^{1}H NMR study of Des-(B26-B30)-insulin was published where the peptide lacks the dimer-forming segment B26-B30 (Hua & Weiss, 1991). The removed residues are not involved in the biological activity of the peptide (Fischer et al., 1985).

2. PRINCIPLES AND THEORY

2.1. PROTEINS

Proteins fall into the general class of polymers which are linear molecules built up from repeating units, the amino acids. Twenty amino acids are essential for mammalians. Proteins have the property of acquiring very specifically folded three-dimensional conformations. The amino acid sequence identifies a given protein, distinguishing it from others. The sequence is known as the primary structure of a protein. The secondary structure is the local arrangement of the polypeptide backbone into random, helical or extended conformations, or turns/bends, respectively. The tertiary structure refers to the overall three-dimensional architecture of a polypeptide chain. The quaternary structure is given by the aggregation of polypeptide subunits after initial folding (Schroeder, 1968; Ramachandran & Sasisekharan, 1968).

2.1.1. THE BACKBONE OF A PROTEIN: THE SECONDARY STRUCTURE

A portion of the backbone of a protein is shown in Figure 2.1.

Figure 2.1: Perspective drawing of a section of polypeptide chain representing two peptide units. The limits of a residue (number i of the chain) are indicated by the dashed lines. The recommended notations for atoms and torsion angles are indicated. The polypeptide is shown in the fully extended conformation, where $\phi = \psi = \omega = 180°$; the amino acid residue is the L-isomer (adapted from Creighton, 1984).

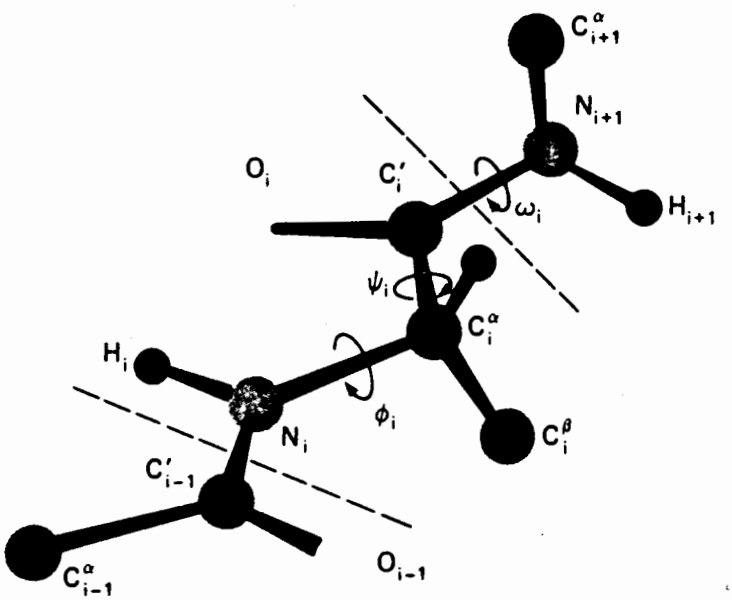

Rotation about the N-Cα bond of the peptide backbone is denoted by the torsion angle ϕ, rotation around the Cα-C' bond, by ψ; and that about the peptide (C'-N) bond, by ω, the maximum value being ±180° for the maximally extended chain with the N, Cα, and C' atoms trans to each other. In the cis-configurations, the angles ϕ, ψ, and ω are given the values of 0. Rotation clockwise is given positive values; rotation counterclockwise negative values. The trans configuration of the peptide bond is favored over the cis bond, since in the latter the Cα atoms, any side chains, and residue i+2 are in too-close proximity. There are also geometrical restraints on possible values of ϕ and ψ, for example the case with $\phi=\psi=0$, where the carbonyl oxygen atom O_{i-1} and the H atom of N_{i+1} would overlap (Ramachandran & Kolaskev, 1974; Ramachandran & Mitra, 1976). The values of the bond angles ϕ and ψ completely define the conformation of the polypeptide chain, when specified for every residue (Ramachandran & Sasisekharan, 1968).

2.1.1.1. THE α-HELIX

The right-handed α-helix has 3.6 residues per turn and a translation of 1.50 Å per residue. The torsion angles in the most favorable case are $\phi=-57°$ and $\psi=-47°$. The backbone carbonyl oxygen of each residue forms a hydrogen bond to the backbone NH of the fourth residue along the chain

(O_i-HN_{i+4}). These bonds are nearly parallel to the helix axis. The side chains point away from the helix and do not interfere with it (Ramachandran & Sasisekharan, 1968). Figure 2.2 shows a model of a right-handed α-helix.

Figure 2.2: The Right-Handed α-Helix (adapted from Pauling, 1960).

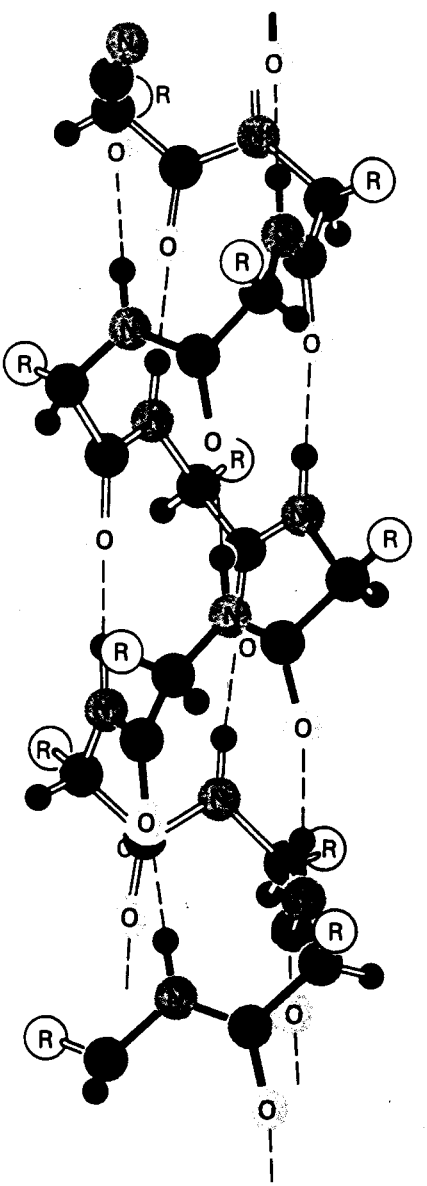

2.1.1.2. β-SHEETS

In the β-sheet conformation, the polypeptide chain is nearly fully extended. Individual strands aggregate side by side with hydrogen bonds between carbonyl and NH groups of the backbone. The adjacent strands may be either parallel with torsion angles ϕ=-119° and ψ=+113° or antiparallel with ϕ=-139° and ψ=+135°, respectively. A β-sheet may involve aggregation of different molecules, or the polypeptide chain may loop back on itself forming an intramolecular sheet. Such loops are called turns or bends. Figure 2.3 shows parallel (A) and antiparallel (B) β-sheets.

Figure 2.3: Parallel (A) and Antiparallel (B) β-Sheets (adapted from Pauling, 1960).

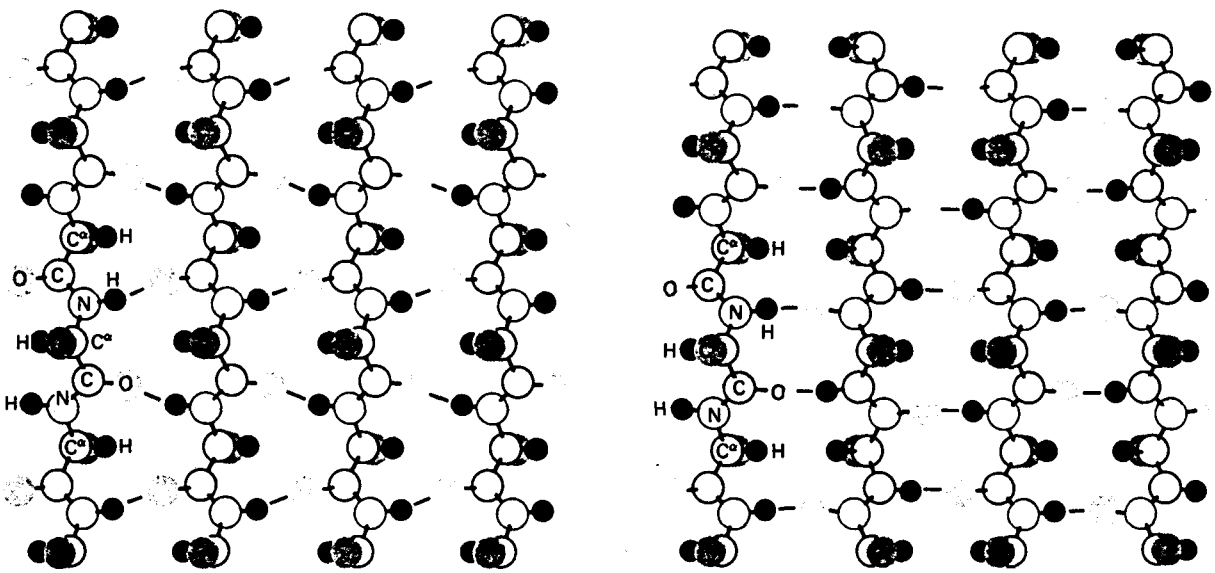

2.1.1.3. OTHER CONFORMATIONS OF THE PEPTIDE BACKBONE

Variations of the α-helix are the 3_{10}-helix and the π-helix. The 3_{10}-helix has 3.0 residues per turn. The torsion angles in the most favorable case are ϕ=-49° and ψ=-26°. The packing of the backbone atoms is very tight in the 3_{10}-helix. Therefore it does not normally occur as a regular structure, but mainly at the end of α-helices. The π-helix has 4.4 residues per turn with torsion angles ϕ=-57° and ψ=-70°. Packing of the backbone atoms is loose in this type of helix; they are not in contact with each other. Therefore the π-helix is not observed as a regular structure (Ramachandran & Sasisekharan, 1968).

Proline residues are not compatible with either α-helix or β-sheet conformations. They may form poly(Pro)I and II helices with all peptide bonds in cis-configuration in the form I and in trans-configuration in the form II, respectively (Sasisekharan, 1959). Glycine residues may form regular conformations, designated I and II, the former being a β-sheet conformation, the latter a threefold helix similar to that of poly(Pro)II (Crick & Rich, 1955). In collagen with repeating sequences $(Gly\text{-}X\text{-}Y)_n$, where one third of the X- and Y-residues are prolines, each chain has a slightly twisted threefold helical conformation like poly(Pro)II and poly(Gly)II. Three such chains are coiled

about each other to give a right-handed super-helix (Traub & Piez, 1971). Such an assembly of secondary structures is called a super-secondary structure.

2.1.1.4. THE RAMACHANDRAN PLOT

Combining different values of the torsion angles ϕ and ψ in a polypeptide results in allowed and forbidden conformational states. In a Ramachandran plot, ψ is plotted versus ϕ. In Figure 2.4, fully allowed regions are enclosed by thin gray lines, the partially allowed regions by thick black lines. The connecting region enclosed by the dashed gray lines is permissible with slight flexibility of the bond angles.

Figure 2.4: Regular polypeptide conformations on a Ramachandran plot. The regular conformations are α_R (right-handed α-helix), α_L (left-handed α-helix), ⧫ (antiparallel β-sheet), ◊ (parallel β-sheet), 3 (right-handed 3_{10}-helix), π (right-handed π-helix), △ (polyproline I, polyproline II, polyglycine II) (adapted from Ramachandran & Sasisekharan, 1968).

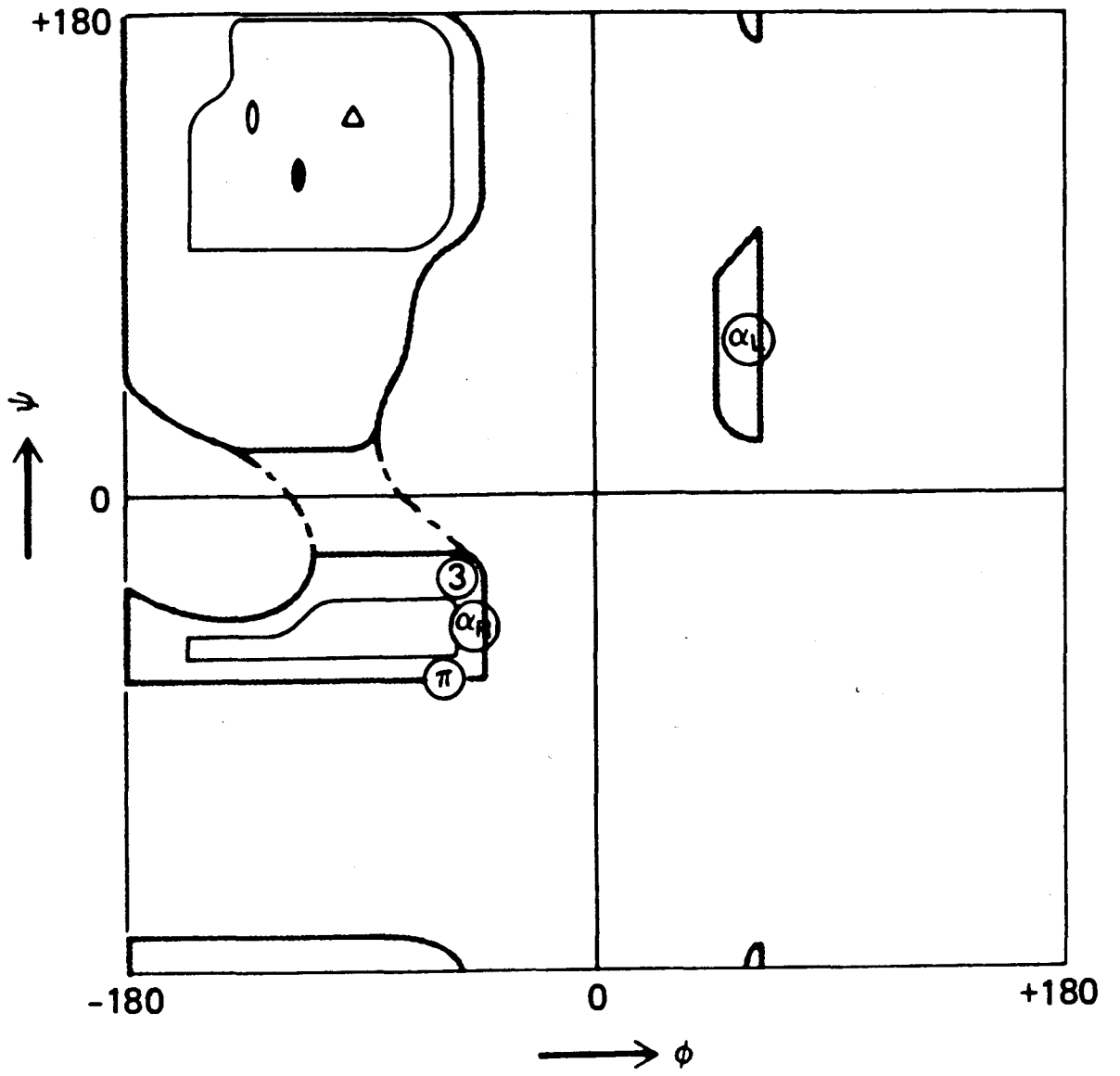

2.1.2. THE TERTIARY AND QUATERNARY STRUCTURE OF PROTEINS

The next higher levels of protein structure are the tertiary and the quaternary structure. Figure 2.5 A shows the tertiary structure of the β_2 chain of hemoglobin. The quaternary structure of this protein is given by the assembly of four identical subunits, the α_1, α_2, β_1, and β_2 chains (Figure 2.5 B).

Figure 2.5: A The Tertiary Structure of the β_2-Chain of Hemoglobin.
B The Quaternary Structure of Hemoglobin, Consisting of Four Identical Subunits (adapted from Zubay G., 1983).

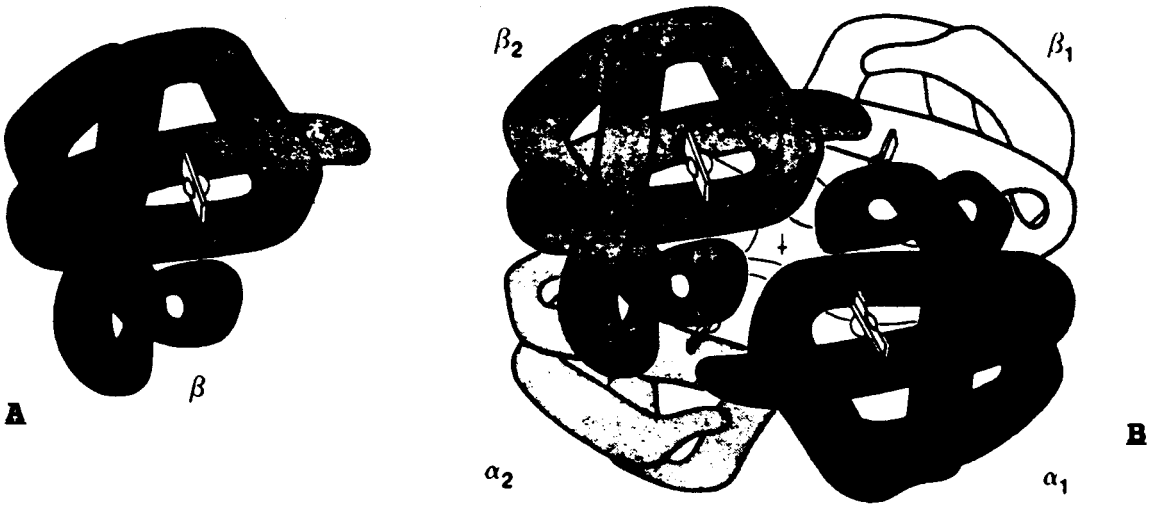

2.1.3. HYDROPHOBIC-FREE FORCES MAINTAINING THE STRUCTURE OF PROTEINS

Hydrophobic-free forces maintaining the structure of proteins are van der Waal's forces, hydrogen bonds, and electrostatic interactions.

Van der Waal's forces originate in oscillating dipoles that are generated in all atoms by the movement of electrons in their orbitals. These oscillating dipoles give rise to a net attractive force between any two atoms.

Hydrogen bonds are an intermediate between covalent bonding and ionic interactions, because a hydrogen atom is shared between a proton donor (acid) and a proton acceptor (base).

Electrostatic interaction is observed between oppositely charged residues (Pauling, 1960), e.g., $-NH_3^+$ and $-COO^-$.

Disulfide bridges do not direct the folding of a protein as can be shown by the spontaneous folding of ribonuclease. This protein contains four disulfide bonds. After denaturing the protein by urea and disrupting the disulfide bonds by β-mercaptoethanol, ribonuclease spontaneously regains its native, active conformation when

the denaturing agents are removed by dialysis (Anfinson, 1973).

2.2. EXAMINATION OF THE PROTEIN STRUCTURE

2.2.1. X-RAY DIFFRACTION

Only a very brief summary of this method will be given here. Reviews describing the technique are given in Dickerson (1964), Eisenberg (1970), Glusker & Trueblood (1972), and Blundell & Johnson (1976). Knowledge of the structure of a protein is almost totally dependent on the technique of X-ray diffraction analysis of crystalline proteins. A crystal has all the molecules arranged in specific positions and orientations on a three-dimensional lattice. The basic unit of a crystal is the unit cell. The individual unit within that cell that yields the entire unit cell when repeated an integral number of times is called the asymmetric unit. Translation of the unit cell parallel to its edges in all three dimensions without rotation gives the crystal lattice. The three dimensions of translation define the three crystal axes. X-rays passed through the crystal are scattered primarily by the electrons of the crystallized compound. Therefore scattering by each atom is proportional to its atomic number. The structure determined by X-ray diffraction analysis is that of the electron density (Schoenborn & Nunes, 1972). Scattering of the X-rays is described by

Braggs law of diffraction

$$d \cdot \sin\theta_n = n\lambda \qquad (2.1)$$

where

d = spacing between molecules in the crystal
θ_n= angle of diffraction for the nth diffraction order
λ = wavelength of the radiation.

The three-dimensional lattice of scattered X-rays is called the reciprocal lattice. The information about the detailed structural features of the protein is contained in the intensity of the diffraction spots. After determination of the phases of each reflection, the latter are recombined by a Fourier synthesis. This computation results in electron densities ρ, at a point (x,y,z) in the unit cell:

$$\rho(x,y,z)=V^{-1}\sum_{h}\sum_{k}\sum_{l} F(h,k,l)\exp[i\alpha(h,k,l)]\exp[-2i\pi(hx+ky+lz)] \qquad (2.2)$$

where

V = volume of the unit cell
F(h,k,l) = amplitude (square root of the intensity) of the reflection with indices h, k, and l
α(h,k,l) = phase of the reflection.

The calculation of the electron density at each point (x,y,z) includes the amplitude and phases of all the reflections of the diffraction pattern. The combination of all electron densities in the unit cell then provides a structural model of the protein (Blundell & Johnson, 1976).

2.2.2. FOURIER-TRANSFORM INFRARED SPECTROSCOPY

The theory of infrared spectroscopy is discussed in detail by Alpert et al. (1970) and Barnes & Orville-Thomas (1977).

In an infrared single beam grating spectrometer, light from an infrared source is focused through the sample and onto an entry slit which is at the focus of a collimating mirror. The collimated beam is dispersed by the grating, and light of a selected narrow frequency band is directed through an exit slit to a detector. A direct plot of detector response versus wavelength is obtained (Alpert et al., 1970). With Fourier-transform infrared spectroscopy, a method was developed that offered advantages compared with conventional dispersion infrared spectroscopy (Green & Reedy, 1978):

1. The signal-to-noise ratio is higher for the same measurement time as a consequence of the concurrent measurement of the detector signal for all resolution elements of the spectrum.

2. A higher accuracy in frequency for spectra taken over a wide range of frequencies is obtained as a consequence of the high optical throughput of the FTIR spectrometer.

Figure 2.6 shows the interferometer unit of an FTIR spectrometer:

Figure 2.6: The Interferometer Unit of a Fourier Transform Spectrometer (adapted from Banwell, 1983).

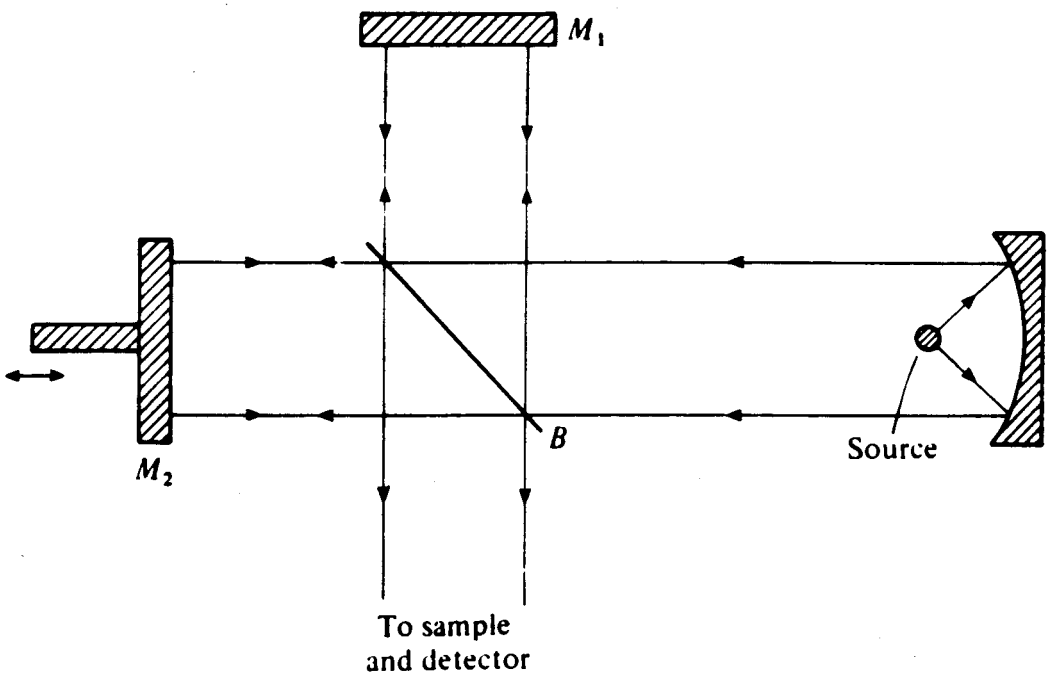

The interferometer consists of a beam splitter, B, and two mirrors M_1 and M_2. The beam splitter is a plate of transparent material, coated so that 50 % of the radiation falling on it is reflected. Half of the radiation from the infrared source goes to the fixed mirror M_1, and half to the moving mirror M_2. The radiation returns along the same path, and is recombined to a single beam at the beam splitter.

The recombined beam shows interference depending on the relative path lengths from the beam splitter to M_1 and M_2, respectively. If the path lengths are identical or differ by an intergral number of wavelengths, the interference gives a bright beam leaving the beam splitter, whereas if the difference is a half-integral number of wavelengths, the beams cancel at the beam splitter. As the mirror is moved towards and away from the beam splitter, the detector sees radiation alternating in intensity. If the recombined beam is directed through a sample before reaching the detector, sample absorption will result in gaps in the frequency distribution. The experiment is repeated and the resulting interferograms added in the computer memory. A Fourier-transform finally yields an absorption spectrum where the signal intensity as a function of the frequency is given by

$$S(\upsilon) = 2\int_0^\infty I(x)\,\cos(2\pi\upsilon x)dx \qquad (2.3)$$

x is the retardation of the moving mirror and I(x) is the damped cosine function

$$I(x) = \exp[-2\pi\sigma|x|]\cdot 2\cos(2\pi\upsilon_0 x) \qquad (2.4)$$

where

σ = Lorentzian half-width at half-maximum
υ_0 = center frequency of the peak

(Braiman & Rothschild, 1988).

The resulting spectrum is a single beam spectrum. An absorbance spectrum is calculated from single beam intensity spectra measured with a sample and a blank ($I_S(\upsilon)$, $I_B(\upsilon)$):

$$A(\upsilon) = - \log_{10} [I_S(\upsilon) / I_B(\upsilon)] \qquad (2.5)$$

2.2.2.1. FTIR SPECTROSCOPY WITH PROTEINS

The secondary structure of proteins is most clearly reflected by the amide I and amide II bands. Particularly the amide I band of proteins is investigated by FTIR. It absorbs around 1600 to 1700 cm^{-1} and is mostly associated with stretching vibrations of the peptide carbonyl groups (Elliot & Ambrose, 1950; Timasheff et al., 1967; Rüegg et al., 1975). The spectrum invariably yields a broad peak in the above frequency range. It has to be deconvoluted in order to obtain resolved components (Kauppinen et al., 1981). If Lorentzian line shape is assumed, the reverse Fourier-transform of the Lorentzian function

$$S(\upsilon) = \sigma / \pi[\sigma^2 + (\upsilon - \upsilon_0)^2] \qquad (2.6)$$

where

σ = Lorentzian half-width at half-maximum, and
υ_0 = center frequency of the peak,

yields the damped cosine function described by equation (2.4).

If equation (2.4) is multiplied by $\exp[2\pi\sigma|x|]$, a Fourier transformation would yield a Lorentzian function with zero half-width (Braiman & Rothschild, 1988). But since time-domain noise persists with equal amplitude throughout the acquisition period, whereas the time domain signal decreases with time, the strongest weight would be given to the noisiest part of the time domain signal. Therefore the time domain is apodized again with a second weighting function in order to give the greatest weight to the earlier part of the time domain signal (Marshal & Verdun, 1990). This procedure is called Fourier deconvolution. Figure 2.7 shows the most commonly used weighting functions with their respective Fourier transforms.

Figure 2.7: Weighting Functions With Their Respective Fourier Transforms. (a) Dirichlet (boxcar); (b) trapezoid; (c) triangle; (d) Hanning (a=0.54); (e) Bessel; (f) Blackman-Harris (3-term); (g) (triangle)^2; (h) exponential; (i) Gaussian (adapted from Marshall & Verdun, 1990).

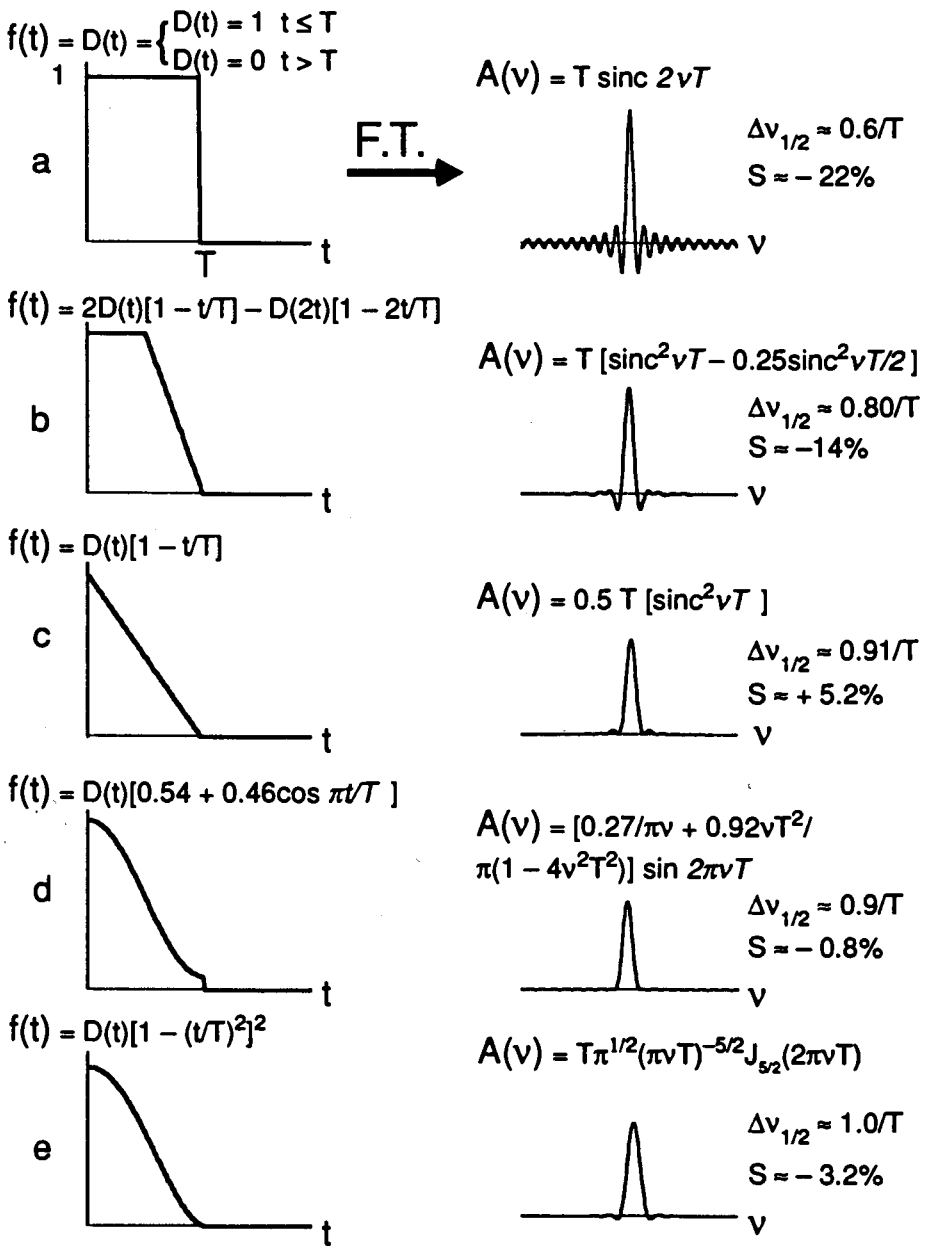

Figure 2.7: (Continued)

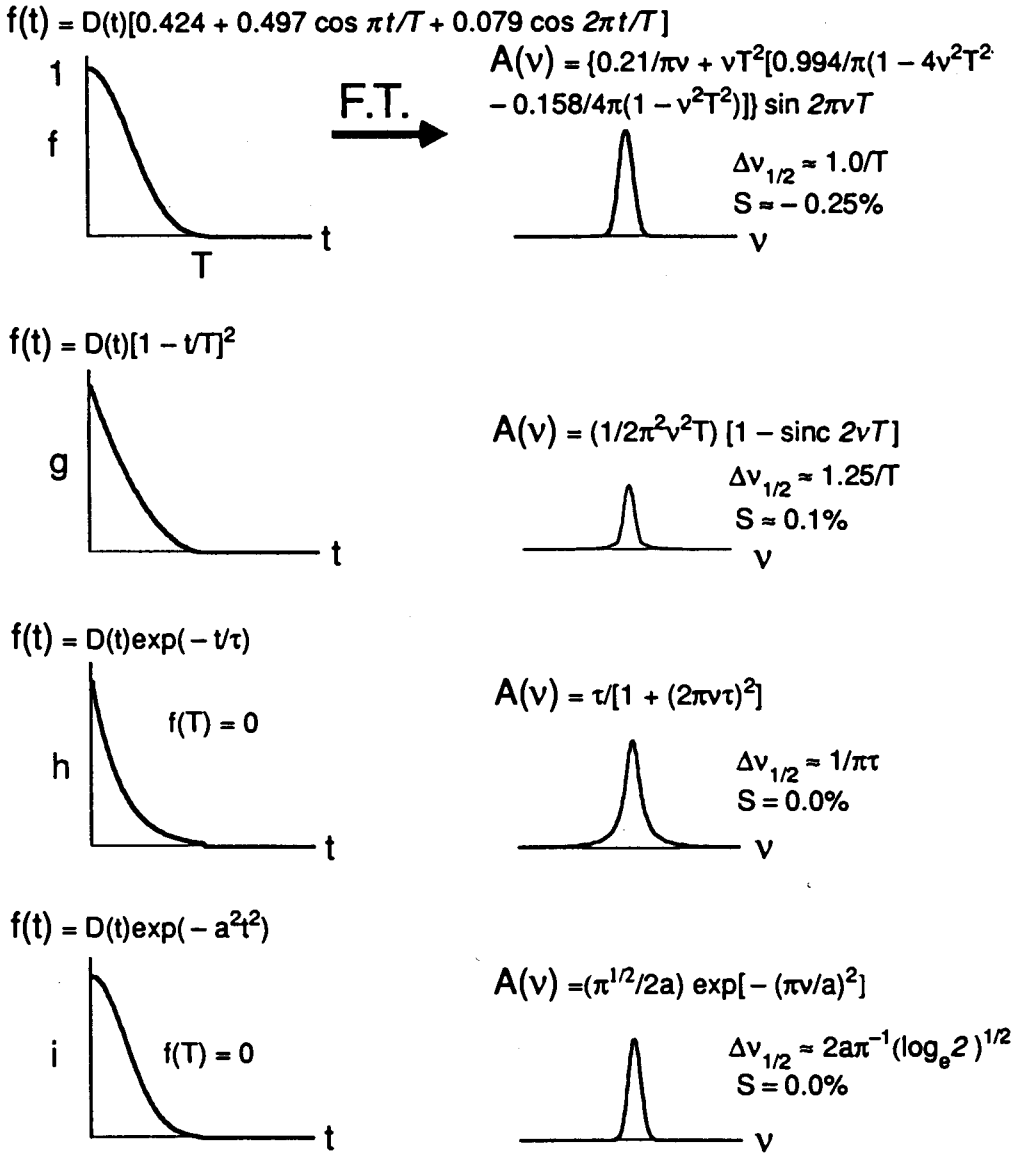

The combination of an exponential function together with a Hanning apodization window (Fig. 2.7d) is shown in Figure 2.8.

Figure 2.8: Weighting function for enhancing the resolution together with a Hanning apodization window to avoid ripple:

$h(t) = 0.5[1 + \cos(\pi t/t_{max})]\exp[2\pi t/t_{max}]$

The weighting function first increases because of the exponential term, and later drops because of the apodization function (adapted from Ernst et al., 1987).

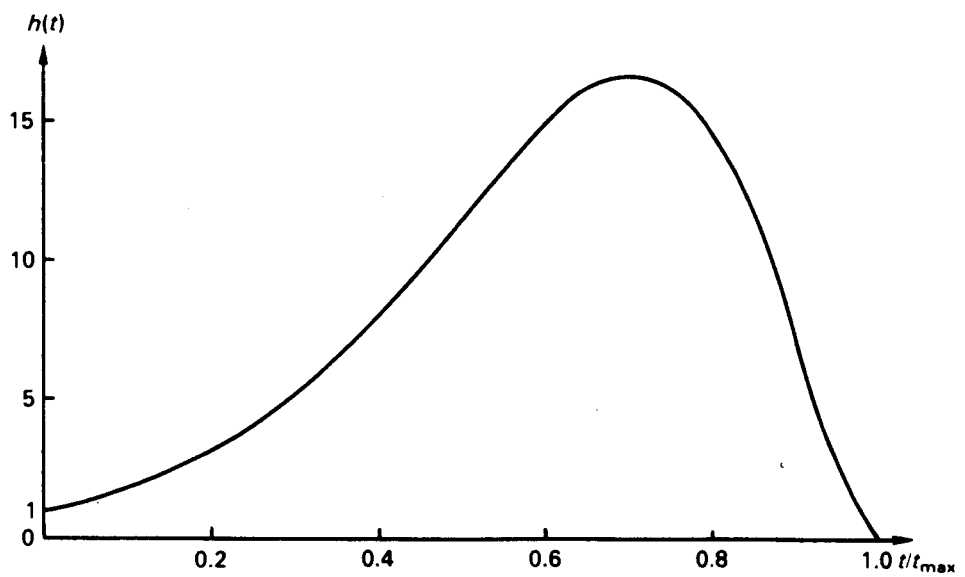

In the next step of quantitative analysis, the peak areas of the single components have to be calculated. For this purpose the bands have to be simulated by varying line width at half-height and percent Gaussian line shape, until

the resulting spectrum shows an optimal fit to the original spectrum. Figure 2.9 shows the deconvolution of two overlapped 8 cm^{-1} wide Lorentzian bands.

Figure 2.9: Results of self-deconvolution of two overlapped 8 cm^{-1} wide Lorentzian bands with relative peak heights of 1.0 and 0.75. **A:** The two bands are 6 cm^{-1} apart, **B:** The two bands are 2 cm^{-1} apart. Deconvolution with a 8 cm^{-1} wide Lorentzian profile improves the spectral resolution by a factor of 5.3; the resultant bandwidths are 1.5 cm^{-1} (Kauppinen et al., 1981).

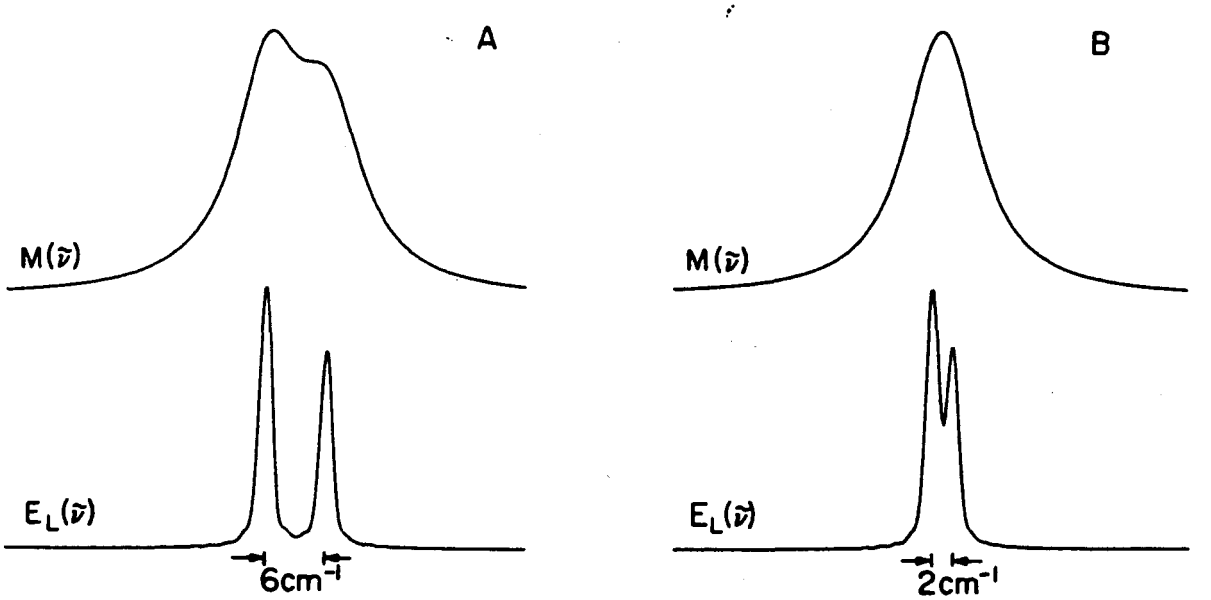

2.2.2.2. ASSIGNMENT OF DECONVOLUTED AMIDE I COMPONENTS

Several approaches are available to assign amide I bands in IR spectra to secondary structures of proteins.

The first is a theoretical approach based on a perturbation treatment applied to a weakly coupled oscillator model (Miyazawa, 1960; Krimm, 1962; Krimm & Abe, 1972).

The second theoretical approach is based on coordinate calculations of polypeptide models representing secondary structure elements (Rabolt et al., 1977; Dwivedi & Krimm, 1984; Krimm & Bandekar, 1980; Bandekar & Krimm, 1980). Since globular proteins have less regular structures than polypeptide models, assignments also have to be based on experimental work with proteins of known three-dimensional structure. Table 2.1 shows the assignments of β-strands, helix, turns and bends, and random coil to deconvoluted amide I frequencies.

Table 2.1: Deconvoluted Amide I Frequencies from 1600-1700 cm^{-1} and Assignments for Proteins in D_2O.

Frequency [cm^{-1}]	Assignment	Reference
<1620	β-strands	1,2
1620-1640	β-strands	3, 4, 5, 6, 7, 8
≈1630	short extended chain connecting α-helices	8
1639, 1666	3_{10}/helix, Type I, II, III β-turns	7, 9, 10
1640-1648	Unordered	8, 11, 12
1650-1658	α-helix	3, 4, 5, 6, 13
1665	Turns	5, 8, 10, 14, 15, 16, 17
1670-1695, 1675	β-strands	7, 8
1670, 1683, 1688, 1694	Turns	8

1 Susi et al., 1967
2 Surewicz et al., 1987a
3 Susi, 1969
4 Parker, 1983
5 Susi & Byler, 1986
6 Koenig & Tabb, 1980
7 Krimm & Bandekar, 1986
8 Byler & Susi, 1986
9 Holloway & Mantsch, 1989
10 Haris & Chapman, 1988a
11 Surewicz et al., 1987b
12 Purcell & Susi, 1984
13 Jakobsen et al., 1983
14 Haris et al., 1986
15 Yang et al., 1987
16 Arrondo et al., 1987
17 Surewicz et al., 1987c

The different frequencies for β-strands probably reflect small differences in hydrogen-bonding, but the assignments of the resonances to parallel, antiparallel, and twisted β-strands have not yet been established (Surewicz & Mantsch, 1988). Theoretical calculations for β-strands predict resonances in the range from 1670-1695 cm^{-1} (Krimm & Bandekar, 1986). However, it was proposed to assign the frequencies of 1670, 1683, 1688, and 1694 cm^{-1} to turns and the band at 1675 cm^{-1} to a β-structure (Byler & Susi, 1986). At present there are no valid criteria for a reliable discrimination of the various bands in the frequency range from 1665 cm^{-1} to 1690 cm^{-1} (Surewicz & Mantsch, 1988).

2.2.3. 2-D ^{1}H NUCLEAR MAGNETIC RESONANCE

The theory of two-dimensional NMR was described in detail by Aue *et al.* (1976), Bax (1982), and Ernst *et al.* (1987).

2.2.3.1. THE HOMONUCLEAR 2-D NMR EXPERIMENT

A 2-D NMR experiment basically includes four successive time periods:

Preparation, evolution, mixing, and detection (Wüthrich, 1986).

The preparation period usually consists of a delay time to attain thermal equilibrium. At thermal equilibrium, the magnetic moment **M** of a sample in a magnetic field $\mathbf{B}_0$ is along $\mathbf{B}_0$ with the spins distributed in their $|\alpha\rangle$- and $|\beta\rangle$ energy state according to Boltzmann's equation

$$n_\alpha - n_\beta = N\Delta E/2kT \qquad (2.7)$$

where

n = spin populations in the $|\alpha\rangle$- and $|\beta\rangle$ state
N = total number of spin-1/2 nuclei in the relevant sample
ΔE= energy difference between $|\alpha\rangle$- and $|\beta\rangle$ state of the spins
k = Boltzmann constant
T = temperature of the sample.

The energy difference is given by

$$\Delta E = \gamma h B_0 / 2\pi \qquad (2.8)$$

where

γ = magnetogyric ratio
h = Planck's constant
B_0= magnetic field (Harris, 1983).

The preparation period is usually followed by a radiofrequency pulse to create coherence. Coherence means that spins of several types have the same phases relative to each other. Corresponding to single quantum transitions it means creation of transverse magnetization (Harris, 1983; Wüthrich, 1986).

During the evolution period, t_1, the chemical shift of the spins evolves according to their precession frequency Ω_1. The state of the spin system at the end of this period depends on the length of t_1 and the energy of the system (Harris, 1983; Wüthrich, 1986).

The mixing period includes one or several radiofrequency pulses which transfer coherence between different spins, determining the frequency pair (ω_1, ω_2). The spins evolve further according to their precession frequency Ω_2 during the mixing period (Wüthrich, 1986).

During the detection period, the resulting free induction decay (FID) is recorded and stored as $s(t_2)$ (Wüthrich, 1986).

In a 2-D NMR experiment, t_1 is incremented between individual measurements resulting in a two-dimensional data set $s(t_1,t_2)$. A two-dimensional Fourier transform gives the coordinates of the signal peaks $S(\omega_1,\omega_2)$ (Wüthrich, 1986).

The two-dimensional Fourier transform is given by

$$S(\omega_1,\omega_2) = \int_{-\infty}^{+\infty} \exp[-i\omega_1 t_1]dt_1 \int_{-\infty}^{+\infty} \exp[-i\omega_2 t_2]s(t_1,t_2)dt_2 \qquad (2.9)$$

(Ernst et al., 1987).

It is calculated as a succession of two one-dimensional Fourier transforms, first along t_2, then along t_1:

$$S(t_1,\omega_2) = \int_0^{t_2} s(t_2)\exp[-i\omega_2 t_2]dt_2, \text{ and} \qquad (2.10)$$

$$S(\omega_1,\omega_2) = \int_0^{t_1} s(t_1)\exp[-i\omega_1 t_1]dt_1. \qquad (2.11)$$

2.2.3.2. PROCESSING OF 2-D NMR SPECTRA

2.2.3.2.1. ABSOLUTE VALUE AND PHASE-SENSITIVE SPECTRA

2-D NMR spectra can either be processed in absolute value mode or in phase-sensitive mode.

The Fourier transform (FT) described by equation (2.9) is in practice performed as a cosine- and a sine-FT, first along t_2, then along t_1, since

$$\exp[-i\omega t] = \cos(\omega t) - i \sin(\omega t) \qquad (2.12)$$

yielding four data matrices

$$S^{cc}(\omega_1,\omega_2),\ S^{cs}(\omega_1,\omega_2),\ S^{sc}(\omega_1,\omega_2),\ S^{ss}(\omega_1,\omega_2) \qquad (2.13)$$

where superscript c means cosine and superscript s sine, respectively. In absolute-value mode, spectra are presented as

$$|S(\omega_1,\omega_2)| = [S^{cc}(\omega_1,\omega_2)^2 + S^{cs}(\omega_1,\omega_2)^2 + S^{sc}(\omega_1,\omega_2)^2 + S^{ss}(\omega_1,\omega_2)^2]^{1/2}. \qquad (2.14)$$

Since they do not contain an imaginary part, less computer data space is needed. Phase corrections can be circumvented. However, the resolution is low.

Phase-sensitive spectra need a phase-correction and are presented with the cross-peaks in pure absorption with alternating sign of the fine structure components

(antiphase cross-peaks) and the diagonal peaks in dispersion. A comparison of an absolute value display and absorption mode peaks is shown in Figure 2.10.

Figure 2.10: Comparison of an absolute-value display (a) and absorption-mode sections (b) taken from a heteronuclear zero-quantum 2-D correlation spectrum of phosphothreonine, showing typical distortions of the ill-resolved multiplet structure in the absolute-value mode (adapted from Ernst et al., 1987).

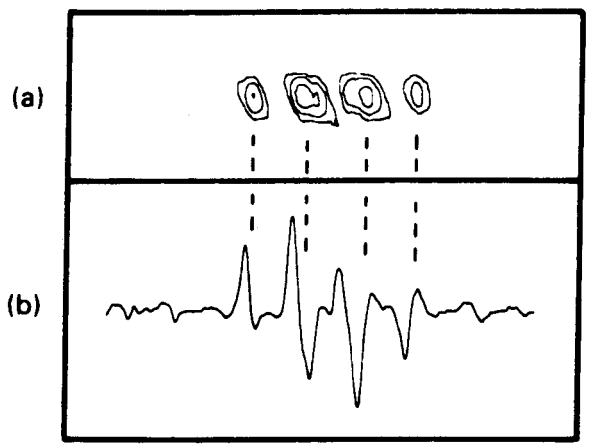

There are two methods for obtaining phase-sensitive spectra. Using the method of time-proportional phase increments (TPPI), the carrier frequency is placed in the middle of the spectrum and the first pulse is incremented in proportion to t_1

$$\varphi^{prep}=(\pi/2N)(t_1/\Delta t_1) \qquad (2.15)$$

where N corresponds to the order p that one wishes to observe (see chapter 2.2.3.3) (Redfield & Kunz, 1975; Bodenhausen et al., 1980; Marion & Wüthrich, 1983). Pure absorption peak shapes are obtained by calculating a real Fourier-transform with respect to t_1 (Ernst et al., 1987).

The other method generates two data sets for each t_1 (Bachmann et al., 1977; States et al., 1982). In one set the signal in t_1 is cosine-modulated, in the other sine-modulated. This is achieved by shifting the phase of the preparation pulse for the second data set:

$$\varphi_A^{(prep)} = 0, \text{ and } \qquad \varphi_B^{(prep)} = \pi/2|p| \qquad (2.16)$$

where p is the order of coherence in the evolution period. Each data set is submitted separately to a complex Fourier-transform. The addition of the two resulting spectra yields the desired spectrum (Figure 2.11).

Figure 2.11: The result of quadrature detection in t_1 according to States et al., 1982. Cosine-modulated signals are accumulated separately from sine-modulated signals. After a complex Fourier-transform, addition of the resulting spectra results in the desired spectrum (adapted from Kessler et al., 1988).

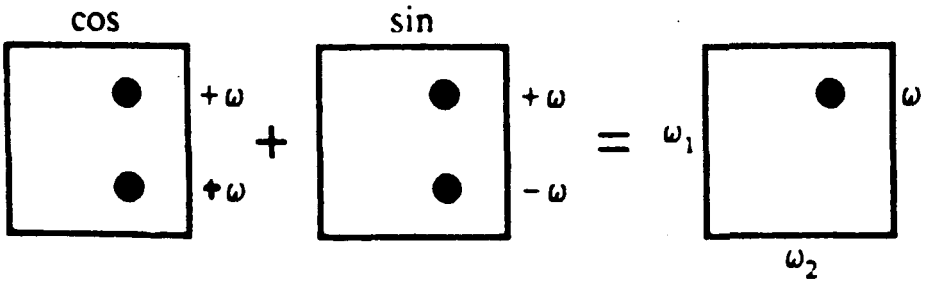

2.2.3.2.2. RESOLUTION ENHANCEMENT

The resolution of an NMR spectrum can be enhanced by multiplying the data set $s(t_1,t_2)$ with a weighting function. Shifted sine- or squared sine-functions (sine-bells) have proven to give the best results in 2-D NMR (DeMarco & Wüthrich, 1976; Guéron, 1978; Wagner et al., 1978). Figure 2.12 shows the resolution enhancement after multiplication of the FID with the shifted sine-bell

$$\sin[(\pi t/t_2) + 0.04\pi]. \qquad (2.17)$$

Figure 2.12: Resolution enhancement by digital filtering before FT. (A) and (B) 1-D FID of BPTI before and after multiplication with the shifted sine bell of Eq. (2.17). (C) and (D) High-field region of the 1-D ^{1}H NMR spectra obtained by FT of (A) and (B), respectively (adapted from Wüthrich, 1986).

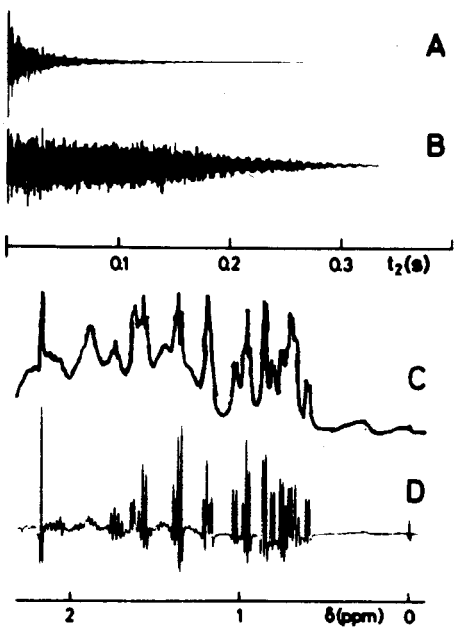

2.2.3.2.3. ZERO-FILLING

According to the sampling theorem the enhancement of the resolution increases with the size of the data set. The number of data points sampled in a 2-D NMR experiment is limited because it would increase considerably the time of the experiment. Therefore the size of a data matrix $s(t_1, t_2)$ is increased by supplementing the recorded data points by a string of zeros up to the next (or higher) power of 2 prior to the FT (Bartholdi & Ernst, 1973). Zero-filling improves the lineshape of a spectrum and thus, its resolution.

2.2.3.3. SELECTION OF COHERENCE TRANSFER PATHWAYS

2-D NMR experiments can be described in terms of pathways through various orders of coherence or energy states of a spin system. Each transition between two energy states is associated with two coherences with order $\pm p_n$. During precession, the quantum number $\pm p_n$ is conserved. Radiofrequency pulses may induce a change in coherence order

$$\pm p_n \longrightarrow \pm p_{n+m}.$$

In NMR, all coherence transfer pathways start with $p = 0$, and end with single-quantum coherence $p = \pm 1$ to be detected (Ernst et al., 1987).

2.2.3.4. SCALAR COUPLING

Scalar coupling is the interaction between neighboring spins that are connected by covalent bonds. It is manifested by the splitting of bands in NMR spectra. The spin states for a system of spin-1/2 nuclei can be labelled using the α,β-notation. The overall state of a spin system is designated by the product of the functions for the individual nuclei (Harris, 1983). The basic product functions of a three-spin system is given in Table 2.2.

Table 2.2: The Basic Product Functions of a Three-Spin System.

m_T	Basis Product Functions
-3/2	$\beta\beta\beta$
-1/2	$\beta\beta\alpha$, $\beta\alpha\beta$, $\alpha\beta\beta$
+1/2	$\beta\alpha\alpha$, $\alpha\beta\alpha$, $\alpha\alpha\beta$
+3/2	$\alpha\alpha\alpha$

where m_T is the total magnetic quantum number (Harris, 1983).

Figure 2.13 shows the energy level diagram for a three-spin system with the assignments of the transitions that are allowed according to the selection rule $\Delta m_T = \pm 1$.

Figure 2.13: Energy level diagram for a system of three spin-1/2 nuclei with the assignements of the allowed NMR transitions for the spins A, M, and X, respectively (adapted from Harris, 1983).

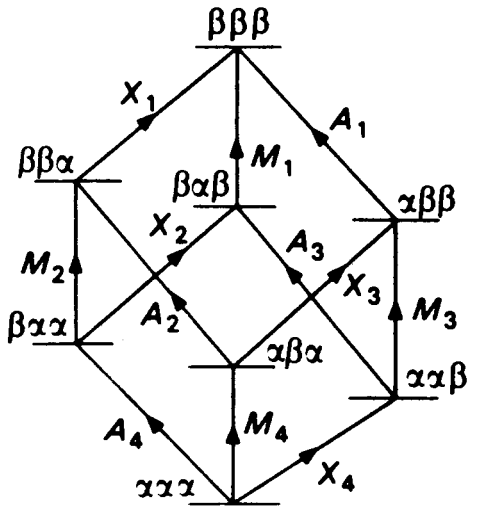

Four transitions are assigned to each spin, therefore each of the three resonances in the NMR spectrum is split into a quadruplet, characterized by the coupling constants J_{AM}, J_{AX}, and J_{MX}. Figure 2.14 shows the splittings for nucleus A of the AMX spin system.

Figure 2.14: Splitting for nucleus A of a three-spin system, showing the effect in first order of coupling to nuclei M and X (adapted from Harris, 1983).

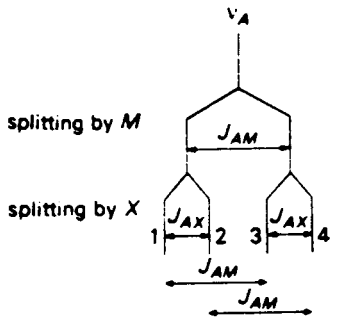

where first order coupling means

$$\begin{aligned} |\upsilon_A - \upsilon_M| &>> |J_{AM}| \\ |\upsilon_A - \upsilon_X| &>> |J_{AX}| \\ |\upsilon_M - \upsilon_X| &>> |J_{MX}|. \end{aligned} \qquad (2.18)$$

υ is the resonance frequency of the respective nucleus.

In 1-D NMR spectra of biological macromolecules it is difficult to detect systems of coupled spins due to the presence of a great number of nuclei and different spin systems. Information about spin systems can be obtained by two-dimensional correlated spectroscopy.

2.2.3.5. 2-D CORRELATED SPECTROSCOPY (COSY)

Two-dimensional correlated spectroscopy has the experimental scheme

$$[t_0 - 90° - t_1 - 90° - t_2(\text{acq.})]_n$$

where

t_0 = preparation period or relaxation delay
t_1 = evolution period
t_2 = mixing and observation period
n = number of experiments

The experiment can be described by means of Cartesian operators (Ernst et al., 1987; Kessler et al., 1988). Only a simplified explanation will be given here for spin A of an AX spin system.

The first radiofrequency pulse creates transverse magnetization. During the evolution period t_1, spin A precesses at two different angular velocities corresponding either to the α- or β-state of spin X. The second radiofrequency pulse transfers magnetization of spin A into transitions of spin X. After a two-dimensional Fourier-transform, magnetization of spin A is observed in peaks at the following frequencies:

1. Magnetization of spin A that was transferred to spin X is observed at $(\omega_{X1}, \omega_{A2})$ as a cross-peak.

2. Magnetization of spin A that was not transferred to spin X, is observed at $(\omega_{A1}, \omega_{A2})$ as a diagonal peak.

3. Magnetization of spin A that was in the ground state $|\alpha\alpha\rangle$ during t_1, appears at $(0, \omega_{A2})$ as an axial peak.

Axial peaks occur as artifacts in the COSY experiment. While the COSY diagonal and cross-peaks are invariant under a 180° phase-shift of the second pulse, axial peaks are not. Thus, they are removed by shifting the phase of the second pulse by 180° between two scans and by adding the resulting signals in the computer memory.

Figure 2.15 shows the pathway of the coherence of the COSY experiment.

Figure 2.15: Coherence Transfer Pathway of the COSY Experiment (adapted from Ernst et al., 1987).

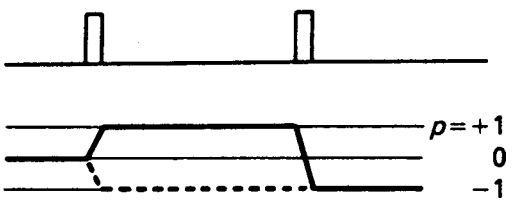

2.2.3.5.1. DOUBLE-QUANTUM-FILTERED COSY

In phase-sensitive COSY spectra, the diagonal peaks are in pure dispersion when the phase is adjusted for pure absorption lines of the cross-peaks, therefore masking cross-peaks close to the diagonal. Routing of the coherence through a double-quantum-filter (2QF) allows one to obtain

both cross-peaks and diagonal peaks in antiphase absorption mode (Ernst et al., 1987). This is illustrated in Figure 2.16.

Figure 2.16: Comparison of conventional, phase-sensitive COSY (A) with phase-sensitive 2QF-COSY (B). The region (ω_1 = 0.5-5.0 ppm, ω_2 = 0.5-5.0 ppm) of a spectrum of BPTI is shown (0.02 M, D_2O, pD 4.6, 36°C; 360 MHz; sine-bell resolution enhancement with phase shifts of $\pi/4$ in t_1 and $\pi/8$ in t_2 applied in both spectra) (adapted from Rance et al, 1983).

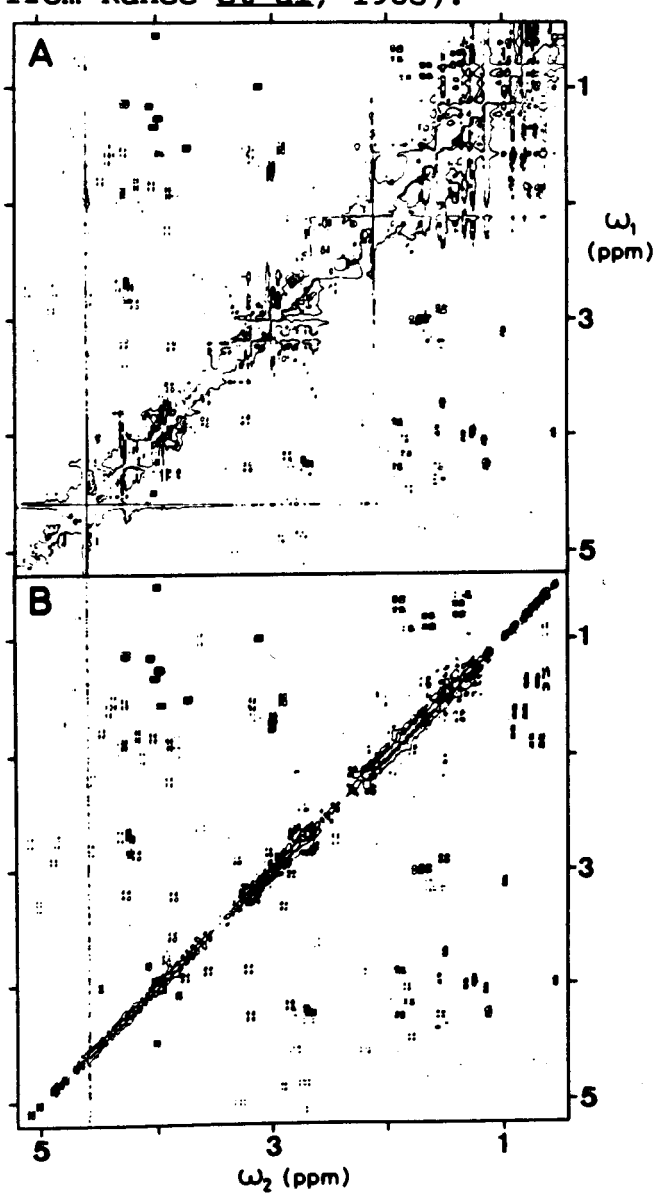

Furthermore, diagonal singlet peaks are suppressed by a double quantum filter, because one-spin systems cannot be routed through a double quantum state.

The pulse sequence of the double-quantum-filtered (DQF) COSY is given by

$$[t_0 - 90° - t_1 - 90° - t_3 - 90° - t_2(\text{acq.})]_n$$

where t_3 is a short delay time (4-5 μs) required to shift the phase of the transmitter.

Figure 2.17 shows the pathway of the coherence transfer in the DQF-COSY.

Figure 2.17: Coherence Transfer Pathway of the DQF-COSY Experiment (adapted from Ernst et al., 1987).

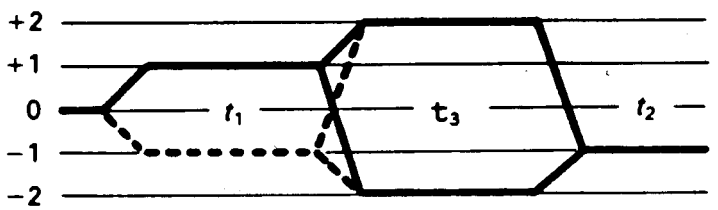

2.2.3.5.2. RELAYED COSY

In a relayed COSY spectrum, cross-peaks are observed between two spins i and k which are not directly coupled but share a mutual coupling partner j:

$$H_i(\omega_1) \longrightarrow H_j \longrightarrow H_k(\omega_2)$$

(Wüthrich, 1986).

The pulse sequence is given by

$$[t_0\text{-}90°\text{-}t_1\text{-}90°\text{-}\tau_R/2\text{-}180°\text{-}\tau_R/2\text{-}90°\text{-}t_2(\text{acq.})]_n$$

where τ_R is the relay time.

A 180° pulse is applied in the middle of the relay time in order to suppress chemical shift evolution.

The efficiency of a relayed magnetization transfer between H_i and H_k is proportional to $\sin(\pi J_i\tau_R)\sin(\pi J_k\tau_R)$, where J is the scalar coupling constant of the respective spins. The maximum of this product is obtained if τ_R matches both $1/(2J_i)$ and $1/(2J_k)$. For most experiments the relay time is estimated.

The coherence transfer pathway of the relayed COSY experiment is given in Figure 2.18.

Figure 2.18: Coherence Transfer Pathway of the Relayed COSY Experiment (adapted from Ernst et al., 1987).

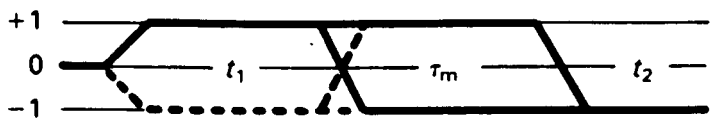

2.2.3.5.3. PHASE-SHIFTS

A coherence transfer pathway cannot be selected by a pulse sequence alone. The key to the separation of coherence transfer pathways is the use of pulses that are shifted in phase (Ernst et al., 1987).

The total signal of an experiment is made up of contributions from all pathways. To restrict the coherence transfer to a particular change Δp_i in coherence order, N_i experiments with systematic increments of the pulse phase (φ_i) are performed:

$$\varphi_i = k_i 2\pi / N_i \qquad (2.19)$$

where

k_i = 0, 1, ..., N-1, and
N_i = number of cycles (normally 4).

The phase increment φ is given by

$$\varphi = \Delta p_i \varphi_i \qquad (2.20)$$

where Δp_i is the change in coherence order (Ernst et al., 1987). The first pulse transfers coherences to all orders. In a DQF-COSY experiment the second pulse has to transfer coherence from $p_1 = 1$ to $p_2 = \pm 2$. Then

$$\Delta p_1 = +1, -3.$$

If we substitute these two values into equations (2.19) and (2.20) we obtain for φ_2 the values

$$\varphi_2 = 0, \pi/2, \pi, 3\pi/2.$$

Similarly, the phase of the receiver is channelled through

$$\varphi^{ref} = -\Delta p_i \varphi_i \qquad (2.21)$$

With $\Delta p_i = -3, +1$, this gives the receiver phases

$$\varphi_{ref} = 0, \pi/2, \pi, 3\pi/2.$$

2.2.3.6. THE NUCLEAR OVERHAUSER EFFECT (NOE)

In addition to scalar coupling between nuclei there is a through space interaction caused by local dipolar fields (Solomon, 1955; Noggle & Schirmer, 1971). A spin 2 which is located close to a spin 1 generates a local magnetic field B_D at the site of spin 1:

$$B_D = \gamma_2(3\cos^2\theta_{12} - 1)(r_{12}^{-3}) \qquad (2.22)$$

where

γ_2 = magnetogyric ratio of spin 2
θ_{12} = angle between the interatomic vector and the magnetic field B_0
r_{12} = internuclear distance between spin 1 and spin 2.

Local magnetic fields lead to exchange of spin polarization between spins and cause the relaxation of a spin system which deviates from the Boltzmann equilibrium (equation 2.7) back to its equilibrium state. This magnetization transfer is termed Nuclear Overhauser Effect (NOE). Figure 2.19 shows the relaxation pathways of a system of two spins I and S with the relaxation rates W. The subscripts 0, 1, and 2 refer to zero-, single-, and double-quantum transitions, respectively.

Figure 2.19: Relaxation of a two-spin system. Zero-, single-, and double-quantum transitions are labelled W_0, W_1, and W_2, respectively (adapted from Kessler et al., 1988).

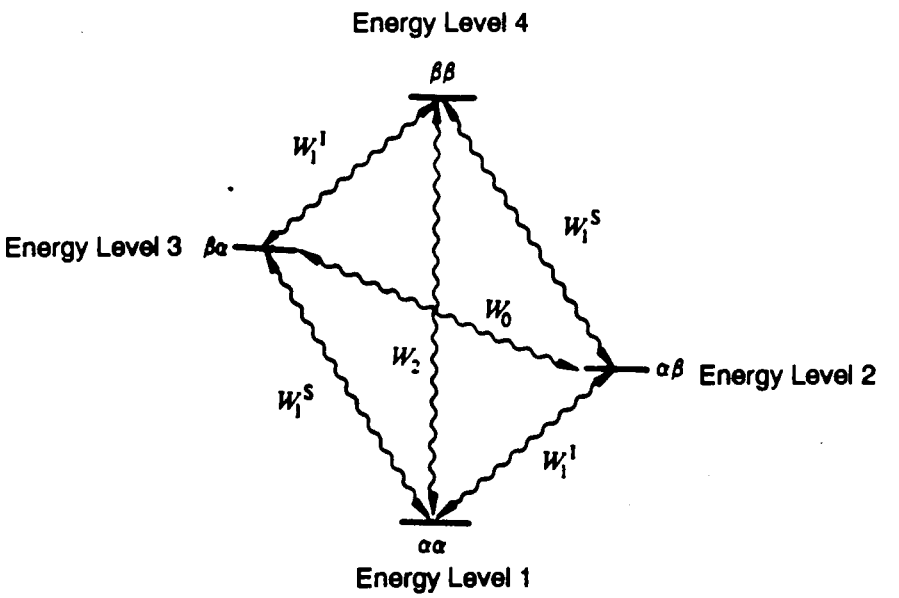

The Nuclear Overhauser Effect will be explained in the following with the transient NOE experiment, which is related to the two-dimensional NOESY (2-D Nuclear Overhauser and Exchange Spectroscopy) (Wüthrich, 1986).

A two-spin system is given with its energy levels as shown in Figure 2.19. Dipolar coupling is assumed between the two spins, but no scalar coupling. The spins are distributed among the energy levels according to the Boltzmann equation (2.7). The energy difference between $|\alpha\beta\rangle$ and $|\beta\alpha\rangle$ is approximately zero, an excess or deficiency in population by δ (Noggle & Schirmer, 1971).

The population differences at equilibrium are given by

$$\begin{aligned} n_{\alpha\alpha} - n_{\alpha\beta} &= \delta \\ n_{\beta\alpha} - n_{\beta\beta} &= \delta \end{aligned} \qquad (2.23)$$

for the W_{1I} transitions;

$$\begin{aligned} n_{\alpha\alpha} - n_{\beta\alpha} &= \delta \\ n_{\alpha\beta} - n_{\beta\beta} &= \delta \end{aligned} \qquad (2.24)$$

for the W_{1S} transitions;

$$n_{\alpha\beta} - n_{\beta\alpha} = 0 \qquad (2.25)$$

for the zero-quantum transition W_0, and

$$n_{\alpha\alpha} - n_{\beta\beta} = 2\delta \qquad (2.26)$$

for the double-quantum transition W_2.

Now a selective 180° pulse is applied on resonance I at a time τ_M before the observation pulse. A 180° pulse inverts the populations of the affected spin.

Immediately after the 180° pulse, the population differences are

$$n_{\alpha\alpha} - n_{\alpha\beta} = -\delta$$
$$n_{\beta\alpha} - n_{\beta\beta} = -\delta \qquad (2.27)$$

for W_{1I};

$$n_{\alpha\alpha} - n_{\beta\alpha} = \delta$$
$$n_{\alpha\beta} - n_{\beta\beta} = \delta \qquad (2.28)$$

for W_{1S}, which leads to

$$n_{\alpha\beta} - n_{\beta\alpha} = 2\delta \qquad (2.29)$$

for W_0, and

$$n_{\alpha\alpha} - n_{\beta\beta} = 0 \qquad (2.30)$$

for W_2.

W_0: During τ_M, magnetization is transferred from $|\alpha\beta\rangle$ to $|\beta\alpha\rangle$ in order to restore the equilibrium given by equation (2.25). This population transfer increases the population of energy level 3 and decreases the population of energy level 2.

W_2: During τ_M, magnetization is transferred from $|\beta\beta\rangle$ to $|\alpha\alpha\rangle$ in order to restore the equilibrium given by equation (2.26). This transfer decreases the population of energy level 4 and increases the population of energy level 1.

The signal intensity after the following observation pulse is proportional to the population differences. Therefore

the signal intensity of spin S is decreased when W_0 is dominant, and increased when W_2 is dominant.

For a homonuclear AB spin system, the balance is given by

$$n_I = 1 + [(W_2 - W_0) / (W_2 + 2W_{1I} + W_0)] \qquad (2.31)$$

(Harris, 1983).

Whether W_2 or W_0 is dominating depends on the rotational correlation time τ_c of the molecule. In small molecules the frequencies of the rotational motions are high enough to allow transitions of the type $|\beta\beta\rangle \longrightarrow |\alpha\alpha\rangle$, whereas in macromolecules transitions $|\alpha\beta\rangle \longrightarrow |\beta\alpha\rangle$ are preferred due to their low frequency of rotational motion (Harris, 1983).

The intensity of the NOE is inversely proportional to the sixth power of the distance r between the spins A and B and depends on the length of τ_M. Experiments with varying τ_M thus allow one to calculate the distance between two spins (Wüthrich, 1986).

2.2.3.7. 2-D NUCLEAR OVERHAUSER AND EXCHANGE SPECTROSCOPY (NOESY)

In the 2-D NOESY experiment, NOEs are created of all dipolar coupled spins in a molecule in a single experiment (Wüthrich, 1986). The results are processed and plotted analogous to the COSY spectrum.

The NOESY has the experimental scheme

$$[t_0 - 90° - t_1 - 90° - \tau_M - 90° - t_2(\text{acq.})]_n$$

where τ_M is the mixing time.

The pathway of the magnetization is shown in Figure 2.20.

Figure 2.20: Pathway of the Magnetization of the NOESY Experiment (adapted from Ernst et al., 1987).

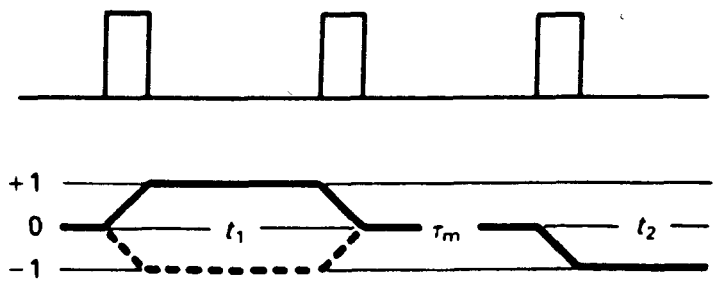

2.2.3.8. IDENTIFICATION OF SPIN SYSTEMS IN PROTEINS BY 2-D ^{1}H NMR

The first step in the analysis of 2-D ^{1}H NMR spectra of peptides is the identification of spin systems of the individual amino acid residues (Wüthrich *et al.*, 1982; Billeter *et al.*, 1982; Wagner & Wüthrich, 1982; Wider *et al.*, 1982). This amounts to recognizing particular geometric patterns of J-coupled resonances in ^{1}H COSY spectra of the peptide in D_2O. Figure 2.21 shows these patterns for the 20 essential amino acids.

Figure 2.21: COSY, relayed COSY, and double-relayed COSY connectivity diagrams for the spin systems of nonlabile protons in the common amino acid residues. Each square represents a 2-D spectrum for an amino acid residue or a group of residues. The positions of the diagonal peaks are represented by filled circles, COSY connectivities by open circles and solid lines, relayed COSY by crosses and broken lines, double-relayed COSY by stars and dotted lines. Additional relayed connectivities may be propagated through the geminal coupling in CH_2 groups, for example, CαH ⟶ CβH ⟶ Cβ'H. Arbitrary chemical shifts have been chosen to enable a clear presentation (adapted from Wüthrich, 1986).

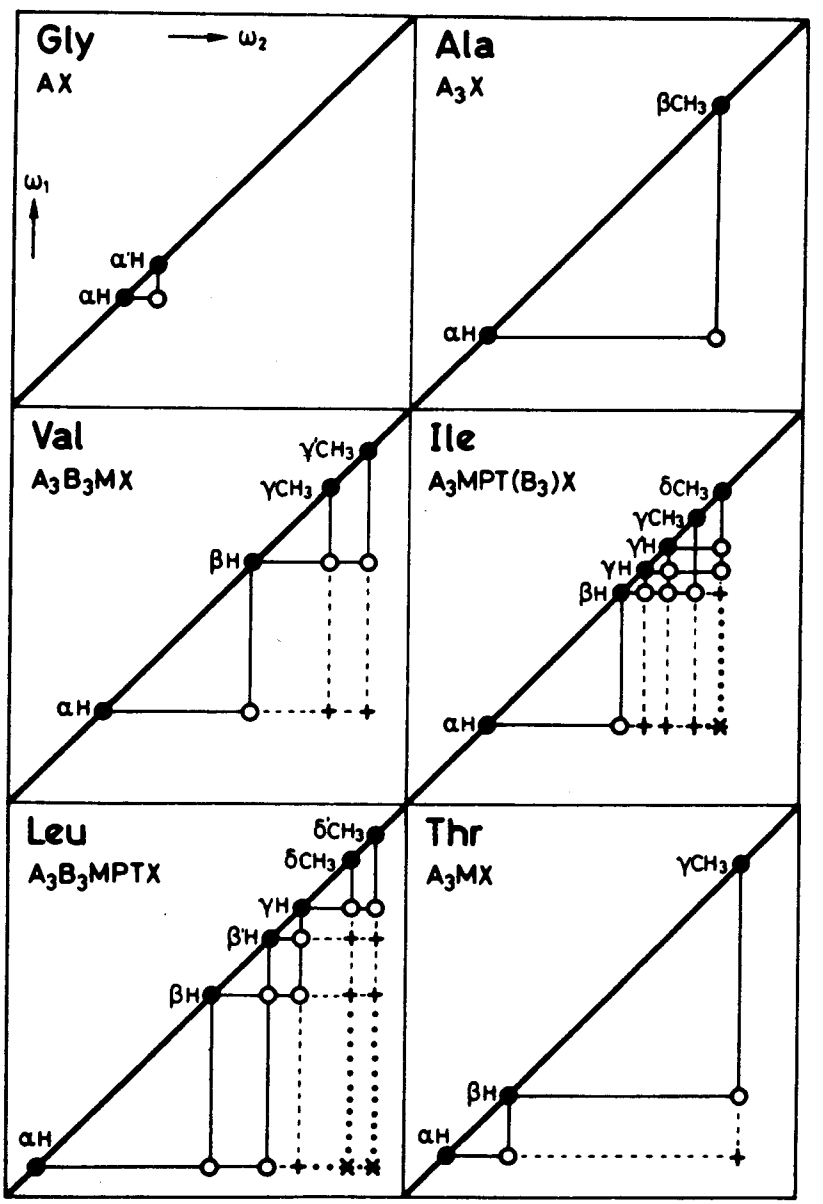

Figure 2.21: (Continued)

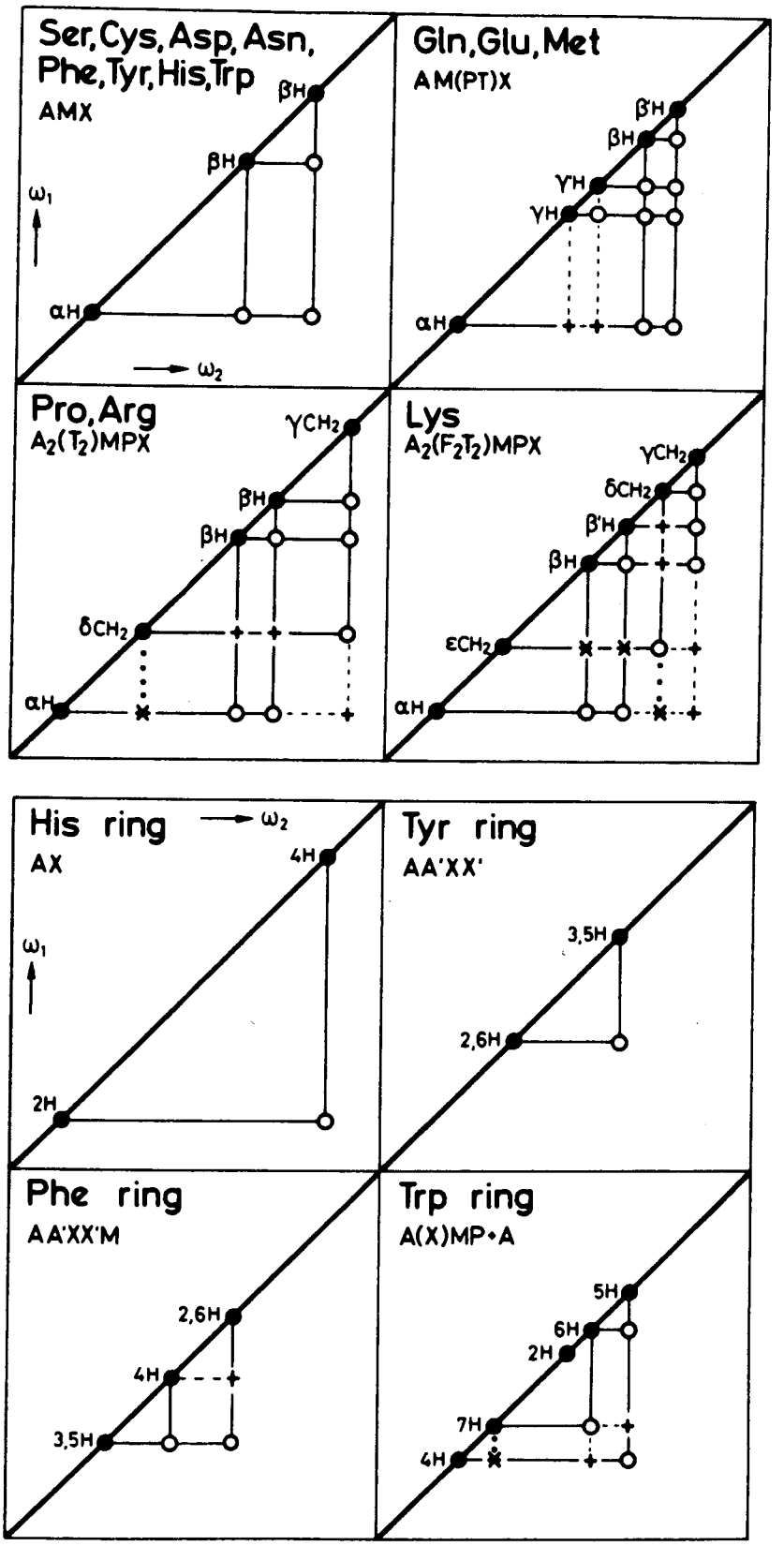

These patterns are often overlapped or incomplete. A series of 2-D ^{1}H NMR spectra thus have to be recorded like COSY, relayed COSY, TOCSY (2-D Total Correlated Spectroscopy) (Braunschweiler & Ernst, 1983) or HOHAHA (2-D Homonuclear Hartmann-Hahn Spectroscopy) (Davis & Bax, 1985), and double-quantum COSY (Braunschweiler et al., 1983) at different temperatures and pH values.

Another important tool is the resolved fine-structure of cross-peaks in phase-sensitive 2-D NMR spectra (Neuhaus et al., 1985), where cross-peaks have antiphase character. This antiphase fine-structure is shown in Figure 2.22.

Figure 2.22: NH/CαH cross-peak fine-structure for Cys-57 in a phase-sensitive COSY spectrum of BUSI. (A) Cross section taken along the dotted line in the contour plot. (B) Contour plot. Positive contours are drawn with solid lines, negative contours with broken lines. (C) Spin-spin coupling scheme (adapted from Marion & Wüthrich, 1983).

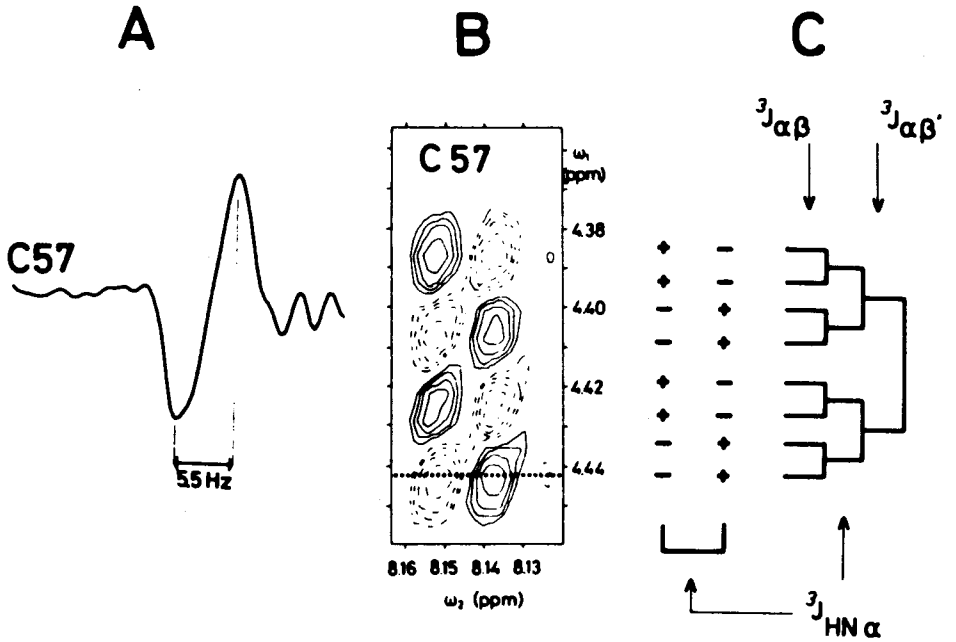

For coupled spins of the type H_i-H_a-H_b-H_j, where H_a and H_b are connected by a cross-peak, the splitting J_{ab} always appears in antiphase along both frequency axes (Sorensen et al., 1983; Neuhaus et al., 1985). The passive couplings J_{ai} and J_{bj} can be observed as additional in-phase splittings along either ω_1 or ω_2. Figure 2.23 shows the cross-peak multiplet structure of the ^1H spin systems AX, AMX, A_3X, and A_3MX, respectively.

Figure 2.23: COSY cross-peak multiplet structures for the ^1H spin systems AX, AMX, A_3X, and A_3MX. The letters on the diagonal indicate the chemical shifts for the different groups of protons. Filled circles represent positive signals, open circles negative signals, and the area of the circles represents the peak intensity. In the lower right of each spectrum, active and passive couplings are indicated with thick and thin lines, respectively (adapted from Neuhaus et al., 1985).

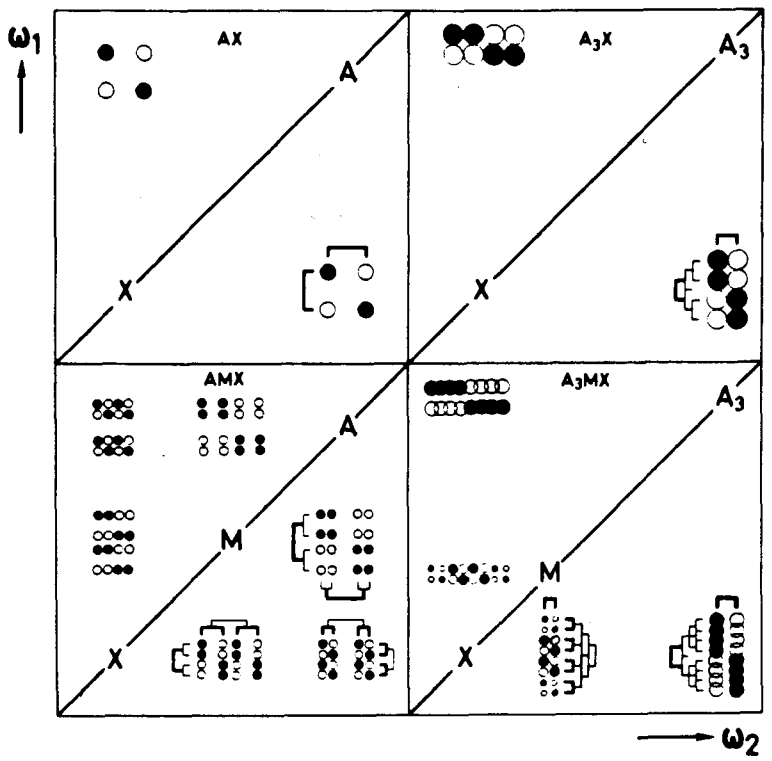

The simplest pattern is that of an AX spin system (glycine). It shows an antiphase square array with no passive couplings.

AMX spin systems are observed for Ser, Cys, Asp, Asn, Phe, Tyr, His, and Trp residues of a peptide, where the AX pattern is split into four identical arrays that are separated by passive couplings. The MX cross-peak in Figure 2.23 at ($\omega_1 = \delta_X, \omega_2 = \delta_M$) shows the antiphase splitting J_{MX} and the in-phase splitting J_{AX} along ω_1. The antiphase splitting J_{MX} and the in-phase splitting J_{AM} are manifested along ω_2. For the A_3X spin system (alanine) the active coupling is to be considered as that between X and one of the three methyl protons, the other two protons of A acting as passive coupling partner of X. Analogously, the cross-peaks of the A_3MX spin system (threonine) can be analyzed. However, the theoretical fine-structure of cross-peaks is often complicated by limited resolution or cancellation of overlapping antiphase cross-peaks.

2.2.3.9. SEQUENCE-SPECIFIC ASSIGNMENTS OF RESONANCES AND IDENTIFICATION OF STRUCTURAL ELEMENTS

Amino acid spin systems in a peptide can only be definitely assigned with COSY and NOESY spectra of the peptide in H_2O where the amide protons of the peptide backbone can be observed (Kumar et al., 1980a,b). Since the

amide protons exchange with the protons of H_2O, the rate depending on the temperature and the pH (Wagner, 1983), their intensity in 2-D NMR spectra may be low. The COSY spectrum connects the CαH with the NH protons of an amino acid. In a NOESY spectrum, cross-peaks should be detected between $C\alpha H_i$ and NH_{i+1} of the next residue in the sequence, between $C\beta H_i$ and NH_{i+1}, and between NH_i and NH_{i+1}. Provided that the protein sequence is known, the amino acid spin systems can then be assigned. Figure 2.24 shows the described connectivities.

Figure 2.24: Polypeptide segment with indication of the spin systems of nonlabile protons in the individual residues (inside dotted lines), the CαH-NH COSY connectivities (broken lines), and the sequential NOE connectivities (arrows) (adapted from Wüthrich, 1986).

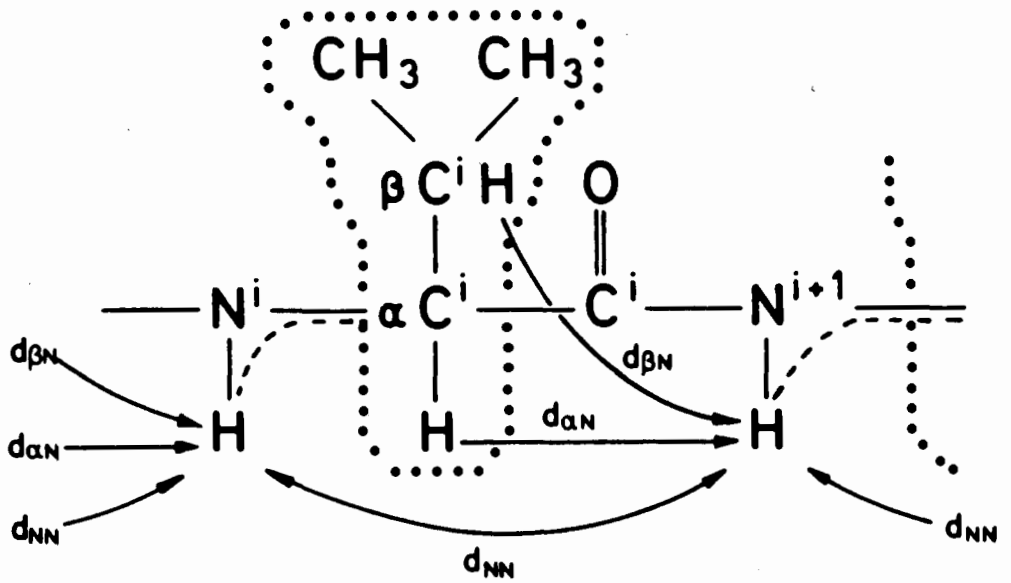

Dipolar coupling between non-neighboring amino acid residues can be detected in NOESY spectra between protons that are less than 0.5 nm apart. In β-sheets, coupling can be observed between amide protons and CαH protons of the opposite chain. In α-helices where the CO_i carbonyl is hydrogen-bonded to the NH_{i+4} proton, a cross-peak between $C\alpha H_i$ and NH_{i+4} can be detected (Kumar et al., 1980a,b; Wagner et al., 1981; Wüthrich et al., 1982).

2.3 BINDING OF INSULIN TO EGG YOLK PHOSPHATIDYLCHOLINE

2.3.1. DYNAMIC LIGHT SCATTERING

The particle size of vesicles in solution can be determined by dynamic light scattering (Berne & Pecora, 1976). The vesicle solution is illuminated by monochromatic photopulses (laser). The intensity of the light scattered by the vesicles is measured at a scattering angle of 90°. Due to the motion of the particles which is dependent upon the viscosity of the solution and the size of the particles, the measured intensities for a series of photopulses are random. One then calculates an autocorrelation function

$$C(t') = \sum_{p=0}^{n} I_s(t) \cdot I_s(t+\tau) \qquad (2.32)$$

where $I_s(t)$ is the intensity measured at a time t and $I_s(t+\tau)$ the intensity at a time τ after. The products of the equation are summed for n photopulses. If τ is very small the measured intensities at t and $(t+\tau)$ are similar, i.e. they are highly correlated. This correlation decreases when τ becomes greater. When a number of autocorrelation functions are computed for increasing values of τ one finally obtains an exponential decay

$$C(\tau) = C(0) \exp[-2DK^2/\tau] \qquad (2.33)$$

where K is the scattering vector

$$K = (4\pi n/\lambda)(\sin\Theta/2) \qquad (2.34)$$

and

λ = wavelength of the monochromatic light
n = index of refraction
Θ = scattered light angle
D = diffusion coefficient of the particles.

From a plot of ln correlator output [$C(\tau)$] vs. τ^{-1} the diffusion coefficient D of the particles can be determined.

The distribution of particle size is then determined by a least-squares fit of the autocorrelation function to a Gaussian distribution, using a chi-square test to assess the goodness of fit. An alternative is a distribution analysis that attemps to determine a set of exponentially decaying functions which yield the measured autocorrelation function when added and squared.

2.3.2. DETECTION OF PROTEIN BINDING TO LIPID MEMBRANES BY FLUORESCENCE EMISSION SPECTROSCOPY

The aromatic side chains of the amino acids tryptophan, tyrosine, and phenylalanine are responsible for the ultraviolet absorbance and fluorescence properties of a protein. They are listed in Table 2.3.

Table 2.3: Spectroscopic Properties of the Aromatic Amino Acids at Neutral pH (adapted from Creighton, 1984).

	Absorbance max. [nm]	Fluorescence max. [nm]
Phenylalanine	257.4	282
Tyrosine	274.6	303
Tryptophan	279.8	348

Fluorescence of the aromatic groups of amino acids is sensitive to their environment. The close proximity of the aromatic groups in a folded protein results in energy transfer between them. Light absorbed by a donor is transferred to an acceptor absorbing at longer wavelength. The rate of this energy transfer is dependent upon the sixth power of the distance R between two chromophores (Stryer & Haugland, 1967):

$$k_T = (1/\tau_D)\,(R_0/R)^{-6} \qquad (2.35)$$

where t_D is the lifetime of the donor in the absence of

the acceptor. R_0 is the characteristic transfer distance

$$R_0 = 9.7 \times 10^3 \cdot (J\kappa^2 n^{-4} \phi_D)^{1/6} \text{ cm} \qquad (2.36)$$

where J is a measure of the spectral overlap between donor emission and acceptor absorbance, κ^2 is a complex geometric factor depending on the orientation of donor and acceptor, n is the refractive index of the medium between donor and acceptor, and ϕ_D is the quantum yield of the donor in the absence of the acceptor. The quantum yield is the ratio between the number of photons emitted and the number of photons absorbed (Cantor & Schimmel, 1980). Since the absorption wavelengths of the aromatic amino acids are in the order Phe < Tyr < Trp, proteins containing all three residues generally emit fluorescent light typical for Trp. In the absence of Trp, fluorescence emission of Tyr is generally observed (Weber, 1972).

When light is absorbed by a chromophore, one or more electrons are promoted from bonding (π) to antibonding (π^*) orbitals. The excited state is more polar than the ground state, therefore an excited molecule is more strongly solvated by polar solvents. The stabilizing solvation lowers the energy of the excited state. When the chromophore is transferred to a non-polar environment such as a membrane, the energy of the excited state is

increased. Since the energy is given by

$$E = h\upsilon \qquad (2.37)$$

where h is Planck's constant, the frequency υ is enhanced. The wavelength λ which is given by

$$\lambda = c/\upsilon \qquad (2.38)$$

where c is the velocity of light, is decreased.

In addition, solvent molecules are much closer to the chromophore in a polar environment, and the collisions between solvent and chromophore molecules in their excited states increase. This leads to a radiationless relaxation, hence, the emission and the quantum yield ϕ_F decrease. If a chromophore is transferred to an unpolar environment, the collisions between solvent and excited states decrease and an enhancement of the emission signal intensity is observed.

Binding of a chromophore to a membrane is therefore accompagnied by an enhancement of the fluorescence and a blue shift of the emission maximum (Weber, 1972). For the peptide hormone glucagon, a small increase in fluorescence intensity and a blue shift of approximately 10 nm of the emission maximum were observed upon binding of the peptide to unilamellar detergent vesicles (Boesch et al., 1980).

3. MATERIALS AND METHODS

3.1. MATERIALS

CHEMICALS	SUPPLIER
Acetic Acid	BHD
d_3-Acetic Acid	SIGMA
Acrodisc filters with a pore diameter of 0.45 µm	Gelman
Acrylamide	SIGMA
Ammonium Persulfate	BIO RAD
Bisacrylamide (N,N'-Methylene-bis-Acrylamide)	SIGMA
Bromophenolblue	SIGMA
Coomassie Blue	SIGMA
Crystalline Egg Albumen	SIGMA
$CuSO_4$	BHD
Dialysis tubing, molecular weight cutoff of 1,000	Spectra/Por
Dialysis tubing, molecular weight cutoff of 12,000 to 14,000	Spectra/Por
d_6-DMSO	SIGMA
D_2O, 99 %	MSD-Frosst
Folin-Ciocalteau Phenol Reagent	Fisher
Glycine	BHD
Hydrochloric Acid	Fisher
d_1-Hydrochloric Acid	SIGMA
KH_2PO_4	BHD
β-Mercaptoethanol	BHD

Methanol	BHD
Na_2CO_3	BHD
NaOH	BHD
Na_2PO_4	BHD
Na-Tartrate	BHD
SDS (Sodium Dodecylsulfate)	BHD
TEMED (N,N,N',N'-Tetramethylethylendiamine)	BIO RAD
Tris (Tris-(hydroxymethyl-)aminomethane)	SIGMA
Urea	BHD

Human insulin was a kind gift of Novo Biolabs Ltd., Willowdale, Ontario.

Porcine insulin was purchased from Novo Biolabs Ltd., Willowdale, Ontario.

Egg yolk phosphatidylcholine was a kind gift of Dr. S. Arumugam.

3.2. METHODS

3.2.1. SDS-PAGE

SDS-PAGE was performed after Swank and Munkres (Swank & Munkres, 1971).

3.2.1.1. SAMPLE PREPARATION

A buffer containing 8 M urea was prepared as follows:

1.0 ml of 10 % SDS solution
0.2 ml of 3 M Tris-HCl, pH 6.8
0.5 ml of bromophenolblue solution (0.05 % $^{w}/_{v}$)

were mixed together.

From a 10 M stock solution, urea was recrystallized by cooling the solution to 6°C in the refrigerator for one hour. The urea was dried at high vacuum after filtration.

Recrystallized urea (4.8 g) was added to the above buffer and the solution diluted to 10 ml with demineralized water.

Insulin (1 mg) was added to 1 ml of sample buffer together with 10 µl of mercaptoethanol. The sample was boiled in a water bath for three minutes before being applied to the SDS gel.

3.2.1.2. RUNNING GEL, 12.5 %, ACRYLAMIDE:BISACRYLAMIDE, 10:1

A buffer composed of

100 µl of 10 % SDS solution
1.25 ml of 3 M Tris-HCl, pH 6.8
1.136 g of acrylamide
0.114 g of bisacrylamide
4.8 g of recrystallized urea

was prepared and diluted to 10 ml with demineralized water. After degassing at vacuum,

7.5 µl of TEMED and
7 mg of ammonium persulfate

were added. The solution was diluted to 10 ml with demineralized water, stirred quickly and poured immediately between the two gel plates. Air bubbles were removed with a Pasteur pipette and the running gel solution carefully overlayed with water. After polymerization, the water was removed with a filter paper, and the running gel overlayed with a 4 % stacking gel solution.

3.2.1.3. STACKING GEL, 4 %, ACRYLAMIDE:BISACRYLAMIDE, 10:1

The stacking gel solution was prepared in the same manner as described above; 10 ml contained

100 µl of 10 % SDS solution
420 µl of 3 M Tris-HCl, pH 6.8
0.364 g of acrylamide
0.036 g of bisacrylamide
4.8 g of recrystallized urea
10 µl of TEMED
7 mg of ammonium persulfate.

Demineralized water was added up to 10 ml.

3.2.1.4. ELECTRODE BUFFER

A five times concentrated stock solution was prepared, containing

9 g of Tris base
43.2 g of glycine
3 g of SDS
Demineralized water up to 600 ml.

For one run, 60 ml of electrode buffer were diluted to 300 ml.

After the samples had been applied, the gel was run at a constant voltage of 120 Volts for 2 hours 15 minutes.

The gels were stained for 2 hours in a solution containing

1.25 g of Coomassie blue
454 ml of 50 % methanol
46 ml of glacial acetic acid,

then destained over night in

40 % $^{v}/_{v}$ methanol
10 % $^{v}/_{v}$ glacial acetic acid
50 % $^{v}/_{v}$ water.

The destaining solution was removed, and the gel further destained in

5 % $^{v}/_{v}$ methanol
7 % $^{v}/_{v}$ glacial acetic acid
88 % $^{v}/_{v}$ water.

The gels were stored in 2 % glacial acetic acid.

3.2.2. FTIR STUDY OF PORCINE INSULIN IN SOLUTION

FTIR was performed on a Bruker IFS 85 spectrometer equipped with an Aspect 2000 computer. The spectra were processed using the program FOUDECONV provided by Bruker. Spikes from water vapor were removed by second derivative spectra subtraction. For quantitative analysis, the program SIMBAND from Bruker was used.

3.2.2.1. SAMPLE PREPARATION

Porcine insulin (16.43 mg, 2.87 x 10^{-3} mmol) was dissolved in 0.5 ml of H_2O/HCl at pH 3.0 and dialyzed against 3 x 1 liter of the same solvent in order to remove zinc. Dialysis tubing with a molecular weight cutoff of 1,000 was used. The sample was then lyophilized overnight at high vacuum and redissolved in 0.5 ml of D_2O/DCl at pH 3.0. The solution was placed in a water bath at a temperature of 50°C for 20 minutes in order to exchange amide protons, and then lyophilized twice from 0.5 ml of D_2O/DCl at pH 3.0. The final solution contained 32.86 mg/ml (5.73 mM) of the peptide. The sample was placed in a Harrick Demountable Precision Liquid Cell (Ossining, NY) with 2 mm thick BaF_2 windows separated by 25 μm thick Teflon spacers.

3.2.2.2. FTIR EXPERIMENT

The spectrometer was continuously purged by air starting 30 min. prior to the experiment in order to remove water vapor.

A 100 % line was established prior to measurements from 400 cm^{-1} to 4,000 cm^{-1} with 64 scans.

The following spectra were recorded:

- Reference single-beam spectrum with an empty light path
- Single-beam spectrum of D_2O
- Single-beam spectrum of insulin in D_2O.

The frequency range from 1,200 cm^{-1} to 1,800 cm^{-1} was recorded with 600 scans and a resolution of 2.0 cm^{-1}. The receiver gain was 3.

From the single-beam spectra, absorbance spectra were calculated. A difference absorbance spectrum between D_2O and insulin in D_2O was obtained with automatic subtraction. Manual subtraction gave no improvement. Water vapor spikes in the resulting difference spectrum were removed by four cycles of second derivative spectra subtraction until the baseline between 1750-2000 cm^{-1} was smooth. The spectrum was then Fourier self-deconvoluted using Bruker's FOUDECONV program and a Blackman-Harris 3-term apodization function.

Curve fitting was carried out using a program written by Qi Zhong of this laboratory. The peak width at half-height (HH) and % Gaussian/% Lorentzian were varied until the root-mean square value (RMS) was as small as possible.

3.2.3. 2-D ^{1}H NMR OF INSULIN IN D_2O

All experiments were performed on a Bruker WM-400 spectrometer equipped with a process controller. The data were processed on a Bruker Aspect 2000 computer. The software was provided by Bruker.

3.2.3.1. SAMPLE PREPARATION

Human insulin (7.35 mg) was suspended in 1 ml of H_2O, dialyzed overnight against 3 x 1 liter of 2 % acetic acid using dialysis tubing with a molecular weight cutoff of 1,000 in order to remove zinc. The sample was then lyophilized overnight at high vacuum and redissolved in 0.5 ml of 2 % d_3-acetic acid at pD 3.4. The solution was placed in a water bath at a temperature of 50°C for 20 minutes in order to exchange amide protons, then lyophilized several times from 2 % d_3-acetic acid. The peptide was redissolved in 2 % d_3-acetic acid at a pD 3.4 and at a concentration of 11.4 mg/ml (2 mM). The sample was spun in a clinical centrifuge for five minutes, degassed and placed in a 5 mm NMR tube under nitrogen.

3.2.3.2. COSY AND RELAYED COSY EXPERIMENTS

The temperature of the sample was adjusted at 37°C. The spectrometer carrier and decoupler frequency were both placed at the frequency of the water resonance. The decoupler power was adjusted to 37 decibel low power, where P_0 = 0.2 W. The sweep-width was 4,000 Hz, and the receiver gain 100. Two thousand and forty eight data points were sampled per scan. Five hundred and twelve experiments were recorded with 64 scans per experiment and a delay time of 1.5 s between experiments, during which the water resonance was saturated by continuous irradiation. The variable delay time, t_1, was incremented by 250 μs between two experiments, i.e. from 3 μs to 128 ms. For the COSY spectrum, the pulse sequence

$$[t_0 - 90°_a - t_1 - 90°_b - t_2(\text{acq.})_c]_n$$

was used, where

t_0 = relaxation delay and preirradiation
t_1 = evolution period (variable delay)
t_2 = observation period, and
n = number of experiments.

The pulse phases were cycled through

a =	x	x	x	x	y	y	y	y	-x	-x	-x	-x	-y	-y	-y	-y
b =	x	-x	y	-y	y	-y	-x	x	y	-y	-x	x	-x	x	-y	y

where

x = 0°
y = 90°
-x = 180°
-y = 270°.

The receiver was cycled through

c =	y	y	-y	-y	-y	-y	y	y	-y	-y	y	y	y	y	-y	-y.

The obtained data set $S(t_1, t_2)$ was processed in absolute value mode. $S(t_1)$ was zero-filled from 512 to 2,048 data points. Both dimensions were multiplied with a sine bell function, shifted by $\pi/9$ in both dimensions.

A relayed COSY experiment was recorded with the same sample, under the same conditions, and with the same processing parameters, using the pulse sequence

$$[t_0\text{-}90°_a\text{-}t_1\text{-}90°_b\text{-}(\tau_R/2)\text{-}180°_b\text{-}(\tau_R/2)\text{-}90°_c\text{-}t_2(\text{acq.})_d]_n$$

where

t_0 = relaxation delay and preirradiation
t_1 = evolution period (variable delay)
τ_R = relay time
t_2 = observation period, and
n = number of experiments.

A relay time of τ_R = 50 ms was chosen for the experiment.

The pulse phases were cycled through

a =	x	x	x	x	x	x	x	x	y	y	y	y	y	y	y	y
	-x	-x	-x	-x	-x	-x	-x	-x	-y	-y	-y	-y	-y	-y	-y	-y
b =	x	x	y	y	-x	-x	-y	-y	y	y	-x	-x	-y	-y	x	x
	-x	-x	-y	-y	x	x	y	y	-y	-y	x	x	y	y	-x	-x
c =	x	-x	y	-y	-x	x	-y	y	y	-y	-x	x	-y	y	x	-x
	-x	x	-y	y	x	-x	y	-y	-y	y	x	-x	y	-y	-x	x

and the receiver through

d =	x	x	-x	-x	x	x	-x	-x	y	y	-y	-y	y	y	-y	-y
	-x	-x	x	x	-x	-x	x	x	-y	-y	y	y	-y	-y	y	y.

3.2.3.3. NOESY EXPERIMENTS

A series of NOESY experiments were recorded in order to evaluate the ideal mixing time τ_M for insulin. A sample of human insulin was prepared as described above. The temperature of the sample was adjusted at 37°C. Spectrometer carrier and decoupler frequency were both placed at the frequency of the remaining water resonance. The decoupler frequency was adjusted at 15 decibel low power, where P_0 = 0.2 W. The sweep width was 4,000 Hz, and the receiver gain 40. Two thousand and forty eight data points were sampled per scan. Two hundred and fifty six experiments were recorded with 64 scans per experiment and a delay time of 1.5 s between two experiments, during which the water resonance was saturated by preirradiation. The delay time was incremented by 250 µs between two experiments, i.e. from 0.9 µs to 64 ms. The pulse sequence

$$[t_0 - 90°_a - t_1 - 90°_b - \tau_M - 90°_c - t_2(acq.)_d]_n$$

was used, where

t_0 = relaxation delay and preirradiation
t_1 = evolution period (variable delay)
τ_M = mixing time
t_2 = observation period, and
n = number of experiments.

The phases of the pulses were cycled through

a =	x	x	x	x	x	x	x	x	x	x	x	x	x	x	x	x
b =	x	y	-x	-y	x	y	-x	-y	x	y	-x	-y	x	y	-x	-y
c =	x	-y	x	-y	y	x	y	x	-x	y	-x	y	-y	-x	-y	-x

and the receiver through

d =	x	-y	x	-y	y	x	y	x	-x	y	-x	y	-y	-x	-y	-x.

The five experiments that were run are listed in Table 3.1 with their mixing times.

Table 3.1: NOESY Experiments With Mixing Times τ_M

	τ_M (ms)
NOESY 1	50
NOESY 2	100
NOESY 3	150
NOESY 4	200
NOESY 5	300

The data set $S(t_1,t_2)$ was processed as described above, but $S(t_2)$ was multiplied with a squared sine-bell function shifted by $\pi/16$ and $S(t_1)$ with a sine-bell function shifted by $\pi/32$.

3.2.4. 2-D ^{1}H NMR OF INSULIN IN d_6-DMSO

3.2.4.1. SAMPLE PREPARATION

Porcine insulin (36.5 mg/ml) was suspended in 1 ml of H_2O and dialyzed overnight against 3 x 1 liter of H_2O/HCl at a pH of 3.0 using dialysis tubing with a molecular weight cutoff of 1,000 in order to remove zinc. The peptide was then lyophilized overnight at high vacuum and dissolved in 0.5 ml of d_6-DMSO. The sample was spun in a clinical centrifuge for five minutes, degassed and placed in a 5 mm NMR tube under nitrogen. The concentration of the peptide was 12.7 mM.

3.2.4.2. DOUBLE-QUANTUM-FILTERED COSY AND RELAYED COSY EXPERIMENTS

The temperature of the sample was adjusted at 37°C. The spectrometer carrier frequency was placed at 8,200 Hz. The sweep-width was 5,000 Hz. Two thousand and forty eight data points were sampled per scan. Six hundred and forty experiments were recorded with a relaxation delay time of 2.0 s between experiments. The variable delay time, t_1, was incremented by 100 μs between two experiments, i.e. from 0.9 μs to 64 ms. In order to obtain phase-sensitive spectra, they were recorded in pure absorption mode, using TPPI (Redfield & Kunz, 1975; Bodenhausen et al., 1980;

Marion & Wüthrich, 1983). As a reference for phase-corrections, a COSY-45 - a COSY experiment with a pulse angle of 45° of the mixing pulse - was recorded with one experiment, 64 scans and a t_1 of 0.9 µs. A relay-time of τ_R = 50 ms was chosen for the relayed COSY. The following pulse sequences were used:

COSY-45: $[t_0 - 90°_x - t_1 - 45°_x - t_2(\text{acq.})_x]_1$

DQF-COSY: $[t_0 - 90°_a - t_1 - 90°_a - t_3 - 90°_b - t_2(\text{acq.})_c]_n$

Relayed-COSY: $[t_0\text{-}90°_a\text{-}t_1\text{-}90°_b\text{-}(\tau_R/2)\text{-}180°_b\text{-}(\tau_R/2)\text{-}90°_c\text{-}t_2(\text{aqc.})_d]_n$

where

t_0 = relaxation delay
t_1 = evolution period (variable delay)
τ_R = relay time
t_2 = observation period
t_3 = delay required to switch the transmitter phase
n = number of experiments.

The pulses of the DQF-COSY experiment were cycled through

a =	x	x	x	x	y	y	y	y	-x	-x	-x	-x	-y	-y	-y	-y
b =	x	y	-x	-y	y	-x	-y	x	-x	-y	x	y	-y	x	y	-x

and the receiver phase through

c =	x	-y	-x	y	y	x	-y	-x	-x	y	x	-y	-y	-x	y	x.

The pulses of the relayed COSY experiment were cycled as described above. Prior to the Fourier-transforms, the data sets were zero-filled to 4,096 data points in $S(t_2)$ and to 1,024 data points in $S(t_1)$ in order to increase the resolution. $S(t_2)$ was then multiplied with a squared sine-bell function, shifted by $\pi/32$, $S(t_1)$ with a sine-bell function, shifted by $\pi/16$. The data sets were phase-corrected using the COSY-45 as a reference.

3.2.5. BINDING STUDY OF INSULIN BY VESICLES OF EGG YOLK PHOSPHATIDYLCHOLINE

Egg yolk phosphatidylcholine (egg PC) in phosphate buffer was sonicated using a Biosonic III probe-type sonicator equipped with a broad tip.

The particle size of egg PC vesicles was measured on a Nicomp Model 270 Submicron Particle Sizer.

Fluorescence emission was measured on a Perkin Elmer MPF 44B Fluorescence Spectrometer, using a 5 ml quartz cuvette.

Optical densities were measured on a Coleman Jr. spectrophotometer at 500 nm.

3.2.5.1. SOLUBILIZATION TEST OF INSULIN BY VESICLES OF EGG YOLK PHOSPHATIDYLCHOLINE

Phosphate buffer was prepared containing 1.179 g/l (8.67 mM) KH_2PO_4 and 4.30 g/l (30.32 mM) Na_2HPO_4 (Bates, 1962). The pH was 7.4. Egg yolk phosphatidylcholine (502.94 mg, ~0.658 mmol) was suspended in 7 ml of phosphate buffer and sonicated for one hour at a 60 % duty cycle and 30 % power output. The sample was constantly cooled with tap water. The remaining 4.2 ml of the solution were centrifuged in a clinical centrifuge for 30 minutes and filtered through a Gelman Acrodisc filter with a pore diameter of 0.45 µm. The lipid concentration was approximately 157 mM. The particle size of the vesicles was measured on a Nicomp Model 270 Submicron Particle Sizer, adjusted to the following parameters:

Channel width	3.9 µs
Prescale factor	1
Temperature	25°C
Viscosity	0.8906 centipoise
Index of refraction	1.333
Scattering angle	90.0°
Autoprint at CH1	2,000K counts.

Zinc-free porcine insulin (23 mg, 4 x 10^{-3} mmol) was suspended in 0.5 ml of phosphate buffer. The concentration of insulin at these conditions was 8 mM. To the insulin suspension, 0.5 ml of vesicle solution in phosphate buffer were added, the mixture gently shaken and let stand for

30 minutes. Then another 0.5 ml of vesicle solution were added, and the procedure repeated, until a final concentration of 0.521 mmol of egg PC was reached.

The final concentration of 4 x 10^{-3} mmol of insulin and 0.521 mmol of egg PC in 3.8 ml were let stand overnight under nitrogen and exclusion of light at room-temperature.

On the next day, the pH of 7.06 was altered by adding small amounts of 100 mM HCl and 100 mM NaOH to pH = 2.1 and pH = 12.0, respectively, and then back to pH = 7.06 to examine whether insulin would reprecipitate at pH = 7.06.

3.2.5.2. FLUORESCENCE EMISSION STUDY

Stock solutions (8.7 mM) of zinc-free porcine insulin and egg PC vesicles were prepared as follows:

Insulin (10 mg, 1.7 x 10^{-3} mmol) was dissolved in 0.2 ml of H_2O/HCl at pH = 3.5. Egg PC (100 mg, 0.132 mmol) was suspended in 7 ml of phosphate buffer (pH 7.4) and sonicated as described above. The remaining 4.5 ml of the solution were centrifuged in a clinical centrifuge for 30 minutes and filtered through a Gelman Acrodisc filter with a pore diameter of 0.45 µm. The solution was diluted to 15 ml with phosphate buffer (pH 7.4) to a final concentration of 8.7 mM.

Fluorescence emission of the tyrosine residues was measured on a Perkin Elmer MPF 44B fluorescence spectrometer with the excitation wavelength adjusted at 275 nm. The emission was scanned manually from 302 nm to 295 nm.

From the stock solutions, 4 µl of insulin solution and increasing amounts of egg PC were mixed and diluted to 4 ml with phosphate buffer. Thus, the peptide concentration was held constant at 8.7 µM, whereas the vesicle concentration was increased from 0 to 4.35 mM in 13 experiments.

Two sets of experiments were carried out with slit widths of 5 mm and 4 mm, respectively.

3.2.5.3. PROTEIN DETERMINATION OF INSULIN WITH VESICLES OF EGG YOLK PHOSPHATIDYLCHOLINE

Egg yolk phosphatidylcholine (200 mg, 0.262 mmol) was suspended in 7 ml of phosphate buffer and sonicated as described above. The remaining 4.3 ml of the solution were diluted to 8.6 ml (30.6 mM), centrifuged in a clinical centrifuge for 30 minutes and filtered through a Gelman Acrodisc filter with a pore diameter of 0.45 µm.

To 700 µl of the above solution, 3.067 mg (5.35×10^{-4} mmol) of zinc-free insulin were added. The

suspension was gently shaken and let stand overnight at room temperature.

Insoluble insulin was then removed by passing the suspension through a Gelman Acrodisc filter with a pore diameter of 0.45 μm. The filter was then placed in 20 ml of 10 mM HCl for 24 hours in order to extract insulin.

The sample containing egg PC vesicles was dialyzed for 24 hours against 2 x 500 ml of phosphate buffer in order to remove free insulin. Dialysis tubing with a molecular weight cutoff of 12,000 - 14,000 was used.

The protein content of the vesicle sample to which insulin had been added, of a vesicle sample without peptide, of the filter extract, and of the dialysis solution, respectively, was measured using Lowry's method of protein determination (Peterson, 1979).

Solution A: Na-tartrate (1.0 ml of a 2 % solution) was mixed well with 100 ml of 2 % Na_2CO_3 in 0.1 M NaOH and then with 1.0 ml of 1 % $CuSO_4$.

Folin-Ciocalteau phenol reagent (5 ml) was diluted with an equal volume of distilled water.

A standard crystalline egg albumen solution (5 ml) at 500 μg/ml was prepared.

A blank sample without protein, a range of standard egg albumen solutions and samples to be investigated were prepared all in duplicate (Table 3.3 and Table 3.4).

Table 3.2: Standard Protein Assay.

Solution [ml]	Blank	1	2	3	4	5
Protein 500 µg/ml	0.0	0.1	0.2	0.3	0.4	0.5
Distilled H_2O	1.0	0.9	0.8	0.7	0.6	0.5
Solution A	2.5	2.5	2.5	2.5	2.5	2.5
µg Protein/tube	0	50	100	150	200	250

Table 3.3: Determination of Insulin Concentrations.

Solution [ml]	1	2	3
Dialysis Solution	0.3	0.4	0.5
Distilled H_2O	0.7	0.6	0.5
Solution A	2.5	2.5	2.5
Filter Extract	0.3	0.4	0.5
Distilled H_2O	0.7	0.6	0.5
Solution A	2.5	2.5	2.5
Vesicles + Insulin	0.1	0.2	
Distilled H_2O	0.9	0.8	
Solution A	2.5	2.5	
Vesicles alone	0.1	0.2	
Distilled H_2O	0.9	0.8	
Solution A	2.5	2.5	

Each tube was mixed well immediately after the addition of solution A and let stand at room temperature for 10 minutes. Then 0.25 ml of Folin reagent were added, the tube contents mixed well immediately after each addition and let stand at room temperature for 30 minutes.

The optical density of the solutions was read at 500 nm on a Coleman Jr. spectrophotometer.

4. RESULTS AND DISCUSSION

4.1. THE SOLUTION PROPERTIES OF INSULIN

Insulin in millimolar concentrations is insoluble in aqueous solutions from pH 3.8 to pH 7.5. At a pH > 7.5, the peptide aggregates to its hexamer form when zinc is present. At a pH < 3.8, and without zinc present, the prevalent form of the peptide is its dimer (Cheshnovsky et al., 1983; Pocker & Biswas, 1981). The association constant of the monomer is in the range of 1.25×10^4 M^{-1} to 7.50×10^5 M^{-1}, depending on the pH of the solvent (Jeffrey & Coates, 1965, 1966; Goldman & Carpenter, 1974; Pekar & Frank, 1972; Lord et al., 1973; Pocker & Biswas, 1981)

4.2. SDS-PAGE

For peptides with a molecular weight < 10,000 Da, high levels of acrylamide/bisacrylamide must be used in SDS gels (Swank & Munkres, 1971). Gels with a content of acrylamide/bisacrylamide ≥ 12.5 % $^{V}/_{W}$ and with a ratio of 10:1 $^{W}/_{W}$ of acrylamide:bisacrylamide became opaque. Gels > 15 % became intractable due to brittleness and difficulties in staining and destaining.

These problems were circumvented in our experiments with gels containing 12.5 % $^{V}/_{W}$ of acrylamide/bisacrylamide and 8 M urea.

Figure 4.1 shows a 12.5 % SDS-Gel containing 8 M urea of human and porcine insulin. Lanes one to five contain human insulin at concentrations of 10 µg, 20 µg, 1 µg, 1.5 µg, and 2 µg, lanes six to eight porcine insulin at concentrations of 10 µg, 15 µg, and 20 µg, respectively. The separation in two bands is not clearly visible because the difference in molecular weight between A- and B-chain is only about 1,000.

Figure 4.1: SDS-Gel (12.5 %) of human and porcine insulin containing 8 M urea.

Lane 1	10.0 µg	Human Insulin
Lane 2	20.0 µg	Human Insulin
Lane 3	1.0 µg	Human Insulin
Lane 4	1.5 µg	Human Insulin
Lane 5	2.0 µg	Human Insulin
Lane 6	10.0 µg	Porcine Insulin
Lane 7	15.0 µg	Porcine Insulin
Lane 8	20.0 µg	Porcine Insulin

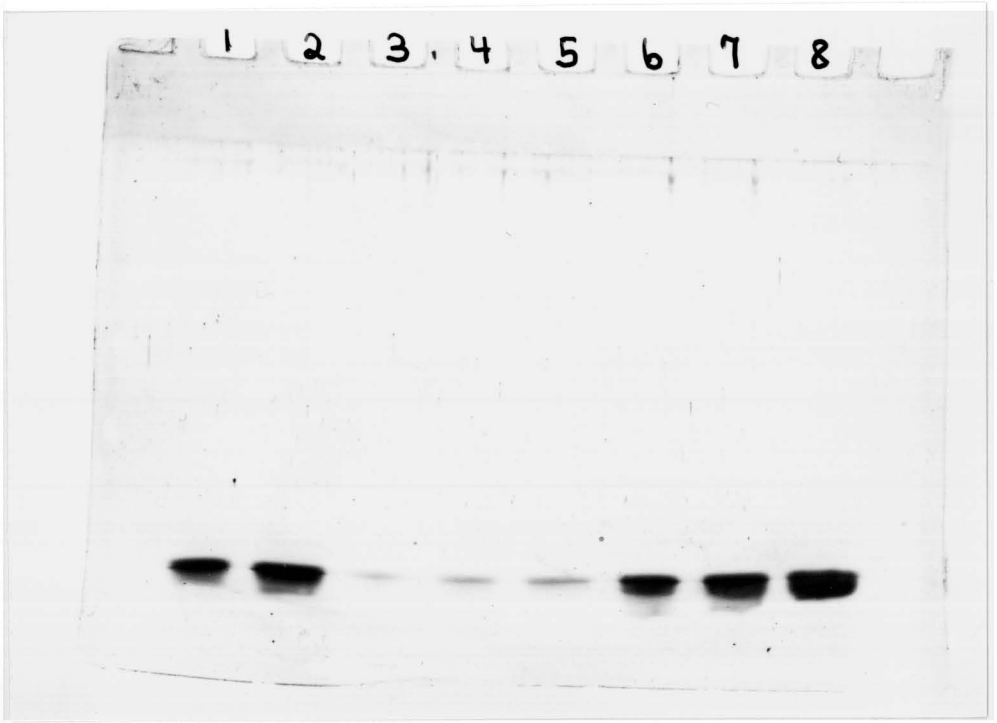

4.3. FTIR STUDY OF INSULIN IN SOLUTION

Porcine insulin (5.73 mM) in D_2O at pH 3.0 was run on a Bruker IFS 85 spectrometer equipped with an Aspect 2000 computer.

Figure 4.2 shows the absorbance spectrum of 5.73 mM porcine insulin in D_2O after subtraction of a D_2O spectrum (light) and the spectrum after subtraction of water vapor (dark).

Figure 4.2: FTIR absorbance spectrum of 5.73 mM porcine insulin in D_2O (dark) and absorbance spectrum after second derivative subtraction of water vapor (light).

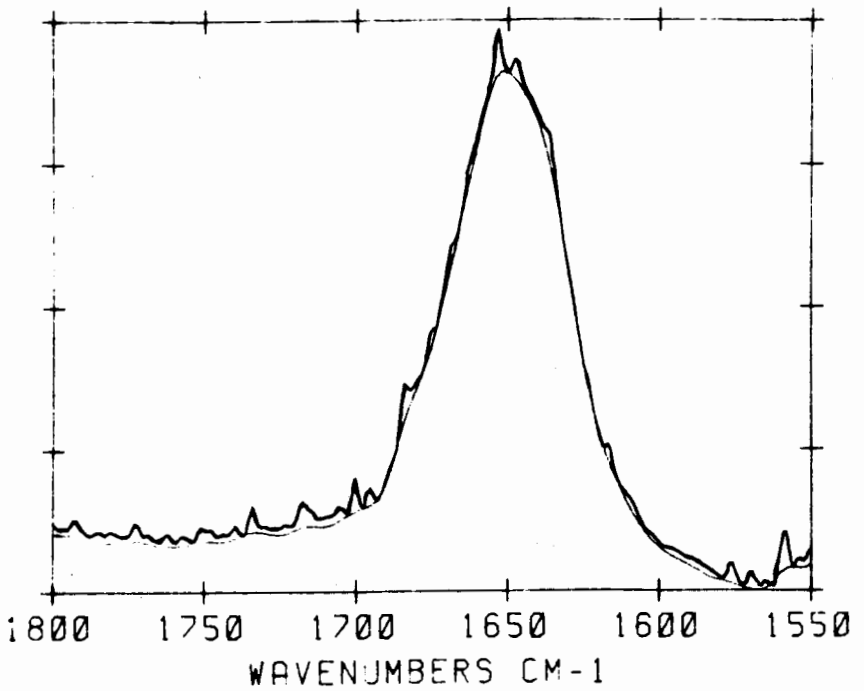

After Fourier-deconvolution, assuming Lorentzian bandshape with a linewidth at half-height of 16 cm^{-1} and a narrowing factor of 1.3, five shoulders were identified between 1600 cm^{-1} and 1700 cm^{-1}. Figure 4.3 shows the spectrum after water vapor subtraction (dark) and the deconvoluted spectrum (light).

Figure 4.3: FTIR absorbance spectrum of 5.73 mM porcine insulin in D_2O after water vapor subtraction (dark) and spectrum after Fourier-deconvolution using a linewidth at half-height of 16 cm^{-1} and a narrowing factor of 1.3.

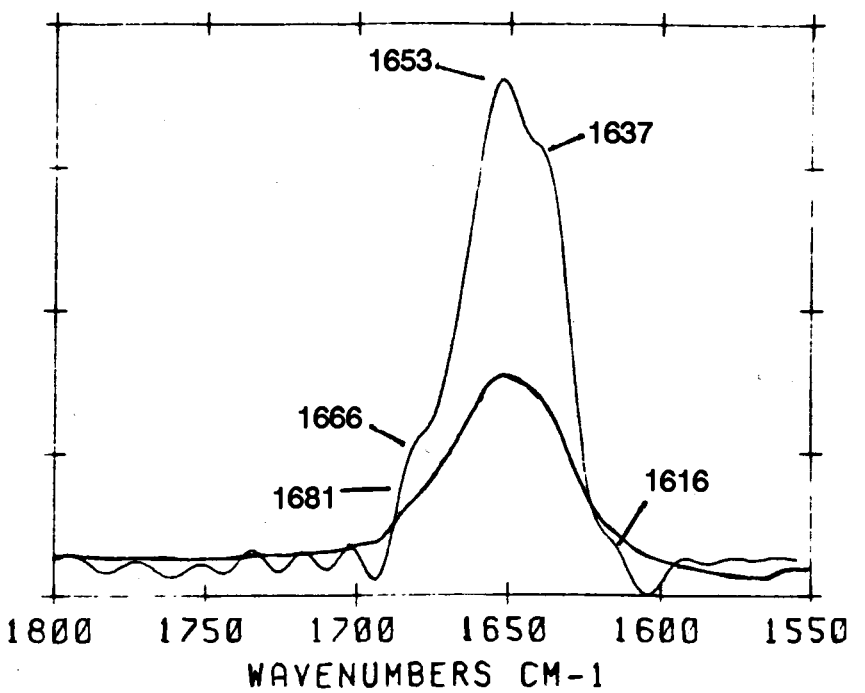

The absorbance spectrum that was obtained after water vapor subtraction was subjected to band-fitting using the program SIMBAND from Bruker until the root-mean-square value was 0.00098. Figure 4.4 shows the absorbance spectrum after water vapor subtraction (dark) and the fitted bands (light).

Figure 4.4: FTIR absorbance spectrum of 5.73 mM porcine insulin in D_2O after water vapor subtraction (dark) and the fitted bands (light).

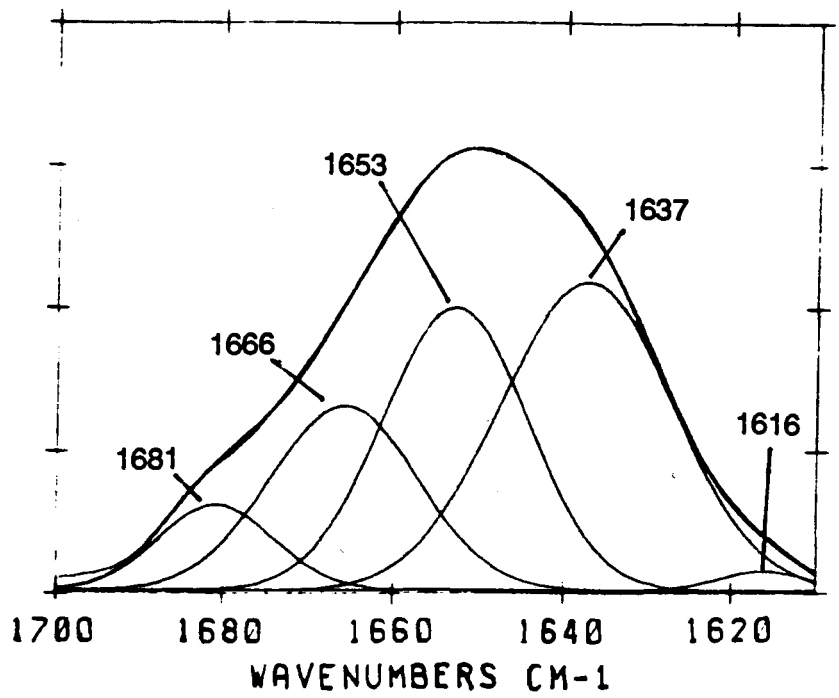

The fitted bands with their position, intensity, linewidth at half-height, % Gaussian lineshape, and area are listed in Table 4.1.

Table 4.1: Positions of the Fitted Bands of 5.73 mM Porcine Insulin in D_2O With Their Intensities, Linewidth at Half-Height, % Gaussian Lineshape, and Area.

Position [cm^{-1}]	Intensity	Linewidth at HH [cm^{-1}]	% Gaussian	Area
1681	0.0224	8.0	100	0.3810
1666	0.0487	10.2	100	1.0540
1653	0.0748	10.0	100	1.5920
1637	0.0817	12.0	100	2.0810
1616	0.0052	6.0	80	0.0634
Total Area				5.1714

According to Table 2.1 (page 36) the bands were assigned to secondary structure elements of the peptide (Susi et al., 1967; Surewicz et al., 1987a; Susi, 1969; Parker, 1983; Susi & Byler, 1986; Koenig & Tabb, 1980; Krimm & Bandekar, 1986; Byler & Susi, 1986; Holloway & Mantsch, 1989; Haris & Chapman, 1988). The results are shown in Table 4.2.

Table 4.2: Assignments of FTIR Bands to Secondary Structure Elements of 5.73 mM Porcine Insulin in D_2O at pH 3.0.					
	Wave-No. [cm^{-1}]	Peak Area	Total Area	%	Res.
β-Strands/Extended	1616	0.0634			
	1637	2.0810	2.1444	41.4	21
α-Helix	1653	1.5920	1.5920	30.8	16
3_{10}-Helix/Turns	1666	1.0540	1.0540	20.4	10
Turns	1681	0.3810	0.3810	7.4	4
Total			5.1714	100.0	51

(Res. = number of amino acid residues.)

According to X-ray crystallographic data (Adams et al., 1969), the A-chain of insulin shows a near helical conformation from Ile A2 to Cys A6 and from Leu A13 to Tyr A19, and a sharp turn induced by a disulfide bond between Cys A6 and Cys A11.

The B-chain forms three turns of an α-helix, slightly opened at its ends, from Cys B7 to Cys B19. The residues Phe B1 to Leu B6 and Glu B21 to Ala B30 are largely extended and packed around the A-chain.

In the insulin dimer, residues Gly B23 to Pro B28 of the monomers form an antiparallel β-sheet.

According to more precise X-ray crystallographic data on insulin dimers in Zn-hexamers (Dodson et al., 1979), the A-chain forms an N-terminal helix from Gly A1 to Cys A6. The intrachain disulfide bridge between Cys A6 and Cys A11

induces a sharp turn involving Cys A7, Thr A8, and Ser A9 followed by an extended segment from A10-A12. Residues A13-A20 form a distorted helix that is close to a 3_{10}-helix.

The B-chain of insulin is extended from B1-B8 and B24-B30, respectively, with an α-helical part from B9-B19. Residues B20-B23 form a sharp turn. An antiparallel β-sheet between B23-B30 links the two monomers of the insulin dimer. The secondary structure of insulin according to Dodson et al. (1979) is listed in Table 4.3.

Table 4.3: Secondary Structure of Insulin According to X-Ray Crystallographic Data (Dodson et al., 1979)

	Segment	Residues	Total Residues
β-Strands/Extended	A10-A12	3	
	A20-A21	2	
	B1-B8	8	
	B24-B30	7	20
α-Helix	A1-A6	6	
	B9-B19	11	17
3_{10}-Helix	A13-A19	7	7
Turns	A7-A9	3	
	B20-B23	4	7

A comparison of the FTIR results with X-ray crystallographic data is summarized in Table 4.4.

Table 4.4: Comparison of FTIR Results With X-Ray Crystallographic Data of the Secondary Structure of Insulin

	FTIR [Residues]	X-Ray Crystallography [Residues]
β-Strands/Extended	21	20
α-Helix	16	17
3_{10}-Helix	10	7
Turns	4	7

The comparison between FTIR- and X-ray diffraction data shows that the number of residues in extended segments and those in α-helical conformation are in good agreement. The difference observed in the 3_{10}-helical part of the peptide and in the number of amino acids involved in turns can be explained by the fact that a 3_{10}-helical turn is identical to a type III turn (Birktoft & Blow, 1972). Both are assigned to 1666 cm^{-1} (Krimm & Bandekar, 1969; Haris & Chapman, 1988a). The 3_{10}-helix is also assigned to 1639 cm^{-1} (Haris & Chapman, 1988a; Holloway & Mantsch, 1989), but at that wavenumber no absorbance was observed.

More FTIR experiments should be performed on both the insulin dimer and monomer, respectively. Self-association of insulin can be removed or reduced by the addition of small amounts of organic solvent (Fredericq, 1957; Weiss et al., 1989), expecially deuterated acetonitrile up to 35 % $^{v}/_{v}$ (Kline & Justice, 1990).

4.4. 2-D ^1H NMR OF HUMAN INSULIN IN D_2O

4.4.1. COSY AND RELAYED COSY EXPERIMENTS

With the application of 2-D NMR methods on insulin, serious problems had to be expected. Other researchers had already unsuccessfully applied these methods on insulin in aqueous solution (Kline & Justice, 1990; Wüthrich K., private communication). Kline & Justice finally published the complete sequence-specific ^1H NMR assignments for human insulin in aqueous solution containing 35 % $^V/_V$ acetonitrile (Kline & Justice, 1990).

Our 2-D ^1H NMR experiments confirmed that no definitive assignments and no elucidation of structural elements of the peptide were feasible with insulin in D_2O or H_2O/D_2O, 9:1.

The major problem arose from the solution properties of the peptide. Complete sequential assignments can only be obtained with a set of experiments being run at different pH and at different temperatures (Wüthrich K., 1986; Klevit R.E., private communication). Varying these parameters causes chemical shifts of some of the resonances. Insulin can only be investigated in a very small pH range, due to its insolubility at pH 3.8 to pH 7.5. At a pH > 7.5, the amide protons of a peptide in aqueous solution would

exchange too fast with water protons and would not be observable (Wagner G., 1983). Therefore, experiments with insulin are restricted to a pH < 3.8.

A second problem arose with the size of the peptide and limitations of the NMR spectrometer. 2-D ^{1}H NMR requires peptide concentrations greater than 2 mM (Wüthrich, 1986). At such concentrations, insulin is self-associating to dimers (Jeffrey & Coates, 1966; Paselk & Levy, 1974). The dimer has a molecular weight of 11,466 Da. Peptides with a molecular weight 10,000 Da may be investigated on a 500 MHz spectrometer by using 2-D ^{1}H NMR techniques. On a 400 MHz spectrometer, the resolution is too low. Resonances are superimposed and cannot be distinguished, or they may cancel each other in phase-sensitive spectra due to their antiphase character.

One might argue that no difference may be seen in a 2-D ^{1}H NMR spectrum between a dimer and a monomer. That is not true for the following reasons:

Firstly, X-ray crystallographic data on insulin indicate that the two molecules that are involved in dimer formation may not have exactly the same conformation (Dodson et al., 1979). Secondly, the rotational correlation time τ_c increases roughly by 1 ns for each 2,400 Da of protein molecular weight (Cantor & Schimmel, 1980). As can

be seen in Figure 4.5, an increasing rotational correlation time decreases the transverse relaxation time T_2.

Figure 4.5: The dependence of T_1, T_2 and $T_{1\rho}$ on the correlation time τ_c and the spectrometer operating frequency υ_0 for relaxation by isotropic random magnetic fields, plotted in a log/log scale. The extreme narrowing scheme is to the left. The solid lines are calculated for $\upsilon_0 \approx 100$ MHz and the dashed lines show the deviations for $\upsilon_0 \approx 400$ MHz. The curves for $T_{1\rho}$ are calculated for $\upsilon_1 = \gamma B_1/2\pi \approx 40$ kHz (adapted from Harris, 1983).

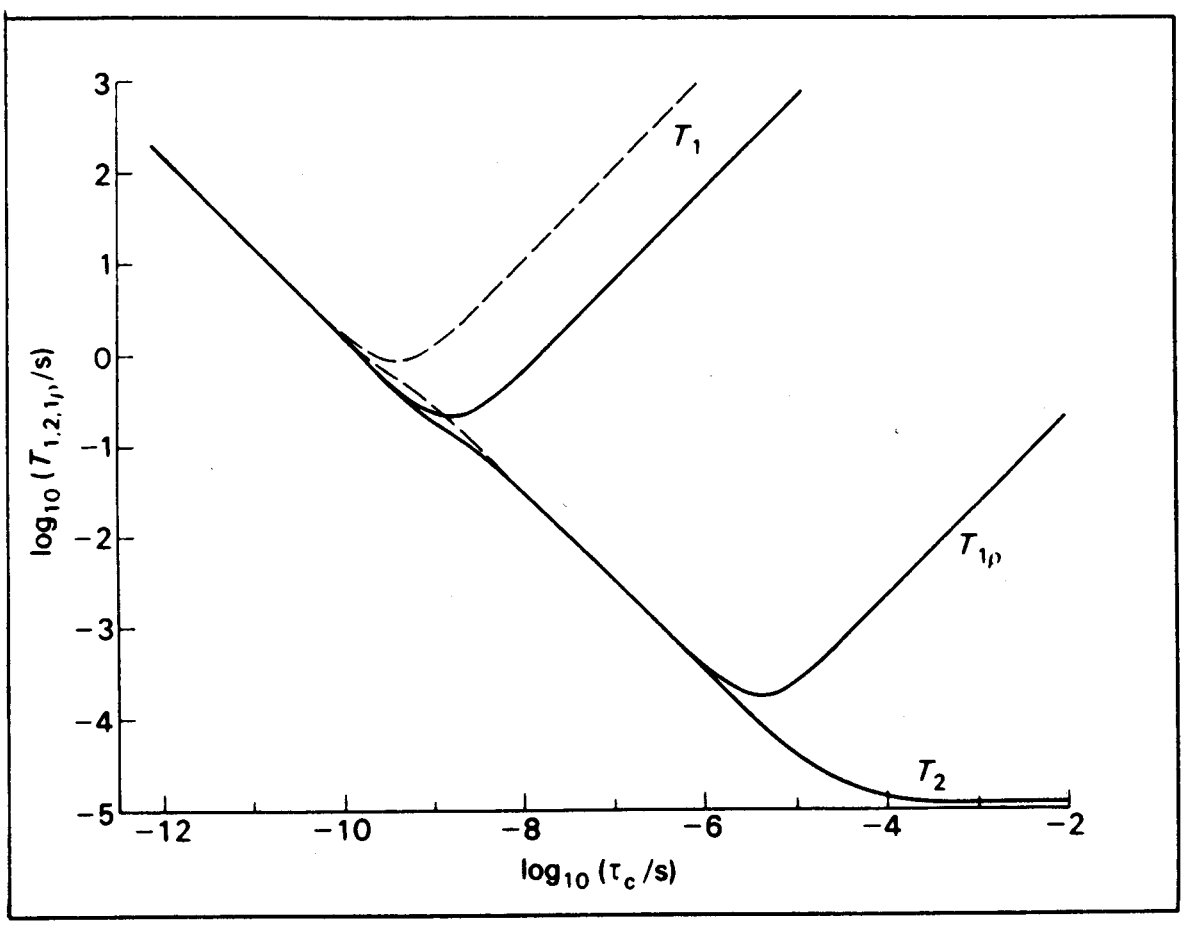

A decreasing transverse relaxation time T_2 on the other hand causes line-broadening (Harris, 1983) and thus a decrease in resolution. Resolution enhancement methods like multiplication of the free induction decay (FID) by a Gaussian-, a sine-bell- or a squared sine-bell function respectively have their limits, since they may introduce artifacts like side lobes into spectra (Wüthrich, 1986).

NOESY spectra of a peptide in water have to be recorded in order to connect exchangeable amide protons of the peptide backbone with the CαH-protons of the next amino acid in the sequence. This requires suppression of the water resonance in order to eliminate the dynamic range problem (Redfield et al., 1975). Furthermore, most of the CαH-protons of a peptide have a chemical shift similar to that of the water resonance. Since a big water peak causes t_1- and t_2-ridges in a 2-D NMR spectrum, no cross-peaks close to this resonance would be observed.

Usually the water resonance is suppressed by preirradiation, either continuously or between two experiments (Wider et al., 1983). Preirradiation between two experiments only, soft pulses (Redfield & Gupta, 1971) or a DANTE pulse (Haasnoot, 1983), respectively, were not efficient in preliminary experiments. Continuous preirradiation had to be applied with strong decoupler

power. This technique led to t_1- and t_2-ridges and also saturated most of the CαH-protons of insulin in preliminary experiments.

Further limitations of the WM-400 spectrometer were caused by the fact that fine tuning was not achievable with insulin in water, thus causing base-line distortions. In addition, inaccuracies in phase-shifts of the analog phase-shifter of the spectrometer may have caused inefficiency in magnetization transfer.

For these reasons, 2-D ^1H NMR experiments with insulin in H_2O/D_2O, 9:1, were not feasible. Spectra of the peptide in D_2O had to be limited to absolute value spectra, where the resolution is very low.

Figure 4.6 shows our absolute value COSY spectrum of human insulin in D_2O. The double-quantum-filtered (DQF) COSY spectrum of human insulin in D_2O/d_3-acetonitrile recorded by Kline & Justice on a 500 MHz NMR spectrometer (Kline & Justice, 1990) is shown in Figure 4.7.

Figure 4.6: Aliphatic region of the absolute value COSY spectrum at 400 MHz of 2 mM human insulin at 37°C dissolved in D_2O/d_3-acetic acid (pD = 3.4)

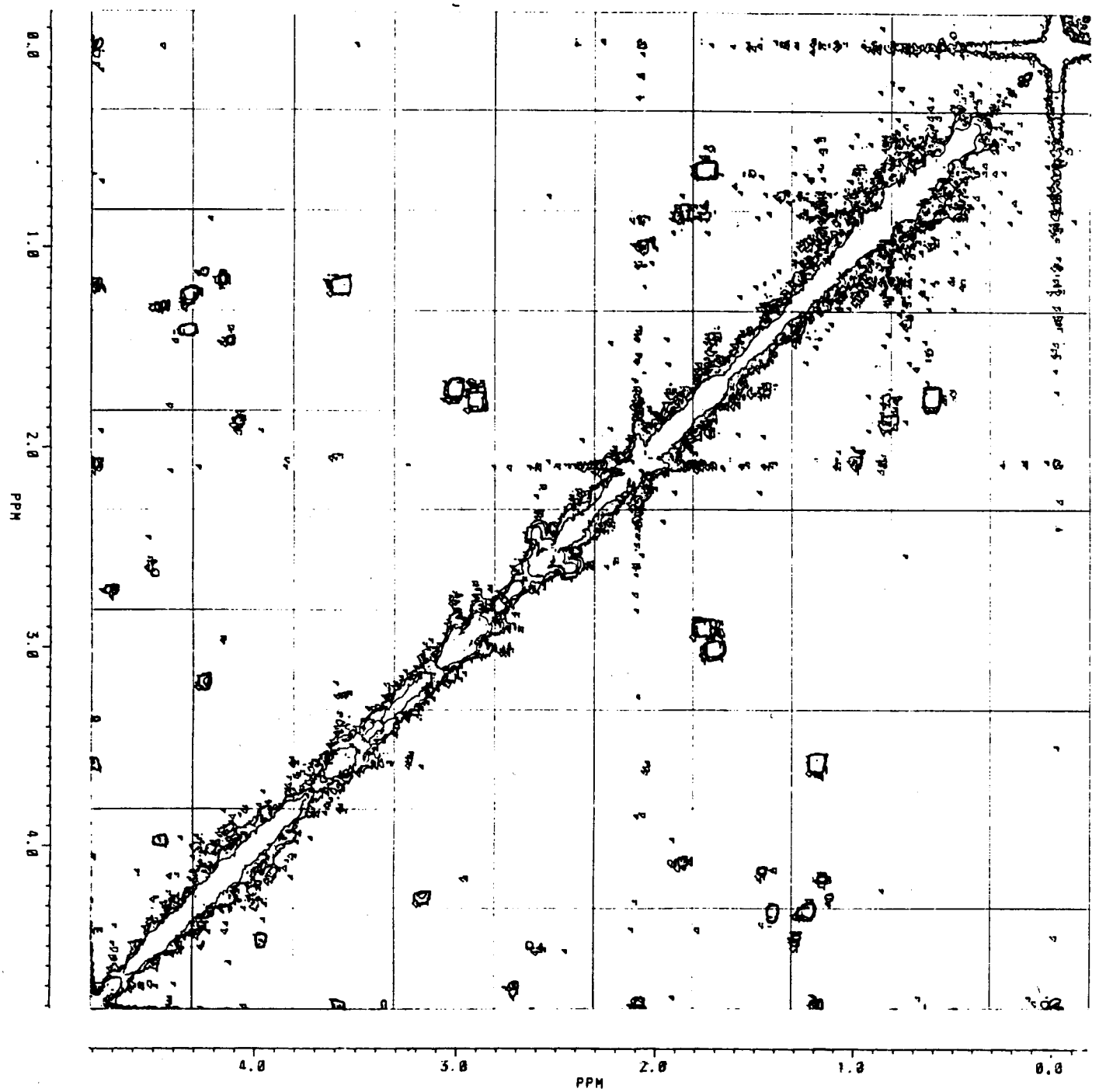

Figure 4.7: Aliphatic region of the DQF-COSY spectrum at 500 MHz of human insulin at 27°C dissolved in completely deuterated solvents. The spectrum was plotted for both ω_1 (vertical axis) and ω_2 (horizontal axis) from 5.08 to 0.34 ppm. Both positive and negative contours are shown (adapted from Kline & Justice, 1990).

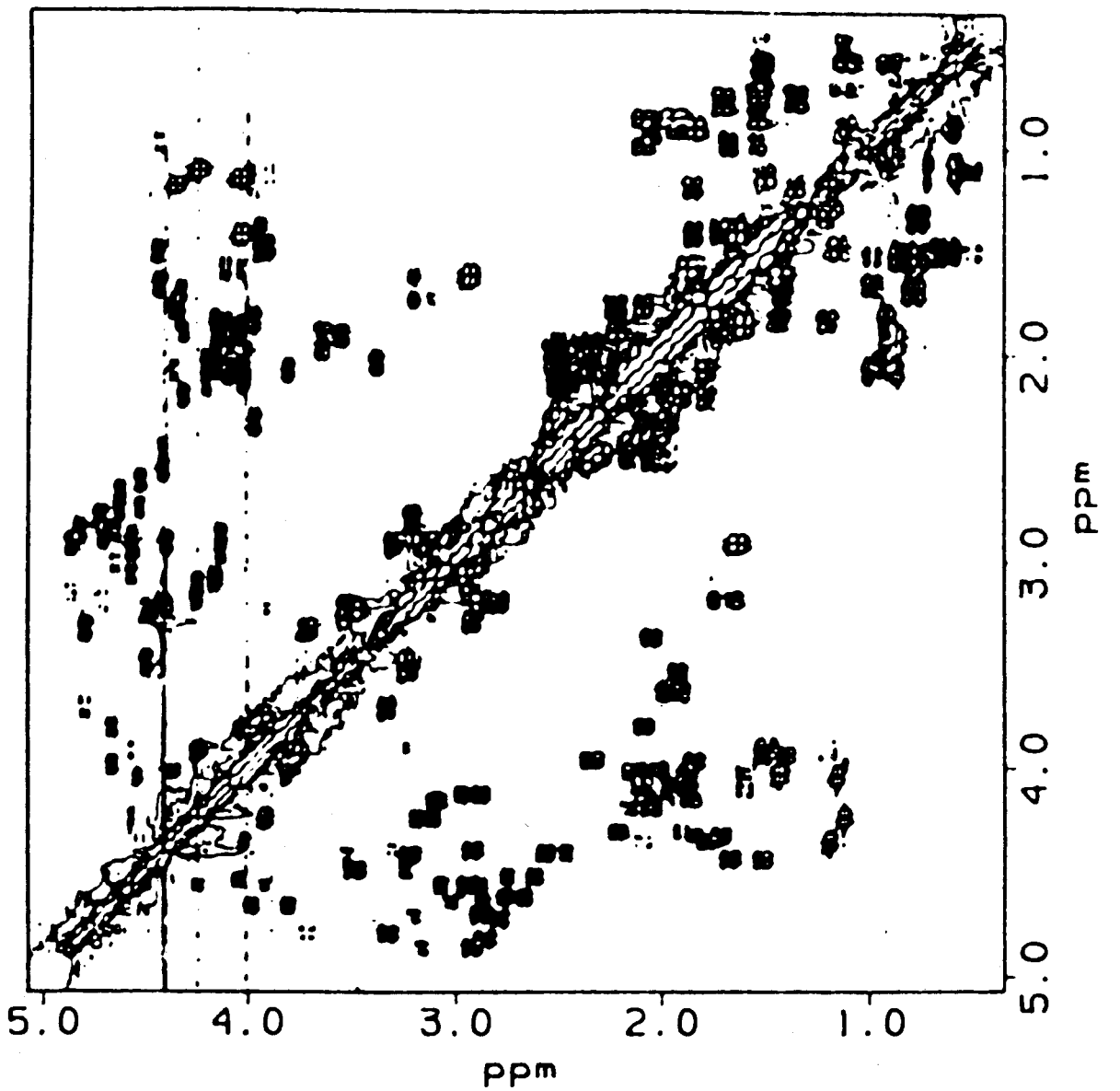

Although the lowest contour level was set near the noise level in our spectrum, cross-peaks close to the diagonal were not observed, especially those belonging to resonances in the range from 1.6 to 2.8 ppm. The chemical shift dispersion of cross-peaks belonging to the side-chain proton resonances of the two isoleucines, the six leucines and the four valines, respectively, was not observed either. Most of the cross-peaks connecting CαH-proton to CβH-proton resonances were not visible in our spectra, due to low sensitivity and the fact that most of the CαH-protons have a chemical shift close to the resonance of the water protons.

Only very few typical spin systems could be recognized in our spectra. Tentative assignments are listed in Table 4.5.

Table 4.5: Tentative Assignments of Cross-Peaks in the COSY Spectrum of Human Insulin in D_2O, Recorded on a WM-400 Bruker Spectrometer.	
Cross-Peaks [ppm]	Tentative Assignment
4.50/3.98	Serines
4.80/3.63	Cysteines
4.84/3.60, 3.60/1.19	Threonines
4.79/3.38	Phenylalanines
4.28/3.19	Tyrosines
4.19/4.53/1.16-1.44	Arginine and Lysine,
4.72/2.73	Asparagines and
4.53/2.64	Aspartic Acid
4.53/2.59	or
4.79/2.12	Glutamines and
4.85/2.11	Glutamic acids

The leucine and isoleucine spin systems were not complete and cross-peaks were superimposed.

The complete sequence-specific assignments published by Kline & Justice are shown in Table 4.6.

Table 4.6: ^1H Chemical Shifts (±0.01 ppm) for Human Insulin at pH = 3.6, 27°C, Dissolved in 65 %/35 % Water/Acetonitrile (adapted from Kline & Justice, 1990).

^1H Chemical Shifts (±0.01) in ppm for Human Insulin at pH = 3.6, 27 °C, Dissolved in 65%/35% Water/Acetonitrile											
residue	NH	$C^{\alpha}H$	$C^{\beta}H$	others		residue	NH	$C^{\alpha}H$	$C^{\beta}H$	others	
Gly A1	n.o.[c]	3.99,[a] 3.92[a]								$C^{\beta}H_3$	0.83, 0.72
Ile A2	8.43	3.78	1.12	$C^{\gamma}H$	1.09, 0.90	Cys B7	8.14	4.86	3.16, 2.91		
				$C^{\gamma}H_3$	0.71	Gly B8	8.82	3.93, 3.74			
				$C^{\delta}H_3$	0.57	Ser B9	8.80	4.04	3.80,[a] 3.80[a]		
Val A3	8.16	3.53	1.91	$C^{\gamma}H_3$	0.92, 0.85	His B10	7.86	4.49	3.49, 3.23	$C^{\delta}H$	7.40
Glu A4	8.29	4.09	2.08, 1.95	$C^{\gamma}H$	2.49, 2.27					$C^{\varepsilon}H$	8.59
Gln A5	8.15	4.01	2.04,[a] 2.00[a]	$C^{\gamma}H$	2.44,[b] 2.33[b]	Leu B11	7.08	3.97	1.84, 1.20	$C^{\gamma}H$	1.35
				$N^{\varepsilon}H$	7.44, 6.73					$C^{\delta}H_3$	0.78, 0.73
Cys A6	8.17	4.82	3.19, 2.86			Val B12	7.23	3.37	2.04	$C^{\gamma}H_3$	0.95, 0.91
Cys A7	8.24	4.79	3.71, 3.32			Glu B13	7.91	4.02	2.13, 2.04	$C^{\gamma}H$	2.48,[a] 2.44[a]
Thr A8	8.10	4.02	4.36	$C^{\gamma}H_3$	1.19	Ala B14	7.72	4.03	1.43		
Ser A9	7.17	4.66	3.98, 3.80			Leu B15	8.04	3.90	1.48, 1.14	$C^{\gamma}H$	1.51
Ile A10	7.70	4.45	1.51	$C^{\gamma}H$	1.12, 0.50					$C^{\delta}H_3$	0.68, 0.57
				$C^{\gamma}H_3$	0.64	Tyr B16	8.15	4.16	3.09,[a] 3.09[a]	$C^{\delta}H_2$	7.08
				$C^{\delta}H_3$	0.57					$C^{\varepsilon}H_2$	6.72
Cys A11	9.39	5.07	3.32, 2.99			Leu B17	7.90	4.02	1.88, 1.60	$C^{\gamma}H$	1.83
Ser A12	8.53	4.57	4.23, 3.91							$C^{\delta}H_3$	0.92, 0.90
Leu A13	8.54	3.94	1.51, 1.40	$C^{\gamma}H$	1.53	Val B18	8.38	3.80	2.08	$C^{\gamma}H_3$	0.99, 0.86
				$C^{\delta}H_3$	0.86, 0.78	Cys B19	8.60	4.70	3.19, 2.87		
Tyr A14	7.38	4.14	2.97, 2.87	$C^{\delta}H_2$	7.05	Gly B20	7.79	3.85,[a] 3.85[a]			
				$C^{\varepsilon}H_2$	6.80	Glu B21	8.13	4.20	2.14, 2.05	$C^{\gamma}H$	2.48, 2.43
Gln A15	7.47	3.96	2.33, 1.96	$C^{\gamma}H$	2.42,[a] 2.33[b]	Arg B22	7.79	4.16	1.93, 1.85	$C^{\gamma}H$	1.71,[a] 1.66[a]
				$N^{\varepsilon}H$	7.37, 6.85					$C^{\delta}H$	3.19, 3.19[b]
Leu A16	7.94	4.11	1.86, 1.59	$C^{\gamma}H$	1.70					$N^{\varepsilon}H$	7.29
				$C^{\delta}H_3$	0.80, 0.75	Gly B23	7.74	3.87, 3.77			
Glu A17	7.96	4.13	2.06, 1.96	$C^{\gamma}H$	2.52, 2.33	Phe B24	7.60	4.64	3.02, 2.86	$C^{\delta}H_2$	6.98
Asn A18	7.38	4.41	2.56, 2.45	$N^{\delta}H$	7.09, 6.34					$C^{\varepsilon}H_2$	7.13
Tyr A19	7.84	4.40	3.29, 2.91	$C^{\delta}H_2$	7.28					$C^{\zeta}H$	7.13[b]
				$C^{\varepsilon}H_2$	6.71	Phe B25	7.99	4.56	3.07, 2.94	$C^{\delta}H_2$	7.19
Cys A20	7.35	4.72	3.20, 2.78							$C^{\varepsilon}H_2$	7.28
Asn A21	7.86	4.52	2.75, 2.61	$N^{\delta}H$	7.35, 6.50					$C^{\zeta}H$	7.22[a]
Phe B1	n.o.	4.24	3.19, 3.10	$C^{\delta}H_2$	7.24	Tyr B26	7.73	4.56	2.96,[a] 2.87[a]	$C^{\delta}H_2$	7.02
				$C^{\varepsilon}H_2$	7.37					$C^{\varepsilon}H_2$	6.73
				$C^{\zeta}H$	7.32[a]	Thr B27	7.61	4.54	4.04	$C^{\gamma}H_3$	1.15
Val B2	8.05	4.08	1.94	$C^{\gamma}H_3$	0.86,[a] 0.86[a]	Pro B28		4.31	2.20, 1.89	$C^{\gamma}H$	1.97, 1.90
Asn B3	8.21	4.62	2.76, 2.66	$N^{\delta}H$	7.42, 6.73					$C^{\delta}H$	3.63, 3.63[b]
Gln B4	8.15	4.36	2.08, 1.78	$C^{\gamma}H$	2.21, 2.21[b]	Lys B29	8.07	4.33	1.84, 1.72	$C^{\gamma}H$	1.42,[a] 1.41[a]
				$N^{\varepsilon}H$	7.29, 6.59					$C^{\delta}H$	1.63, 1.63[b]
His B5	8.35	4.42	3.53, 3.22	$C^{\delta}H$	7.36					$C^{\varepsilon}H$	2.92, 2.92[b]
				$C^{\varepsilon}H$	8.48					$N^{\zeta}H_3$	7.39
Leu B6	8.77	4.44	1.67, 0.98	$C^{\gamma}H$	1.53	Thr B30	7.63	4.20	4.24	$C^{\gamma}H_3$	1.12

[a] Uncertainty in the chemical shift value is ±0.03 ppm. [b] Assignment is not definitive; that is, it relied on NOE data or the lack of cross peaks to other shift values. [c] n.o. = not observed.

The relayed COSY spectrum of insulin in D_2O gave only very few cross-peaks (see Figure 4.8).

Figure 4.8: Aliphatic region of the absolute value relayed COSY spectrum at 400 MHz of 2 mM human insulin at 37°C dissolved in D_2O/d_3-acetic acid (pD = 3.4).

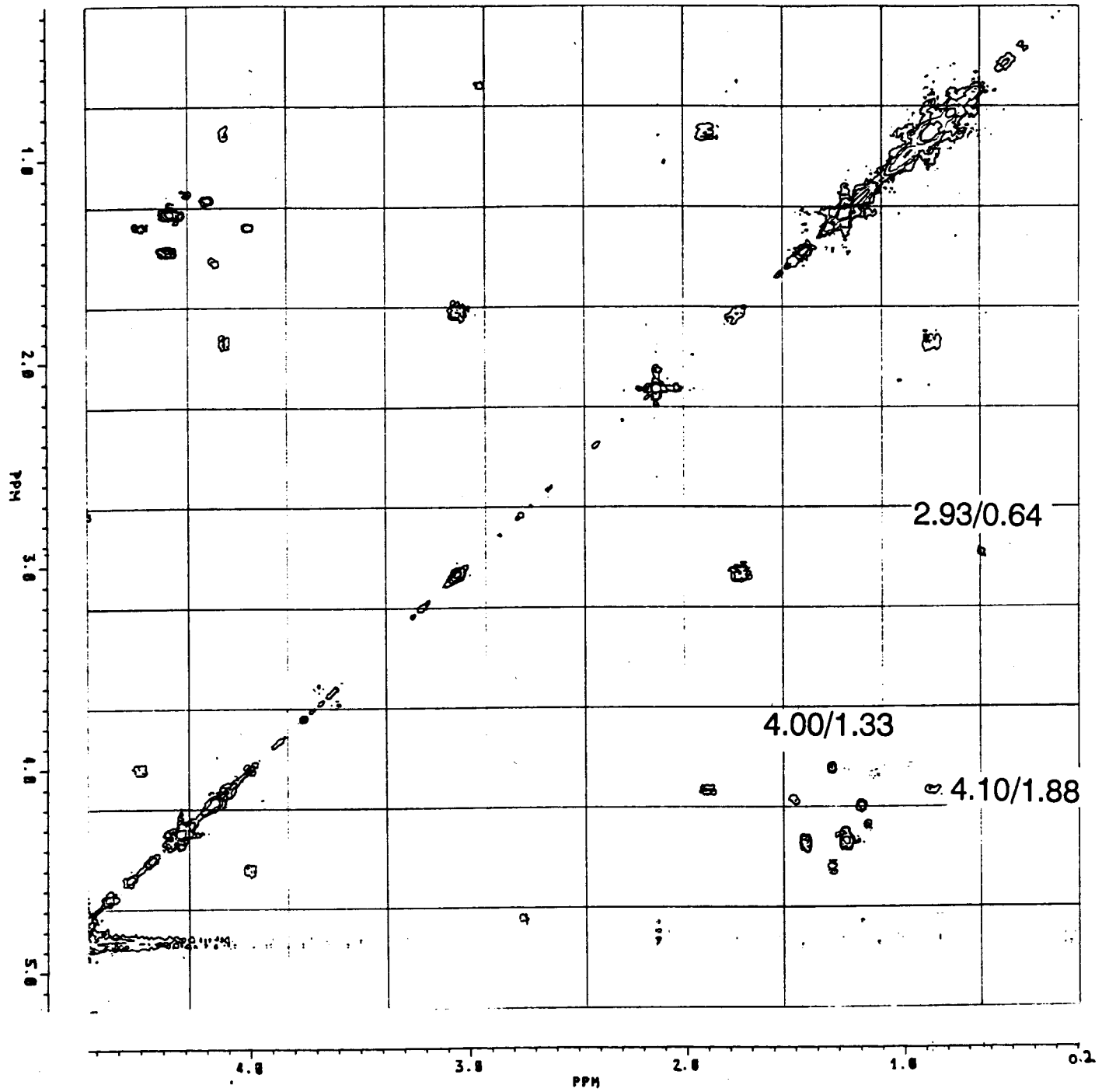

The cross-peaks at

2.93/0.64 ppm
4.00/1.33 ppm
4.10/1.88 ppm,

respectively, stem from relayed magnetization transfer from a spin 2 to a spin 3. The cross-peaks belonging to the magnetization transfer from the respective spin 1 to spin 2 were not observed or very weak in the relayed COSY spectrum. This fact may indicate, that the relay time τ_R chosen for the experiment was too long. A series of relayed COSY experiments with different relay times would have to be recorded in order to find the ideal τ_R. TOCSY (Total Coherence Transfer) or HOHAHA (Homonuclear Hartmann-Hahn) spectra would be an alternative (Braunschweiler & Ernst, 1983; Davis & Bax, 1985).

4.4.2. NOESY EXPERIMENTS

A series of NOESY spectra of human insulin in D_2O were recorded in order to find the ideal mixing time τ_M for the peptide. These spectra are shown in Figures 4.9 to 4.13.

Figure 4.9: Absolute value NOESY spectrum at 400 MHz of 2 mM human insulin at 37°C dissolved in D_2O/d_3-acetic acid (pD = 3.4) with a mixing time τ_M = 50 ms.

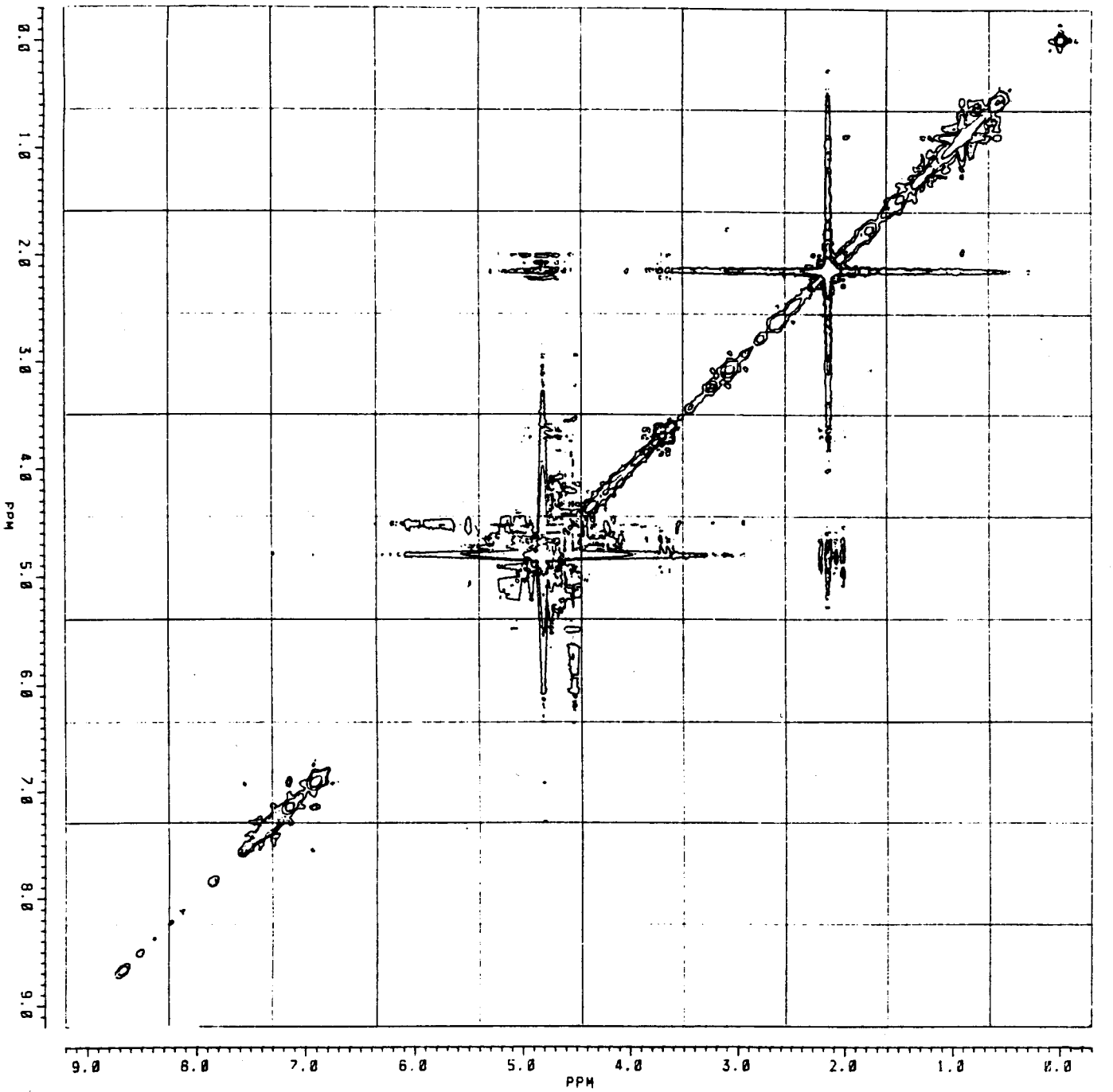

Figure 4.10: Absolute value NOESY spectrum at 400 MHz of 2 mM human insulin at 37°C dissolved in D_2O/d_3-acetic acid (pD = 3.4) with a mixing time τ_M = 100 ms.

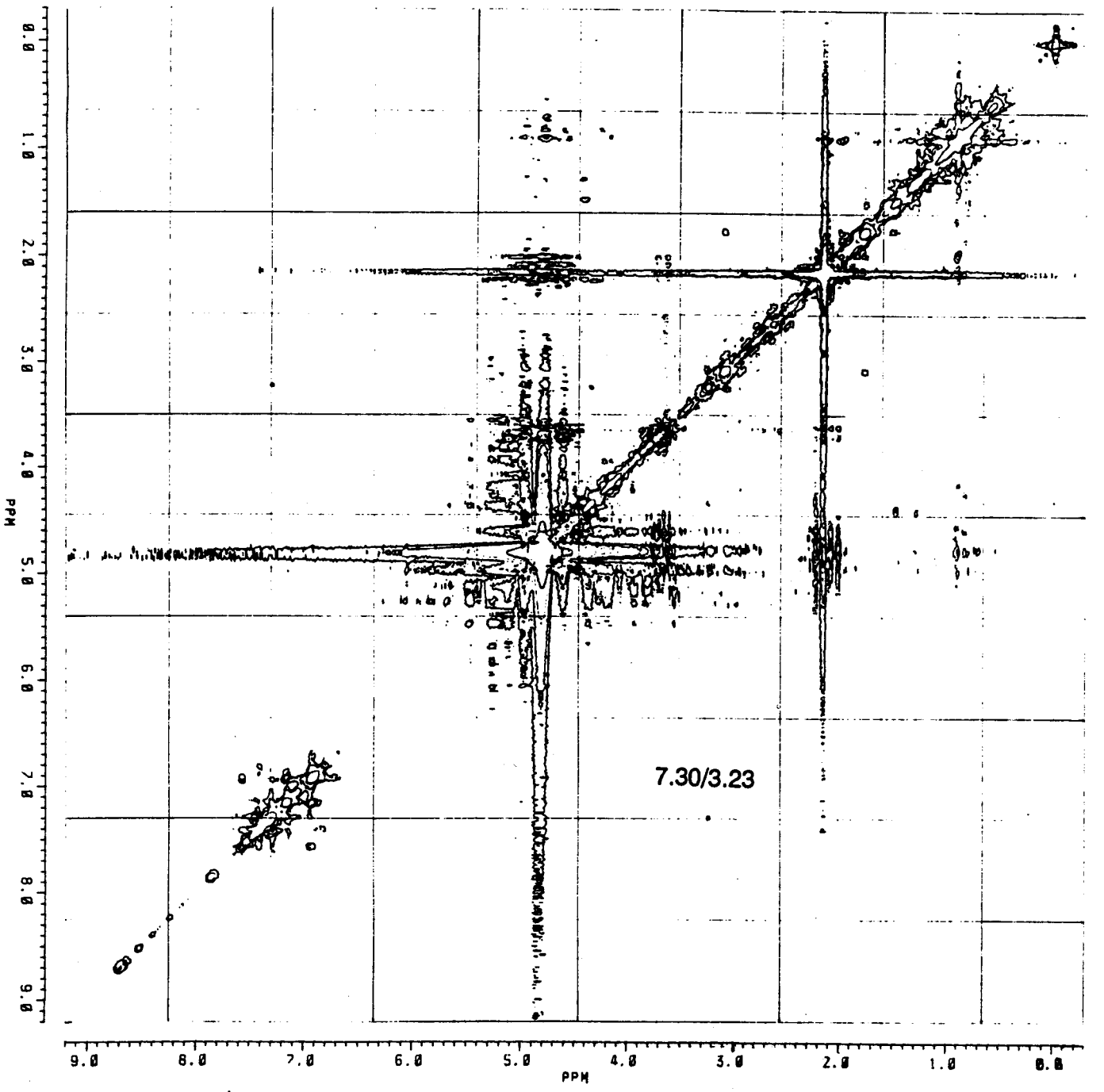

Figure 4.11: Absolute value NOESY spectrum at 400 MHz of 2 mM human insulin at 37°C dissolved in D_2O/d_3-acetic acid (pD = 3.4) with a mixing time τ_M = 150 ms.

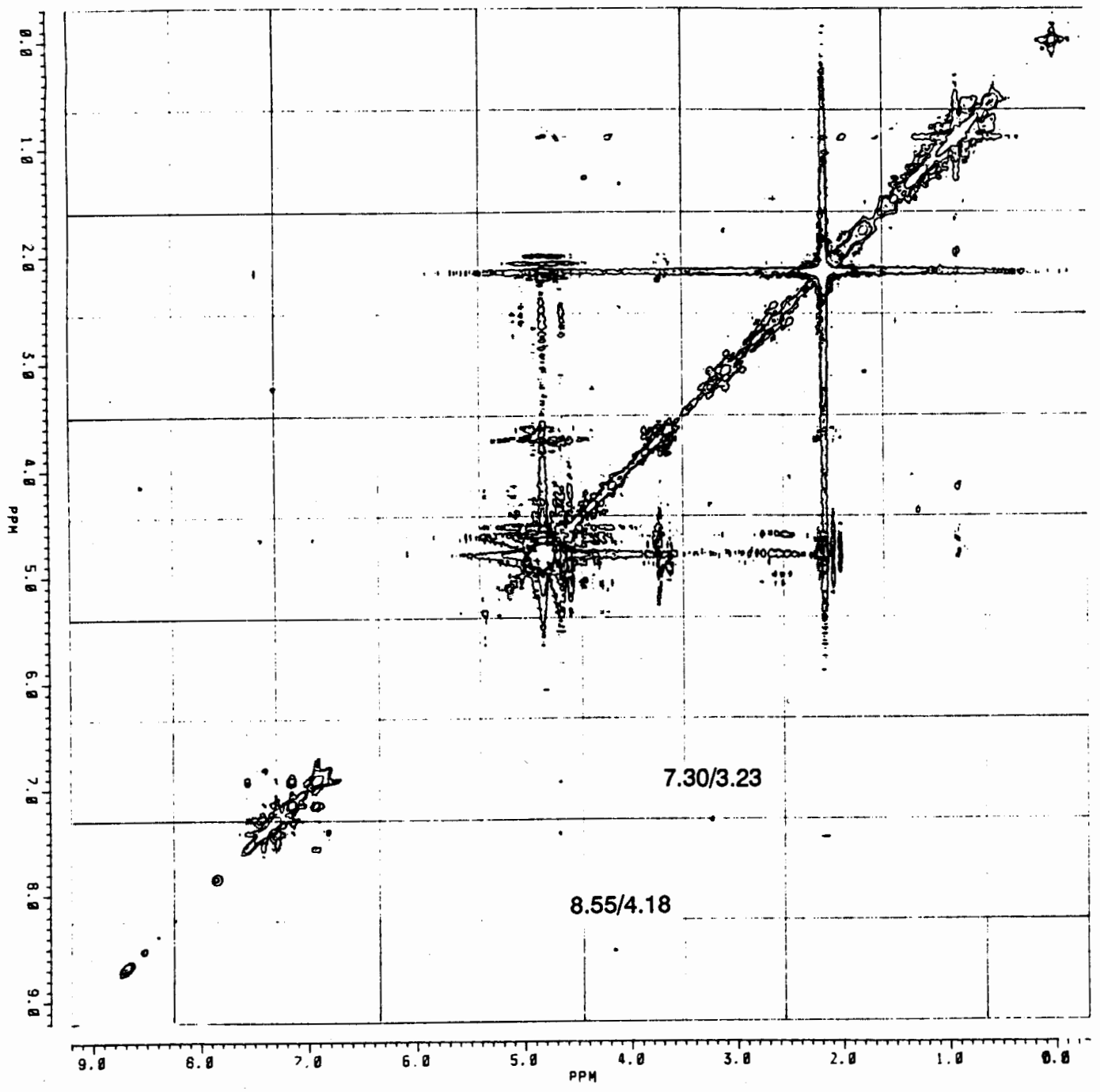

Figure 4.12: Absolute value NOESY spectrum at 400 MHz of 2 mM human insulin at 37°C dissolved in D_2O/d_3-acetic acid (pD = 3.4) with a mixing time τ_M = 200 ms.

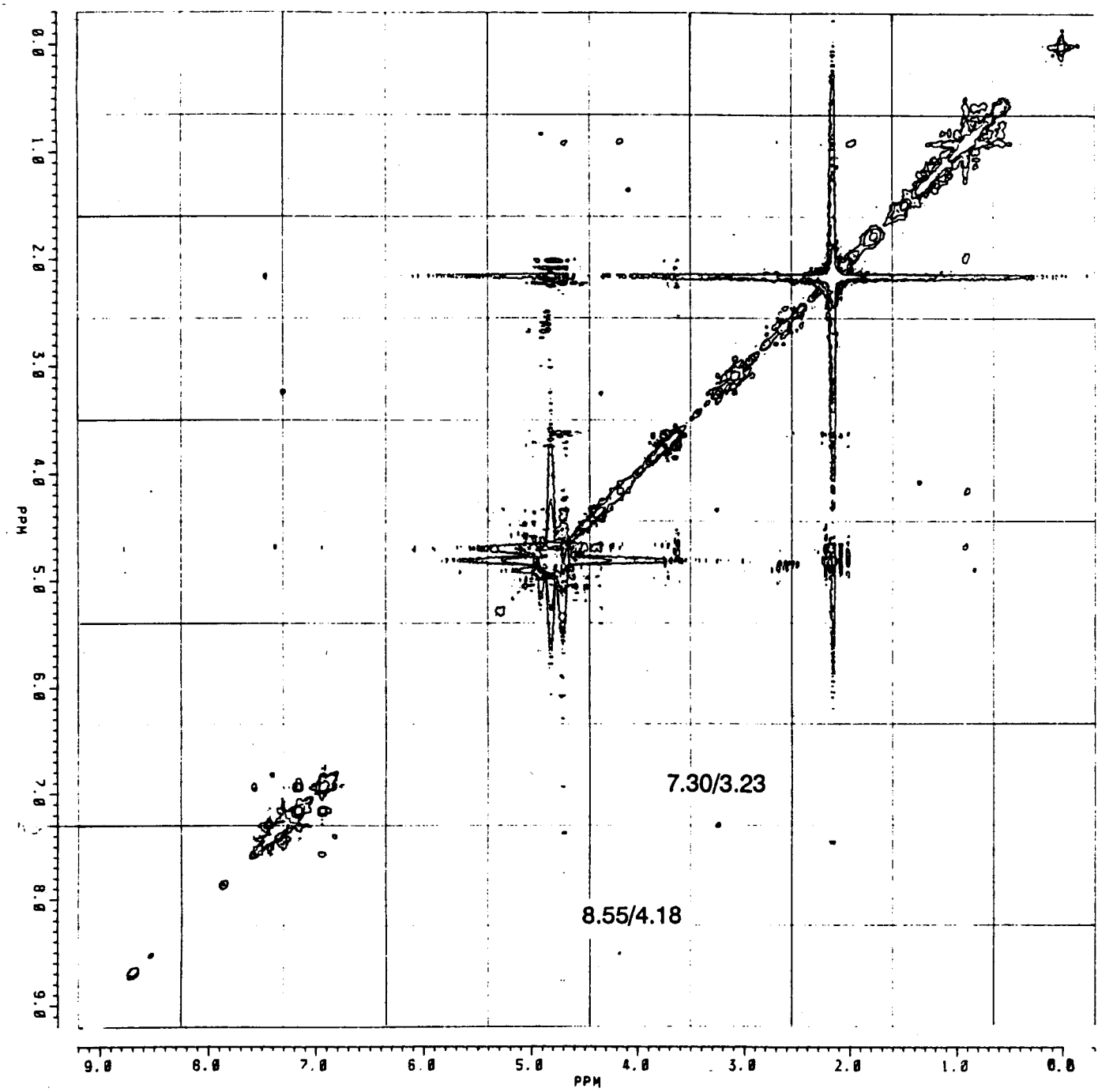

Figure 4.13: Absolute value NOESY spectrum at 400 MHz of 2 mM human insulin at 37°C dissolved in D_2O/d_3-acetic acid (pD = 3.4) with a mixing time τ_M = 300 ms.

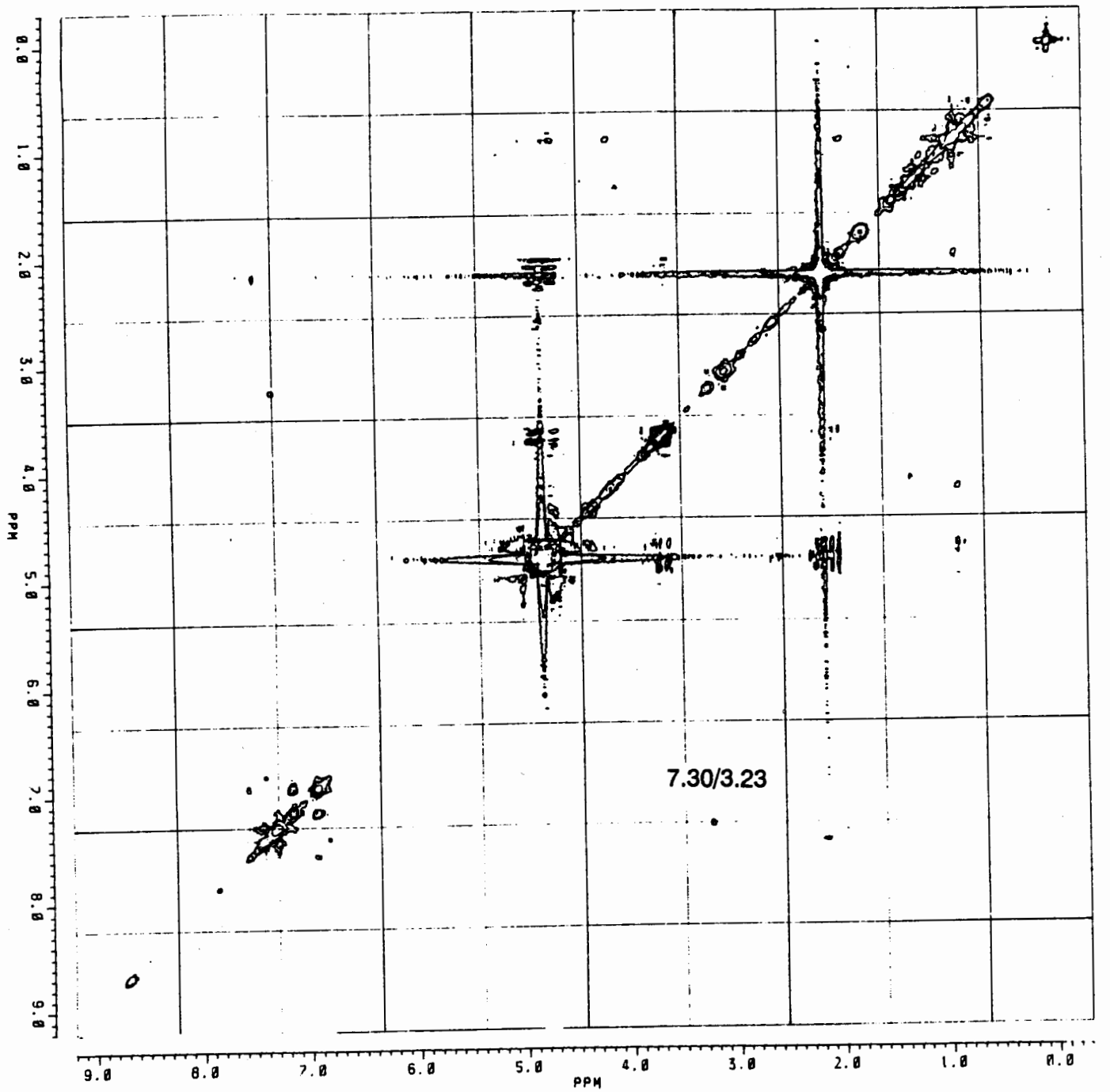

The spectra show strong t_1- and t_2-ridges (Wüthrich, 1986; Klevit, 1985). Only few cross-peaks were visible in all spectra. By comparing the cross-peaks at 7.30/3.23 ppm, and 8.55/4.18 ppm, respectively, we can conclude, that a mixing time of τ_M = 150 to 200 ms would be optimal for insulin.

4.5. 2-D ^{1}H NMR OF PORCINE INSULIN IN d_6-DMSO

In order to circumvent self-association of insulin in aqueous solution, d_6-DMSO was used as a solvent in a series of experiments. However, the question had to be posed, whether a chemical shift dispersion typically for globular proteins would be observed, or if the peptide would be partially or completely denatured. Again, the double-quantum-filtered COSY of Kline & Justice (Kline & Justice, 1990) recorded on a 500 MHz NMR spectrometer can be compared with a double-quantum-filtered COSY and a relayed COSY spectrum from our experiments, recorded on the WM-400 spectrometer (Figures 4.7, 4.14 and 4.15).

Figure 4.14: Aliphatic region of the DQF-COSY spectrum at 400 MHz of 12.7 mM porcine insulin at 37°C dissolved in d_6-DMSO. Both positive (light) and negative (dark) contours were plotted.

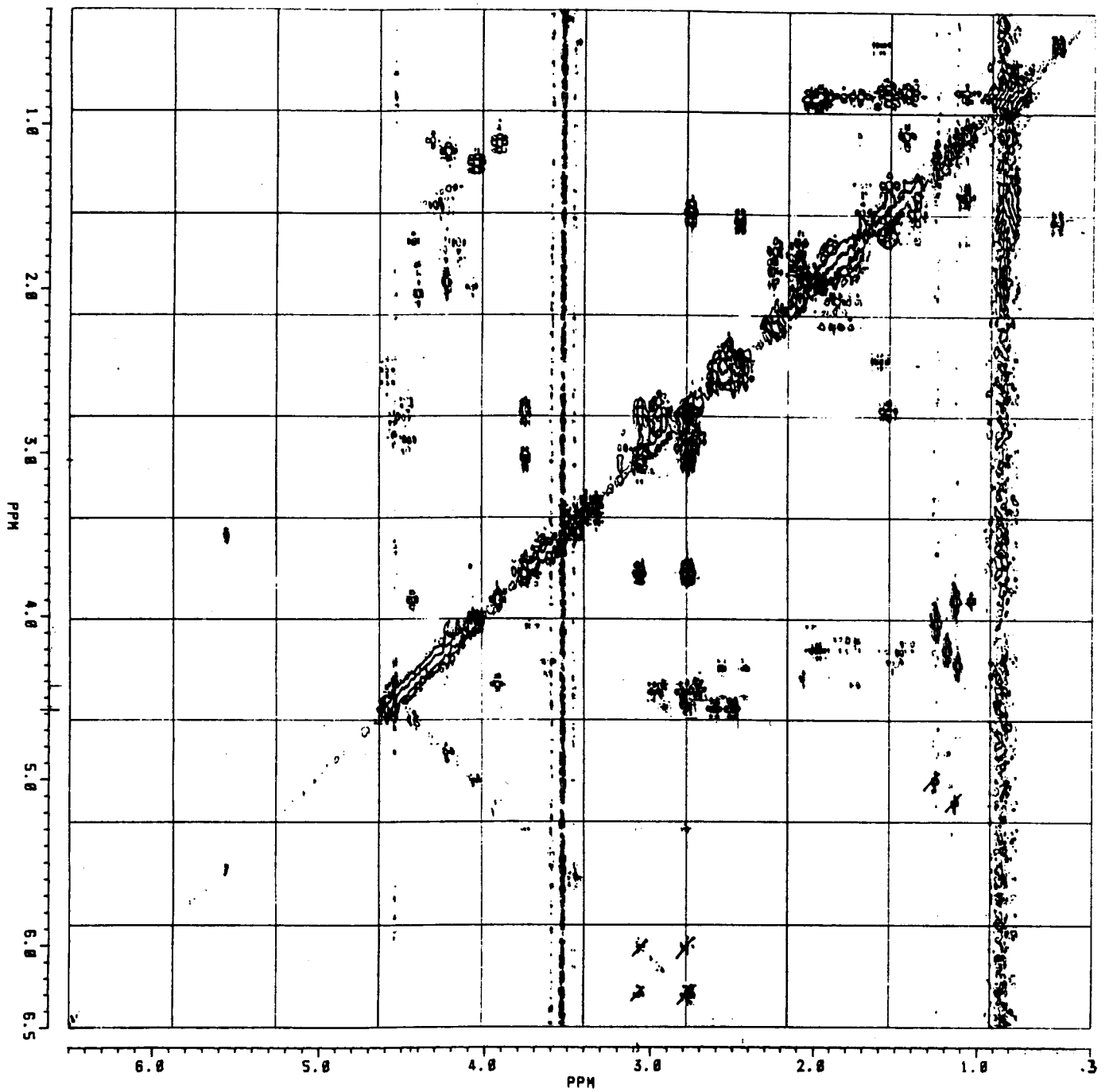

Figure 4.15: Aliphatic region of the relayed COSY spectrum at 400 MHz of 12.7 mM porcine insulin at 37°C dissolved in d_6-DMSO. Both positive (light) and negative (dark) contours were plotted.

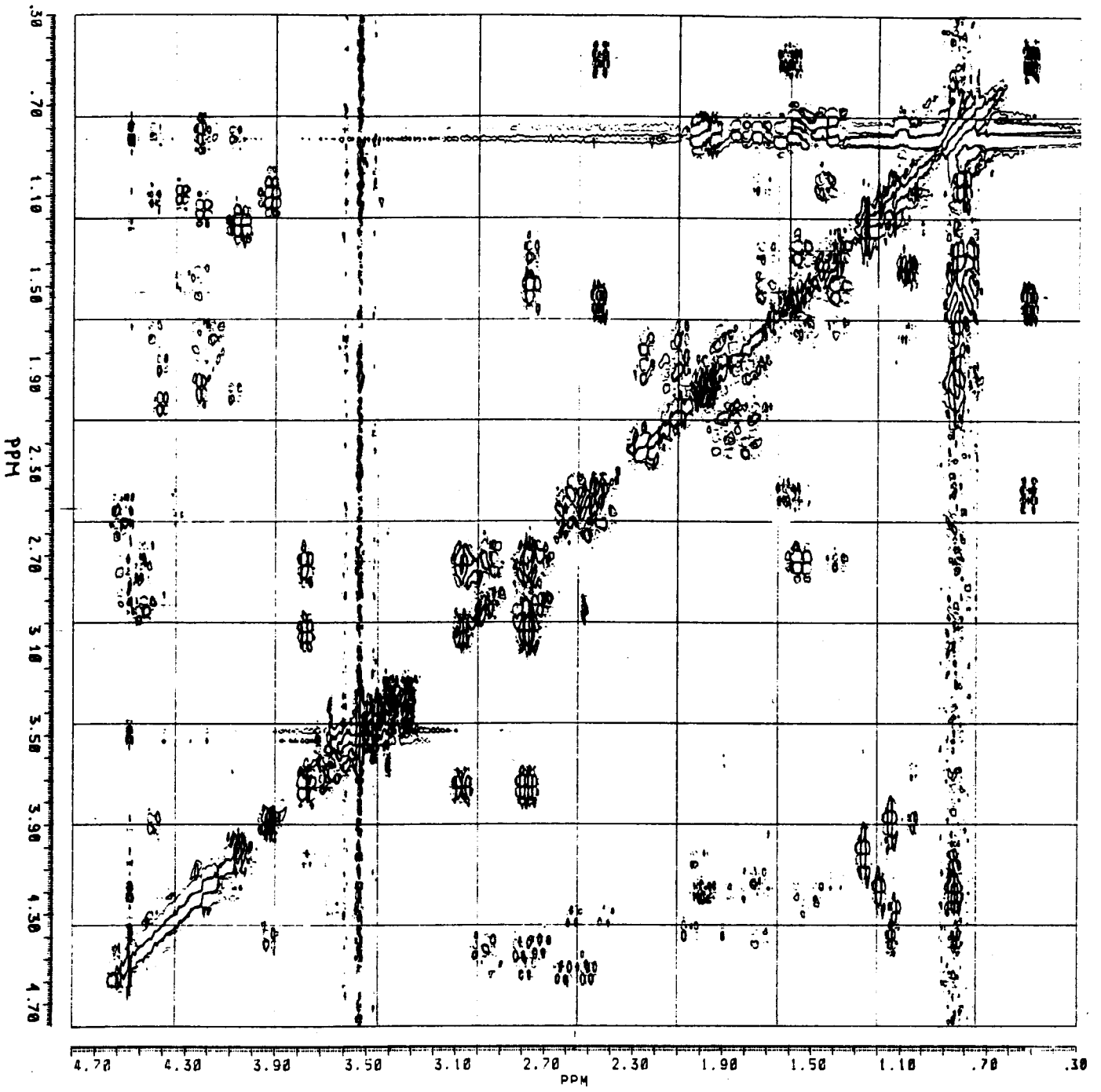

A comparison of the two spectra does not show the same chemical shift dispersion in our experiment as it can be observed in the spectrum of Kline & Justice. Some very intensive cross-peaks in our spectra may indicate superimposition of resonances, especially the cross-peaks in the range of ω_2 = 0.7 ppm to 1.0 ppm, belonging to the methyl resonances of the two isoleucines and the six leucines respectively. The peak intensity of these resonances caused a strong t_1-ridge with a base-plane distortion. Thus, cross-peaks in the range of ω_2 = 1.4 ppm to 2.0 ppm were very weak. Figure 4.16 shows our DQF-COSY spectrum in the range of 0.3 ppm to 3.0 ppm.

Figure 4.16: DQF-COSY spectrum at 400 MHz of 12.7 mM porcine insulin at 37°C dissolved in d_6-DMSO in the range of 0.3 ppm to 3.0 ppm. Both positive (light) and negative (dark) contours were plotted.

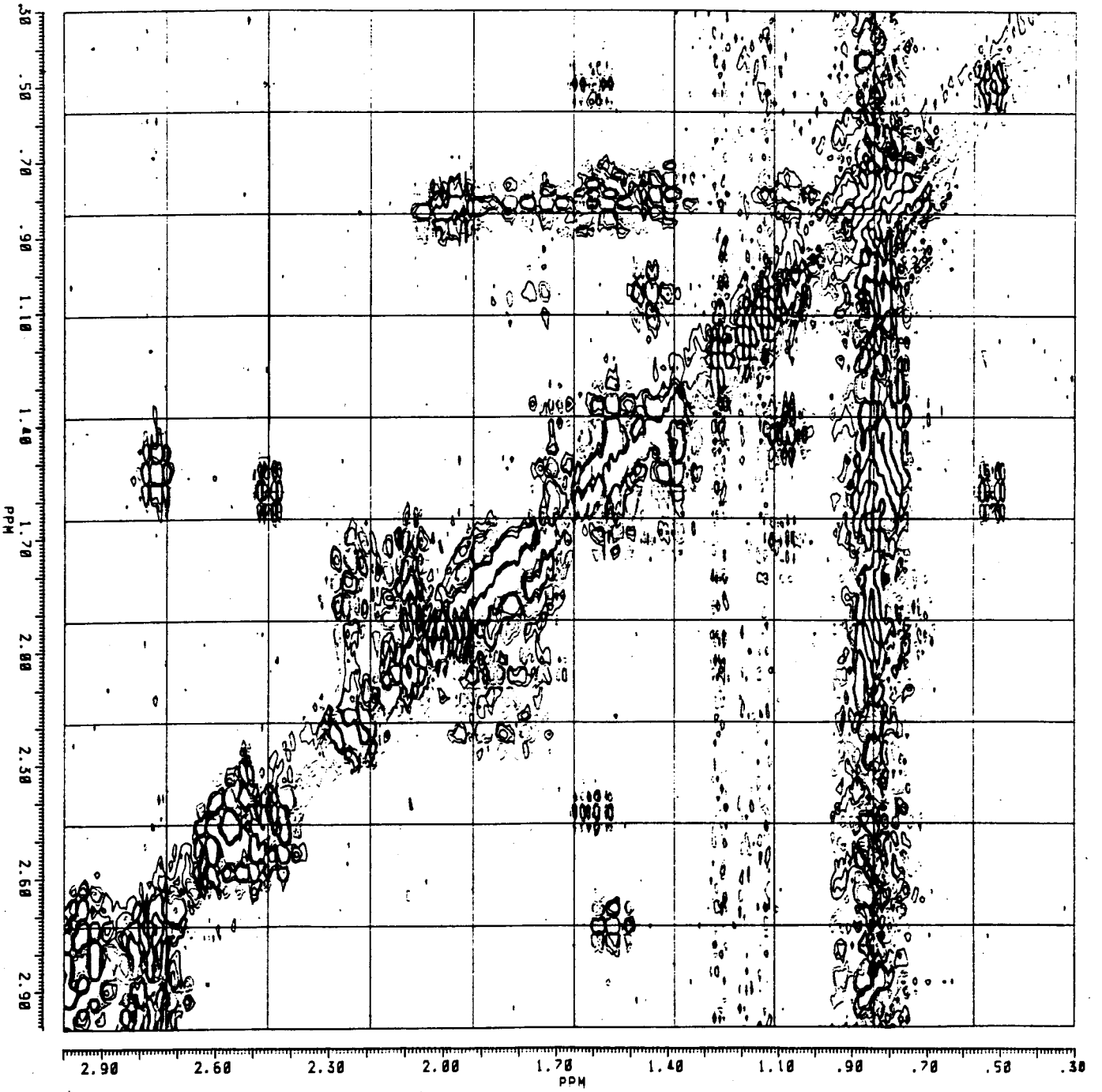

The application of TPPI on the WM-400 spectrometer in order to get phase-sensitive spectra, led to a weak mirror image of the spectrum at the carrier frequency, probably due to inaccuracies in phase-shifts of the analog phase-shifter.

The method of generating two data sets for each t_1 (States et al., 1982) could not be applied with the software available on the Aspect 2000 computer.

Ile A2, A10

The cross-peak at 1.58/0.50 ppm connects the $C\delta H_3$ to the $C\gamma H_2$ of both Ile A2 and Ile A10, respectively. $C\beta H$ can be assigned to the resonance at 2.44 ppm with a cross-peak at 2.44/1.58 ppm. A cross-peak at 2.44/0.50 ppm in the relayed COSY spectrum connects $C\beta H$ to $C\delta H_3$. The ridge in the range from 0.8 ppm to 0.9 ppm did not allow identification of the cross-peak between $C\beta H$ and $C\gamma H_3$. The cross-peak between $C\beta H$ and $C\alpha H$ is not resolved, but must be in the range of ω_1 = 4.5 to 4.6 ppm (see Fig. 4.17). The cross-peak between $C\alpha H$ and $C\gamma H_3$ can be found in the relayed COSY (Fig. 4.15) at ω_1 = 0.82 ppm. Our spectra gave no chemical shift difference between the spin systems of Ile A2 and A10. This chemical shift difference is also small in the spectrum of Kline & Justice. Furthermore, the chemical shift difference between the $C\gamma H_2$ protons, which are not chemically

equivalent, is not visible in our spectra. This may have been caused by low resolution. On the other hand, it may indicate faster rotation of the side-chains in DMSO than in aqueous solution. The CβH resonances are considerably shifted downfield compared to the spectrum of Kline & Justice. This may be explained by structural changes of the peptide caused by disruption of intramolecular hydrogen bonds by DMSO.

Figure 4.17: Cross-peaks in the range of ω_1 = 3.6 to 4.7 ppm/ω_2 = 2.3 to 3.4 ppm of the relayed COSY spectrum at 400 MHz of 12.7 mM porcine insulin at 37°C dissolved in d_6-DMSO. Both positive (light) and negative (dark) contours were plotted.

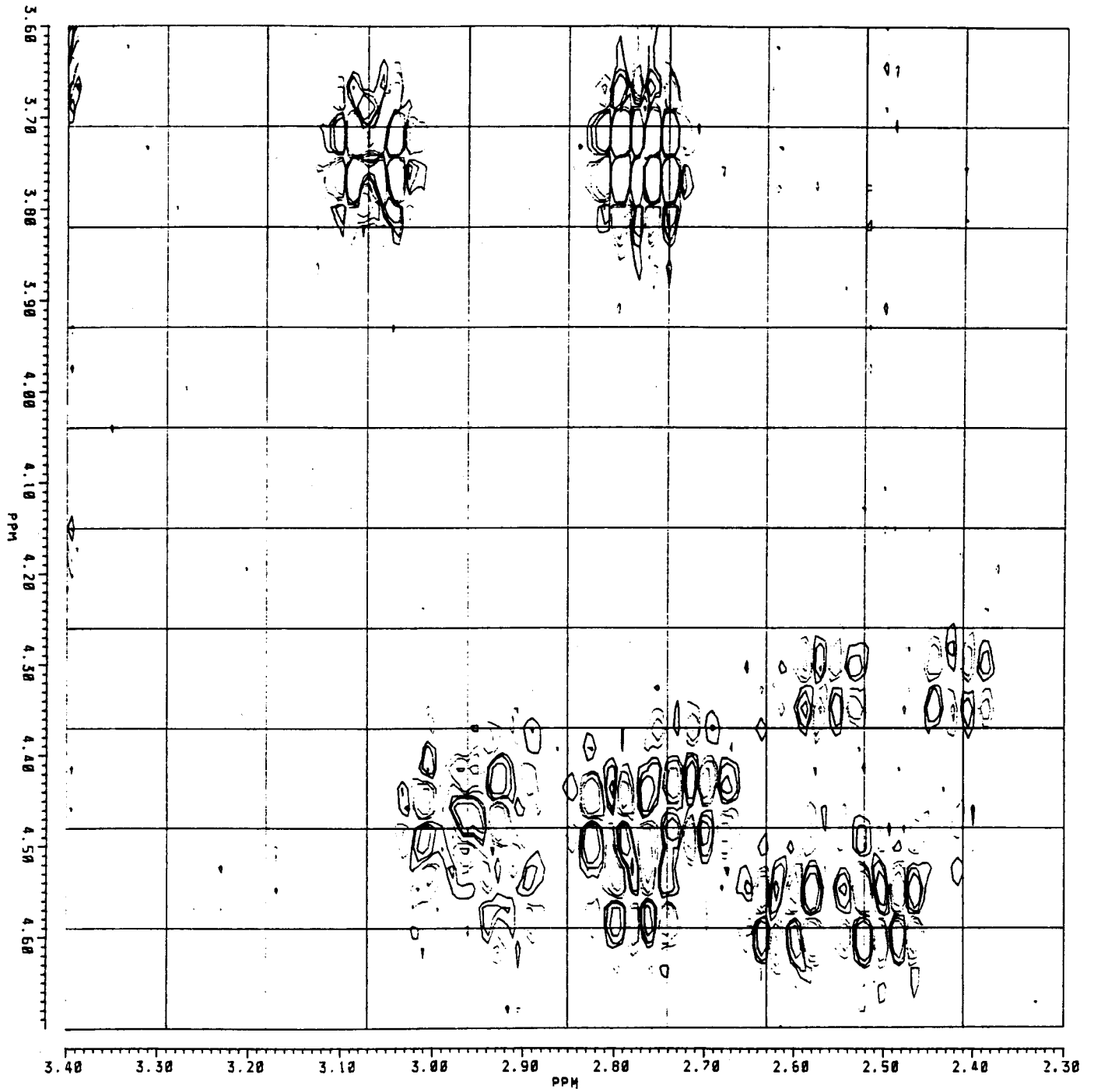

Leu A13, A16, B6, B11, B15, B17

A series of cross-peaks in the range of 0.83/1.35 to 2.07 ppm and one at 0.83/1.08 ppm can be observed in our spectra (Fig. 4.14 and 4.15). They connect the $C\delta H_3$ with the $C\gamma H$ resonances. $C\gamma H$ and $C\beta H_2$ protons have approximately the same chemical shift. Cross-peaks must therefore be found very close to the diagonal in the range 1.2 to 2.0 ppm. Cross-peaks between $C\beta H$ and $C\alpha H$ are observed in the range of ω_1 = 1.2 to 2.0 ppm (Fig. 4.14), but are either weak or superimposed. They cannot be assigned unambiguously. Cross-peaks at 0.83/1.08 ppm and at 1.46/1.08 ppm may also belong to a leucine spin system, probably the one of Leu B15. The spectrum of Kline & Justice gave the $C\delta H_3$ resonances in the range of 0.75 ppm to 0.92 ppm, except the one for Leu B15 at 0.57/0.68 ppm. The chemical shift dispersion of the leucine resonances indicates that insulin is not completely denatured in DMSO.

Val A3, B2, B12, B18

The series of strong cross-peaks at 0.83/1.35 to 2.07 ppm (Fig. 4.16) can be assigned to the valine residues, connecting the $C\gamma H_3$ and $C\beta H$ resonances. Again, the $C\beta H/C\alpha H$ cross-peaks are not clearly visible in our COSY spectra. The leucine and valine resonances thus cannot be distinguished from each other (Fig. 4.18). Therefore, for a

peptide with a high content of isoleucine, leucine and valine residues, high resolution is a prerequisite for the assignment of their resonances.

Figure 4.18: Cross-peaks in the range of ω_1 = 3.6 to 4.6 ppm/ω_2 = 0.8 to 2.1 ppm of the relayed COSY spectrum at 400 MHz of 12.7 mM porcine insulin at 37°C dissolved in d_6-DMSO. Both positive (light) and negative (dark) contours were plotted.

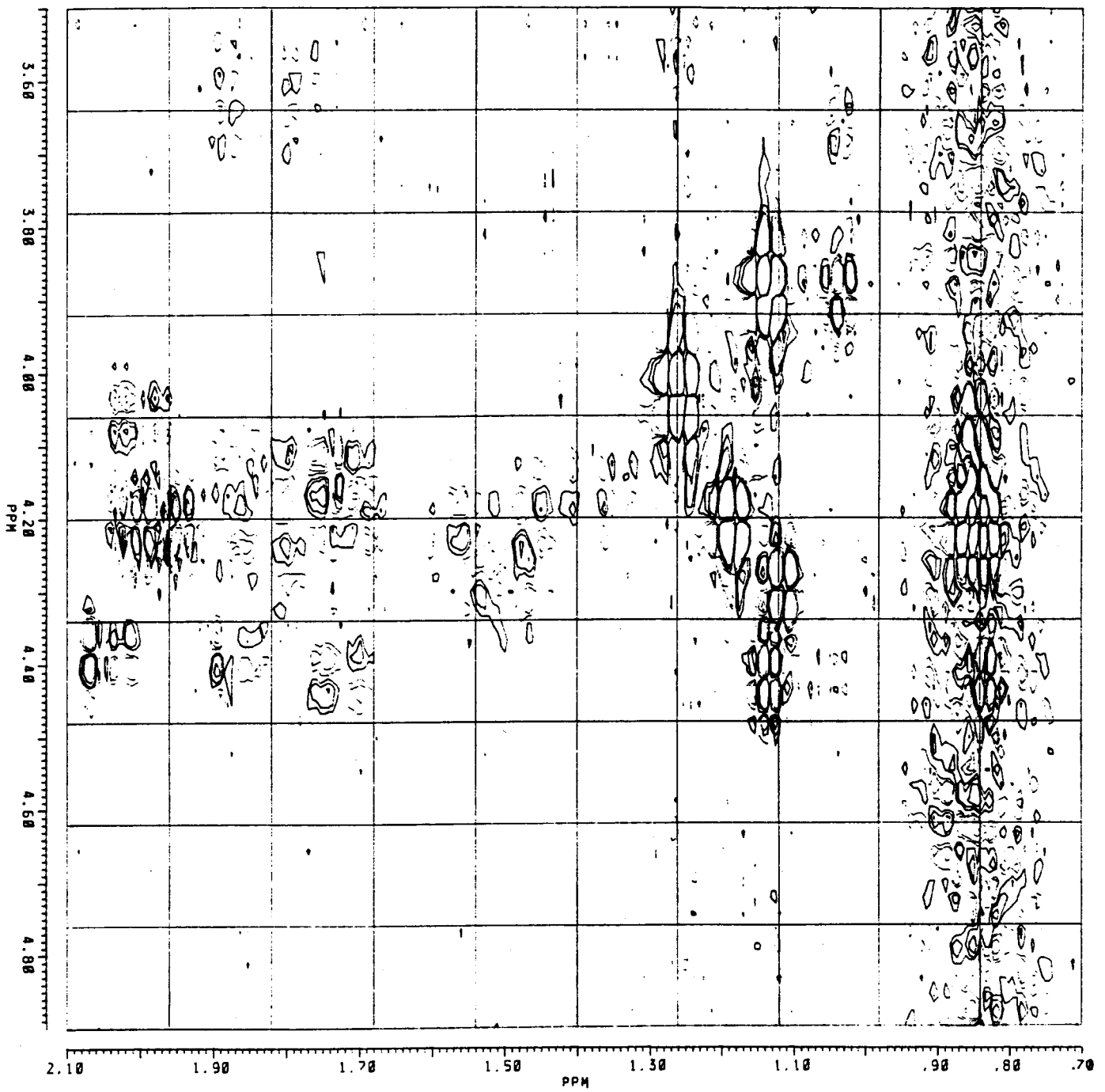

Ala B14, B30

The $C\beta H_3$ resonance should be observed in the range from 1.4 ppm to 1.5 ppm. The cross-peaks that connect $C\beta H_3$ to $C\alpha H$ must also be assigned to the range of ω_1 = 4.0 to 4.4 ppm/ω_2 = 1.3 to 1.6 ppm (Fig. 4.18).

Glu A4, A17, B13, B21; Gln A5, A15 B4; Asn A18, A21, B3

Our spectra gave cross-peaks between 1.71 - 2.00/2.05 - 2.32 ppm (Fig. 4.15). The $C\gamma H_2$ resonances were observed in the range from 2.27 ppm to 2.52 ppm by Kline & Justice, the $C\beta H_2$ resonances in the range from 1.78 ppm to 2.33 ppm, respectively. The $C\gamma H_2$ resonances of glutamic acid and glutamines must be shifted downfield compared with the $C\beta H_2$ resonances due to the carboxy group in the side chain. The connection between $C\beta H_2$ and $C\alpha H$ is unclear, except the cross-peak at 2.05/4.40 ppm (Fig. 4.15). For the glutamine residues, cross-peaks between the amide protons of the side chain at 7.29 ppm to 7.44 ppm and the $C\gamma H_2$ resonances should be observed in the relayed COSY. The $C\beta H_2$ of the asparagine residues in the range from 2.45 - 2.76 ppm should be connected by cross-peaks to the $N\delta H_2$ protons from 6.34 ppm to 7.42 ppm in the relayed COSY. Four weak cross-peaks at 7.95/2.71 ppm, 8.24/2.80 ppm, 8.38/2.62 ppm and 8.38/2.50 ppm were observed in the relayed COSY spectrum (Fig. 4.19 and 4.20). They are in line with cross-peaks at

4.45/2.80 ppm, 4.47/2.71 ppm, 4.27/2.62 ppm and 4.27/2.50 ppm, connecting $C\beta H_2$ with $C\alpha H$ of asparagine or $C\gamma H_2$ with $C\beta H_2$ of glutamine residues respectively. Again, the side-chain amide protons are shifted downfield compared to those in the spectrum of Kline & Justice.

Figure 4.19: Relayed COSY spectrum at 400 MHz of 12.7 mM porcine insulin at 37°C dissolved in d_6-DMSO. Both positive and negative contours were plotted. The weak cross-peaks at 7.79/2.71 ppm, 8.24/2.80 ppm, 8.38/2.62 ppm and 8.38/2.50 ppm are encircled.

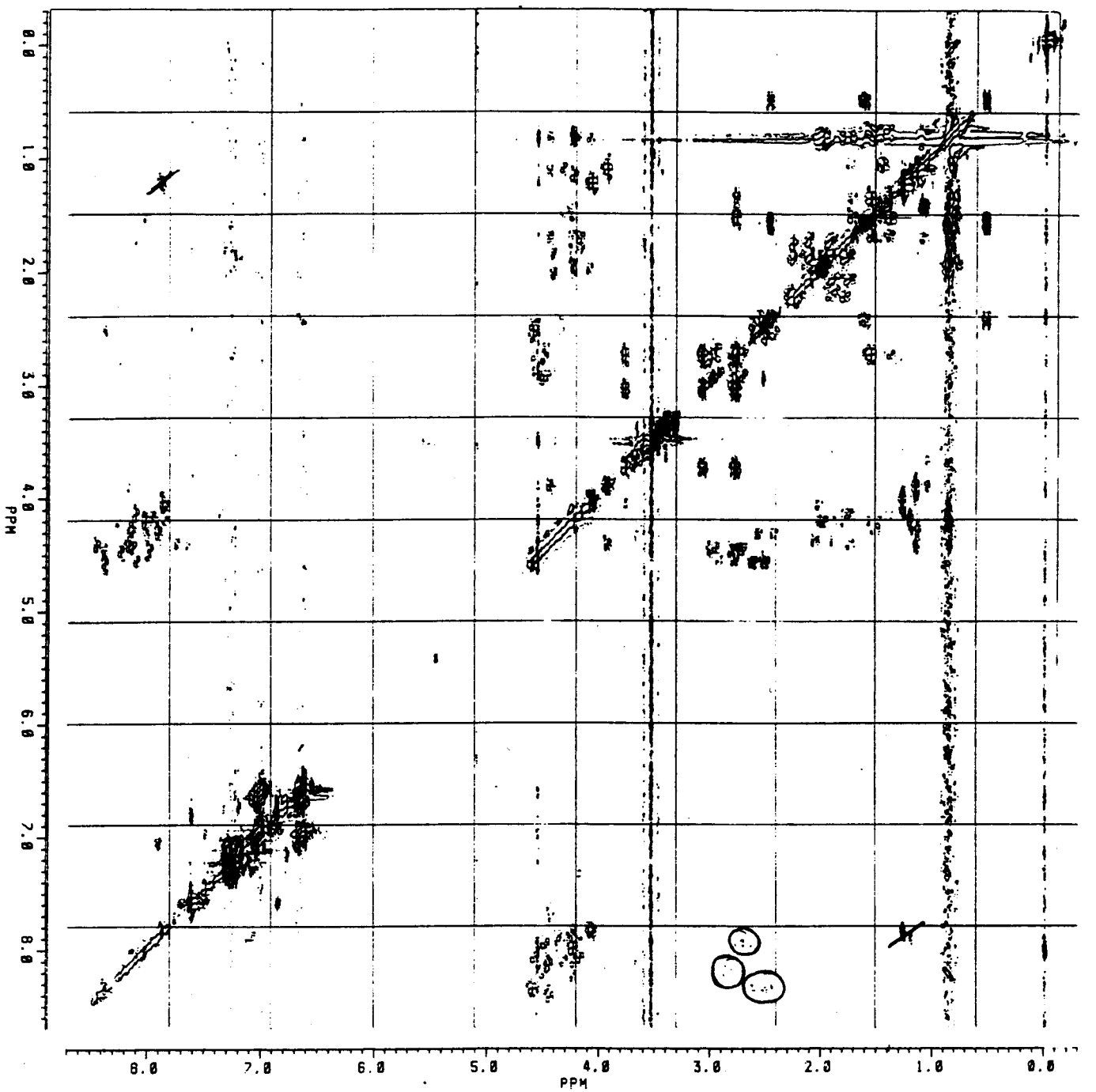

Figure 4.20: Cross-peaks in the range of ω_1 = 7.9 to 8.4 ppm/ω_2 = 2.4 to 2.9 ppm of the relayed COSY spectrum at 400 MHz of 12.7 mM porcine insulin at 37°C dissolved in d_6-DMSO. Both positive (light) and negative (dark) contours were plotted.

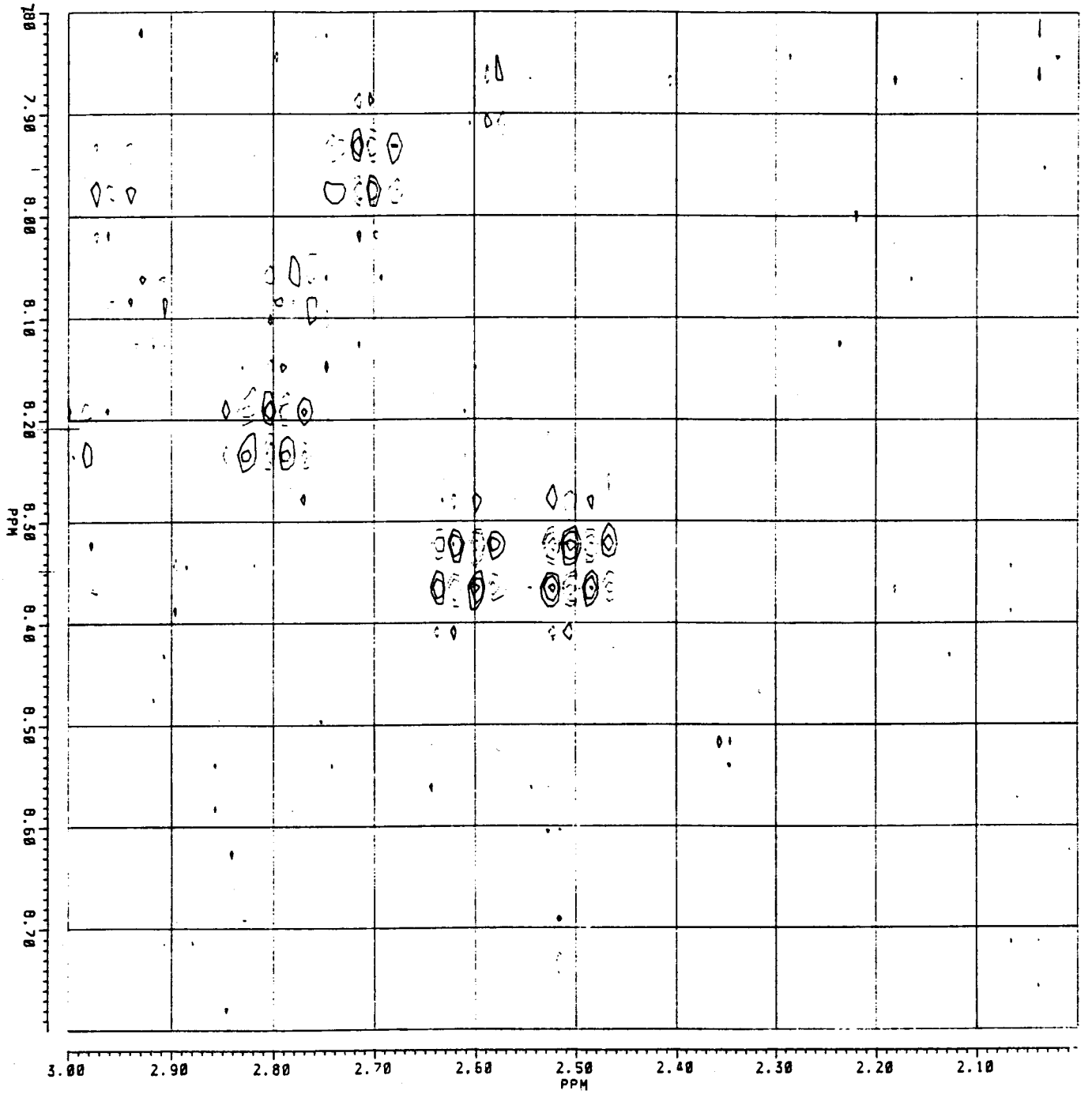

Cys A6, A7, A11, A20, B7, B19; Ser A9, A12, B9; Tyr A14, A19, B16, B26; Phe B1, B24, B25; His B5, B10

Cross-peaks connecting $C\beta H_2$ with $C\alpha H$ protons in our COSY spectrum (Fig. 4.14) in the range of 4.25 - 4.65/2.40 - 3.10 ppm and at 3.74/3.05 ppm and 3.74/2.78 ppm, respectively, may be assigned to Cys, Ser, Tyr, Phe, or His resonances; but an assignment to the $C\beta H_2$ and the $C\alpha H$ protons of glutamic acid, glutamine or asparagine spin systems is also possible. The cross-peaks between $C\beta H_2$ and $C\alpha H$ of Cys, Ser, Tyr, Phe, and His were observed in the range from 2.78 - 4.23/4.04 - 4.86 ppm by Kline & Justice. The cross-peak at 4.43/3.89 ppm may identify one or more serine spin systems. Our relayed COSY spectrum gave no cross-peaks between $C\beta H_2$ and the aromatic $C\delta H_2$ of the tyrosine and phenylalanine residues.

Thr A8, B27

The $C\alpha H$ and $C\beta H$ resonances of the threonine residues in human insulin were assigned to the range of 4.02 ppm to 4.54 ppm by Kline & Justice. Cross-peaks close to the diagonal in that range were not detected in our spectra. Characteristic for threonines are cross-peaks in the range of 4.04 - 4.36/1.12 - 1.19 ppm, connecting $C\beta H$ to $C\gamma H_3$. Cross-peaks at 4.43/1.13 ppm and 4.43/1.04 ppm are observed

in our spectra (Fig. 4.14 and 4.18), but they may also be assigned to alanine.

Arg B22; Lys B29

CαH and $C\beta H_2$ of the arginine and lysine residues would be observed in the range of 4.16 - 4.33/1.72 - 1.93 ppm according to Kline & Justice. Our COSY data in that range are weak (Fig. 4.14). Cross-peaks in the range of 1.80 - 2.20/1.70 - 2.20 ppm in our COSY experiment linking $C\beta H_2$ to $C\gamma H_2$ may be assigned to these residues (Fig. 4.15). Our spectra gave no cross-peaks in the range of 1.66 - 1.71/3.19 ppm, linking $C\gamma H_2$ to $C\delta H_2$ of arginine, in the range of 1.41 - 1.42/1.63 ppm linking $C\gamma H_2$ to $C\delta H_2$ of lysine, and at approximately 1.63/2.92 ppm, linking $C\delta H_2$ to $C\varepsilon H_2$ of lysine. Cross-peaks at 7.29 - 7.39/2.92 - 3.19 ppm, linking $C\delta H_2$ to NεH of arginine and $C\varepsilon H_2$ to $N\zeta H_2$ of lysine, respectively, were detected in our relayed COSY spectrum at 7.79/2.71 ppm, 8.24/2.80 ppm, 8.38/2.62 ppm, and 8.38/2.50 ppm (Fig. 4.20). They may also be assigned to glutamine and asparagine spin systems, thus overlapping them.

We can conclude from our experiments that the complex chemical shift dispersion of insulin observed by Kline & Justice requires higher resolution for 2-D ^1H NMR experiments. Figure 4.21 shows parts of a NOESY spectrum of

insulin in water/acetonitrile 65 %/35 % recorded by Kline & Justice. The mixing time was τ_M = 200 ms. Due to significant amount of α-helix present the NOESY CαH/NH cross-peaks are weak and one must use NH/NH cross-peaks in order to find connectivity patterns used to predict protein secondary structure. In particular NH/NH connectivities between A4-A5, A7-A8 (Fig. 4.21 A, their paper), B4-B5, B11-B12, B13-B14, B14-B15, B16-B17, B21-B22, B23-B24, and B25-B26 (Fig. 4.21 B, C, their paper) can hardly be resolved at 400 MHz. This should indicate the difficulty in doing protein work at fields less than 500 MHz for even moderate sized peptides like insulin.

Figure 4.21: Amide diagonal region of a 200 ms NOESY spectrum at 500 MHz of human insulin at 27°C dissolved in H_2O/acetonitrile. Region A shows the sequential NH/NH cross-peaks for the A chain, while regions B and C show the sequential cross-peaks for the B chain. The spectra were plotted for both ω_1 (vertical axis) and ω_2 (horizontal axis) from (A) 8.71 to 6.98 ppm, (B) 8.87 to 7.53 ppm, and (C) 8.88 to 6.93 ppm. Only positive contour levels have been drawn. Sequence positions are shown along the diagonal with lines connecting the appropriate cross-peaks (adapted from Kline & Justice, 1990).

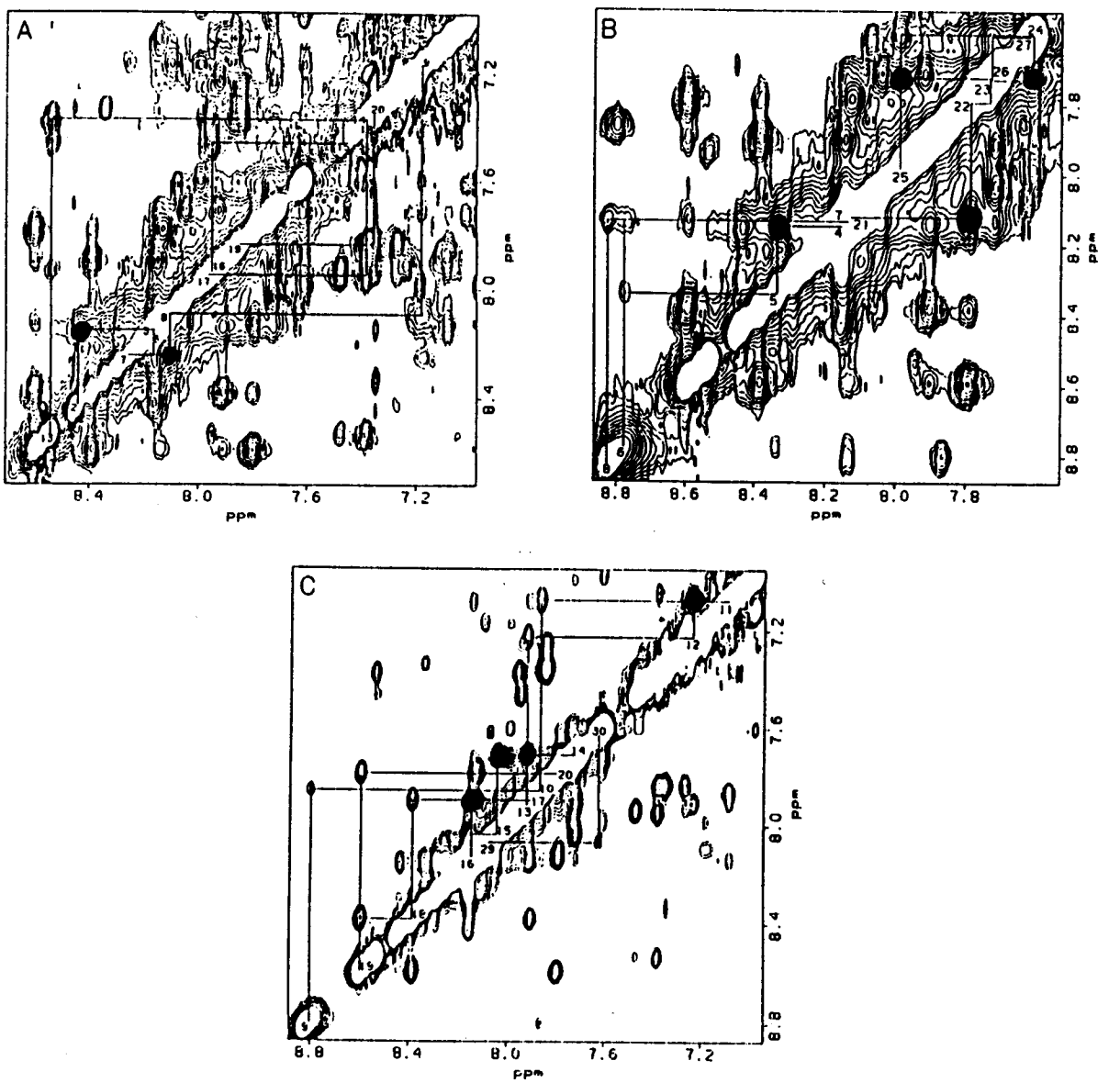

Software for base-plane corrections would be another necessary prerequisite. The fact that many cross-peaks were either weak or not detectable in our spectra may be due to base-plane distortions, overlapping antiphase cross-peaks that cancel each other, and the application of strongly shifted sine-bell functions in order to increase the resolution. Pure DMSO is not the ideal solvent for NMR experiments with insulin. Although some chemical shift dispersion can be observed, the structure of the peptide in DMSO must be between its native structure and the denatured state. To illustrate this, Figures 4.22 and 4.23 show a comparison of the fingerprint region in the range of 3.0 - 5.0/7.5 - 8.7 ppm of our DQF-COSY spectrum and of the DQF-COSY of Kline & Justice.

Figure 4.22: Fingerprint region of our DQF-COSY spectrum at 400 MHz of porcine insulin at 37°C dissolved in d_6-DMSO. The spectrum was plotted for ω_1 (vertical axis) from 3.8 ppm to 5.0 ppm and for ω_2 (horizontal axis) from 7.5 ppm to 8.5 ppm. Both positive (light) and negative (dark) contours have been plotted.

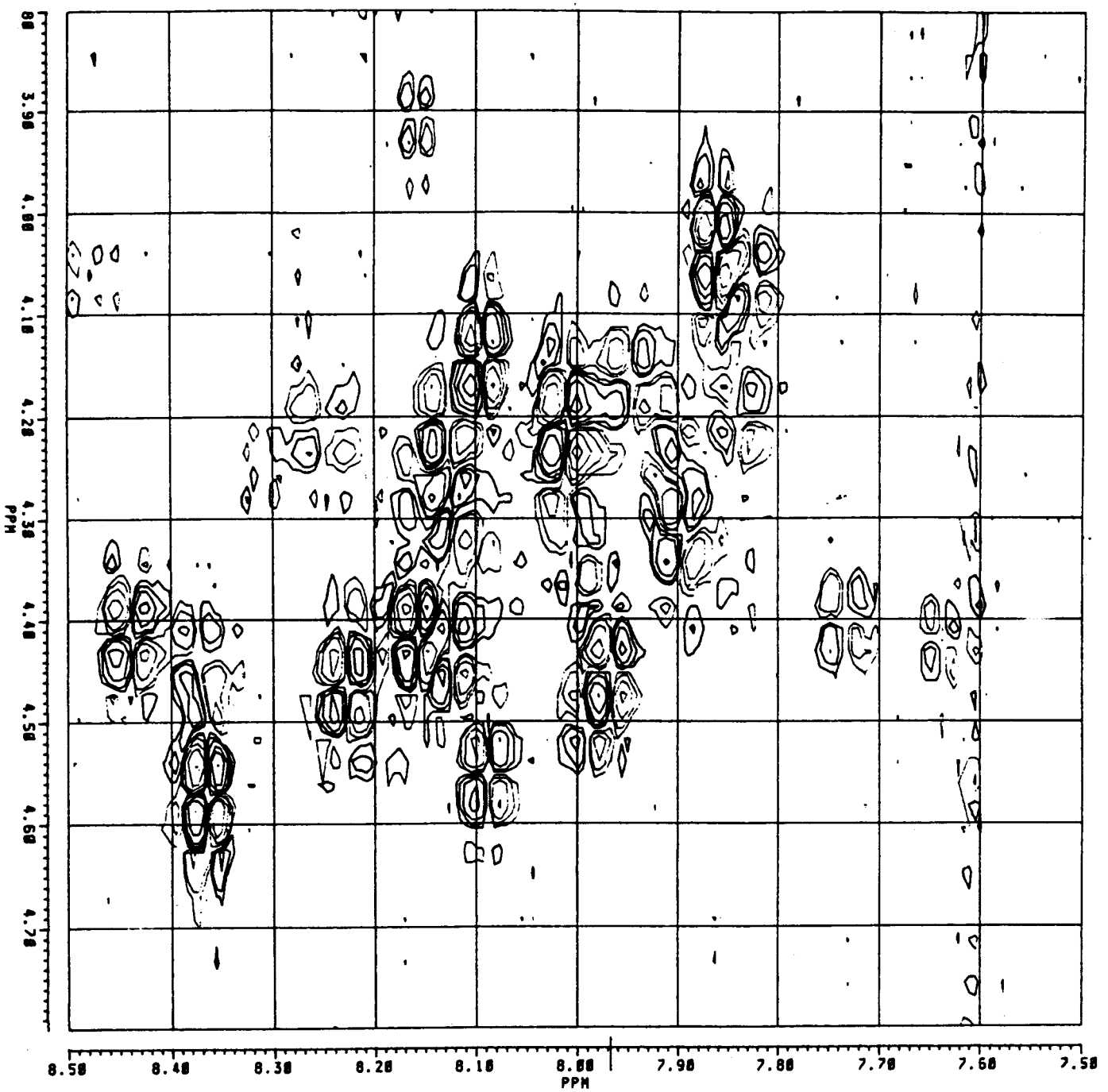

Figure 4.23: Fingerprint region of a DQF-COSY spectrum at 500 MHz of human insulin at 27°C dissolved in H_2O/acetonitrile. The spectrum was plotted for ω_1 (vertical axis) from 5.19 to 2.78 ppm and for ω_2 (horizontal axis) from 9.51 to 6.95 ppm. Both positive and negative contours have been plotted. Each NH-CαH cross peak has been labeled with the assigned chain and sequence position. Boxes have been drawn to clearly indicate the peak positions in crowded regions. The two cross-peaks marked with the asterisk are due to side-chain protons (adapted from Kline & Justice, 1990).

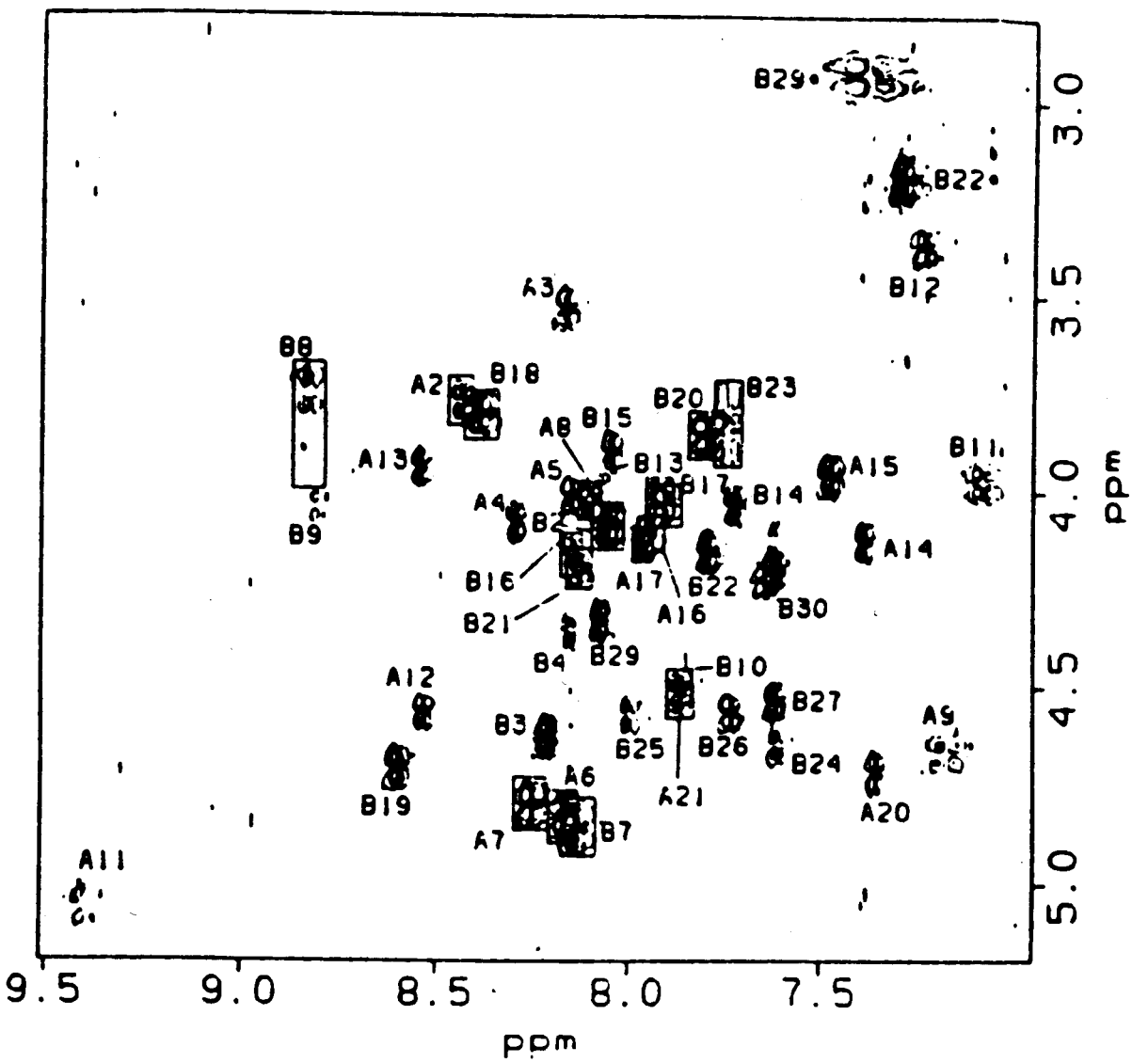

We can conclude from our 2-D ^1H NMR experiments, that for every peptide that is to be investigated by 2-D ^1H NMR, the following steps should be observed:

1. The solution properties of a peptide, expecially self-association behavior, have to be investigated prior to any NMR experiments.

2. A set of 1-D ^1H NMR experiments should be recorded prior to any 2-D ^1H NMR experiments in order to investigate chemical shift dispersions at different temperatures and pH-values.

3. 2-D ^1H NMR COSY experiments of a peptide in D_2O have to be recorded in order to investigate the number of cross-peaks, chemical shift dispersion and possible base-plane distortions.

4. Only then should a set of 2-D ^1H NMR experiments be recorded (DQF-COSY, relayed COSY and TOCSY/HOHAHA, NOESY, Double-Quantum COSY) of the peptide both in D_2O and H_2O/D_2O 9:1.

4.6. BINDING STUDY OF INSULIN WITH VESICLES OF EGG YOLK PHOSPHATIDYLCHOLINE

4.6.1. PARTICLE SIZE

Nicomp Distribution Analysis and Nicomp Gaussian Analysis of vesicles of egg yolk phosphatidylcholine yielded the following mean diameters (Table 4.7):

Table 4.7: Mean Diameters of Egg Yolk Phosphaditylcholine Vesicles.

Experiment	Mean Diameter [nm]				Chi-Square
	DA	SD	GA	SD	
1	34.1	61 %	26.5	36 %	120.7
2	32.9	55 %	26.5	36 %	96.0
3	37.2	76 %	26.6	36 %	118.8
4	32.3	51 %	26.6	36 %	102.0
5	32.9	54 %	26.5	36 %	103.1
Average	33.9	59 %	26.5	36 %	

where

DA: Distribution Analysis
GA: Gaussian Analysis
SD: Standard Deviation

Two populations of vesicles were observed, one with diameters between 19.3 nm and 23.0 nm, and a smaller subfraction with diameters between 40.0 nm and 85.7 nm. The values of chi-square indicate that the Gaussian analysis was not a good fit.

4.6.2. SOLUBILIZATION OF INSULIN BY VESICLES OF EGG YOLK PHOSPHATIDYLCHOLINE

The purpose of the experiment was an answer to the question whether insulin suspended in phosphate buffer would be solubilized by binding to vesicles of egg yolk phosphatidylcholine. Increasing amounts of vesicles in phosphate buffer at pH 7.4 were added to a solution of 4×10^{-3} mmol of insulin suspended in 0.5 ml of phosphate buffer at pH 7.4. The suspension was cloudy. The results are listed in Table 4.8.

Table 4.8: Solubilization Experiment of Insulin with Vesicles of Egg Yolk Lecithin.

Time [min.]	EYL added [ml]	Conc. EYL [mmol]	Solubil.
0	0.5	0.079	no
30	0.5	0.158	no
60	0.5	0.237	no
90	0.5	0.316	no
120	0.5	0.395	no
150	0.8	0.521	no

The final lipid:peptide molar ratio was 130:1. The sample was let stand overnight under nitrogen and exclusion of light. The following day, the solution was still cloudy with some of the insulin precipitated at the bottom of the tube. The pH was lowered to pH = 2.1 by the addition of 100 mM HCl and then increased to pH = 12.0 by the addition of 100 mM NaOH. As expected, insulin dissolved at pH values

< 3.8 and > 7.5, but the peptide always reprecipitated when the pH was adjusted to pH = 7.0.

4.6.3. FLUORESCENCE EMISSION STUDY

Tables 4.9 and 4.10 show the results of the experiments described in chapter 3.2.5.2. Fluorescence intensity and emission maximum of the tyrosine residues of porcine insulin were measured at different molar ratios lipid:peptide after the addition of egg yolk phosphatidylcholine vesicles. The slit width of the spectrometer was adjusted to 5 mm in experiment 1, to 4 mm in experiment 2, the excitation wavelength to 275 nm, and the emission wavelength to 302 nm. The volume of the samples was 4 ml.

Table 4.9: Fluorescence Signal Intensities of the Tyrosine Residues of Porcine Insulin at Different Molar Ratios Lipid:Peptide After the Addition of Egg Yolk Phosphatidylcholine Vesicles.

Sample	Vesicles [μM]	Ratio L:P	Signal Intensity at 302 nm
1	0.0	-----	2
2	8.7	1:0	10
3	0.0	0:1	95
4	8.7	1:1	90
5	43.5	5:1	107
6	87.0	10:1	102
7	174.0	20:1	106
8	435.0	50:1	100
9	696.0	80:1	98
10	870.0	100:1	92
11	1044.0	120:1	94
12	1305.0	150:1	90
13	1740.0	200:1	88
14	2610.0	300:1	80
15	4350.0	500:1	64

Table 4.10: Fluorescence Emission Maximum of the Tyrosine Residues of Porcine Insulin at Different Molar Ratios Lipid:Peptide After the Addition of Egg Yolk Phosphatidylcholine Vesicles.

Sample	Vesicles [μM]	Ratio L:P	Emission Maximum	Signal Intensity
1	0.0	-----	300-303	0
2	8.7	1:0	300-303	0
3	0.0	0:1	301.2	30
4	8.7	1:1	301.0	30
5	43.5	5:1	302.4	42
6	87.0	10:1	302.4	42
7	174.0	20:1	300.0	42
8	348.0	40:1	300.0	40
9	522.0	60:1	301.0	39
10	696.0	80:1	301.0	35
11	870.0	100:1	300.0	34
12	1044.0	120:1	301.0	13
13	1305.0	150:1	300-303	10
14	1740.0	200:1	300-303	0
15	4350.0	300:1	300-303	0

Sample 1 was a blank, sample 2 contained 8.7 μM vesicles without peptide, and sample 3 was 8.7 μM insulin without vesicles. Samples 3 to 15 contained 8.7 μM insulin from a 8 mM stock solution. Increasing amounts of vesicles from a 8.7 mM stock solution were added to the different samples.

In experiment 1, the intensity of the emission signal started to drop slightly at a molar ratio lipid:peptide of 80:1.

In experiment 2, a small range around the emission maximum was scanned in order to examine whether a blue shift would occur. There was no significant shift of the emission maximum observed, while the signal intensity again started to drop, when a molar ratio lipid:peptide of 80:1 was reached.

4.6.4. PROTEIN DETERMINATION OF INSULIN WITH VESICLES OF EGG YOLK PHOSPHATIDYLCHOLINE

A solution of vesicles to which insulin had been added was passed through a Gelman Acrodisc filter in order to remove insoluble insulin. The filter was then placed in 10 mM HCl in order to extract insulin. Free insulin that was dissolved in the vesicle solution was removed by dialysis.

Table 4.11 and Figure 4.24 show the results of the Lowry standard assay. The results of the protein determination performed on the vesicle sample to which insulin had been added, on a vesicle sample without peptide, on the filter extract, and on the dialysis solution, respectively, are shown in Tables 4.12 and 4.13.

Table 4.11: Lowry Standard Protein Assay.

Protein	50 µg	100 µg	150 µg	200 µg	250 µg	Blank
O.D. Standard 1	0.147	0.261	0.400	0.501	0.613	0
O.D. Standard 2	0.141	0.271	0.408	0.510	0.589	0
Average O.D.	0.144	0.266	0.404	0.506	0.601	0

Figure 4.24: Lowry Standard Protein Assay

COEFFICIENTS 3.80000E-02 2.30800E-03

STD DEVNS 1.63066E-02 9.83328E-05

WEIGHTED STD DEVN OF FIT =1.555E-02

X	Y EXP	Y CALC	DEVN	ERR EST
50.00	.14400	.15340	9.400E-03	1.000E-02
100.0	.26600	.26880	2.800E-03	1.000E-02
150.0	.40400	.38420	-1.980E-02	1.000E-02
200.0	.50600	.49960	-6.400E-03	1.000E-02
250.0	.60100	.61500	1.400E-02	1.000E-02

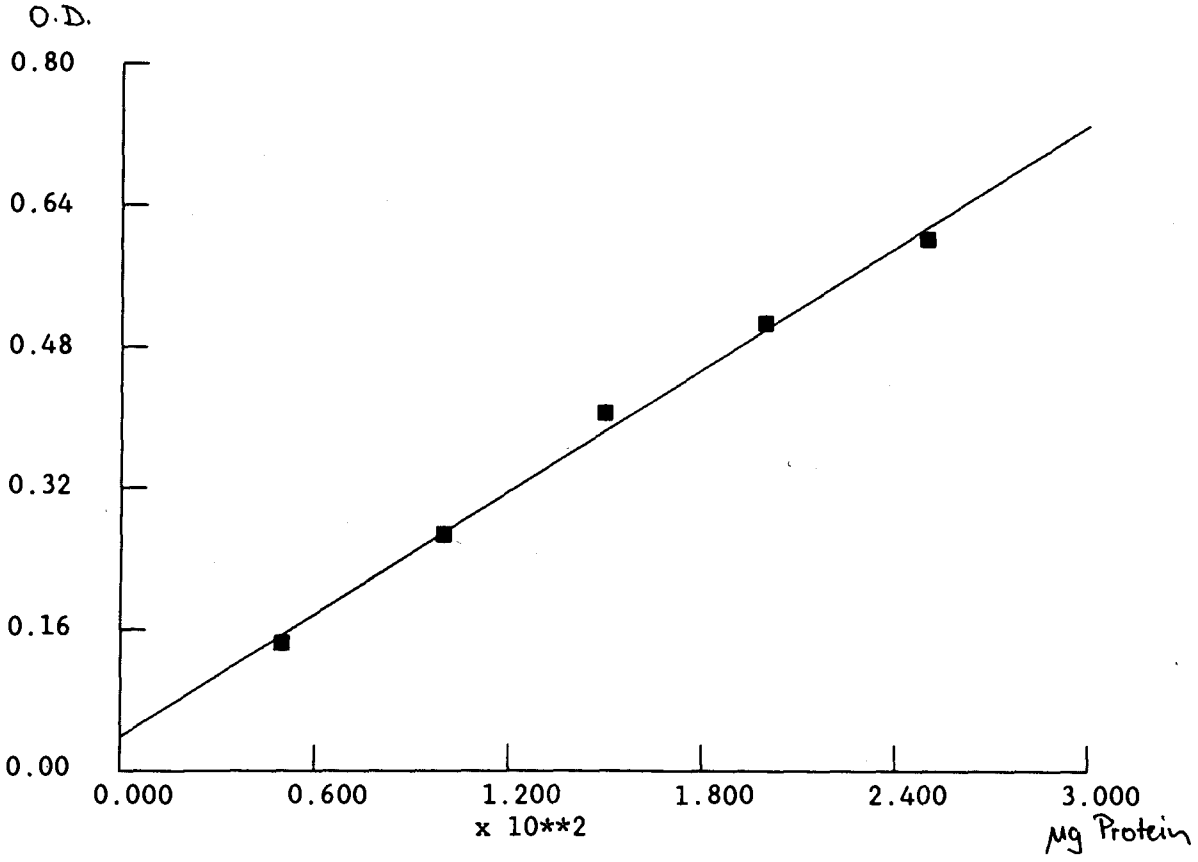

Table 4.12: Protein Determination of Insulin with Vesicles of Egg Yolk Phosphatidylcholine.

Dialysis Solution [ml] (Total Volume: 1 l)	0.3	0.3	0.4	0.4	0.5	0.5
O.D.	0	0	0	0	0	0
Filter Extract [ml]	0.3	0.3	0.4	0.4	0.5	0.5
O.D.	0.040	0.039	0.055	0.050	0.069	0.073
Average O.D.		0.040		0.053		0.071
Insulin [µg]		15		19		26
Vesicles + Insulin [ml]		0.1	0.1	0.2		
O.D.		0.875	0.975	1.500	(discarded)	
Average O.D.			0.925 ± 0.050			
Vesicles alone [ml]		0.1	0.1	0.2		
O.D.		0.521	0.459	1.500	(discarded)	
Average O.D.			0.490 ± 0.030			
Corrected O.D. Vesicles + Insulin		0.354	0.516			
			0.435 ± 0.050			
Peptide [µg]			170 ± 30			

Table 4.13: Insulin with Vesicles of Egg Yolk Phosphatidylcholine; Peptide Concentrations.			
	Peptide Concentration [mg/ml]		%
Filter Extract	0.050	0.048 0.052	
Average		0.050 ± 0.002	1
Vesicles + Insulin		1.7 ± 0.3	39
Total Insulin added to Vesicles		4.4	100

The O.D. measured for insulin with vesicles had to be corrected by the O.D. of vesicles alone due to light scattering.

A total of 4.4 mg/ml of insulin were added to the buffer containing 0.264 mmol of egg yolk phosphatidylcholine vesicles. When the solution was passed through a Gelman Acrodisc filter, 50 µg/ml or 1 % of the peptide were retained by the filter. The solution was then dialyzed in order to remove free insulin. No peptide was detected in the dialysis buffer due to dilution. A total of 2.7 mg of free insulin should have been detected according to the above calculation in 1 liter of dialysis buffer. A total of 1.7 mg/ml of insulin was measured in the vesicle solution after dialysis. In 700 µl of vesicle solution, this would correspond to 1.2 mg (1.9×10^{-4} mmol) with 2.15×10^{-2} mmol of vesicles.

5. CONCLUSION

Insulin, suspended in phosphate buffer at pH 7.4, was not visibly solubilized by the presence of vesicles of egg yolk phosphatidylcholine.

The results of the fluorescence study yielded no evidence for the interaction of the tyrosine residues with egg yolk PC vesicles. Neither a blue shift of the tyrosine fluorescence emission maximum of insulin nor a significant intensity enhancement were observed upon addition of egg PC vesicles to an insulin solution. The signal intensity started to drop at a lipid:peptide molar ratio > 80:1 due to a decrease in excitation intensity caused by light scattering. Tyrosine is a polar amino acid. In an amphipathic helix bound to the surface of a membrane tyrosine would be exposed to the aqueous environment of the membrane. In future work, interaction of insulin with dodecylphosphocholine-d_{38} micelles, with sodium dodecyl-d_{25} sulfate, or with vesicles of different classes of phospholipids may be investigated by measuring a possible blue-shift and enhancement of the emission maximum of site-directed mutant insulin containing tryptophan residues in the peptide segments that are expected to interact with the non-polar face of membranes.

The results of the protein determination experiment of insulin with egg yolk PC vesicles are inconclusive. According to Table 4.13, 60 % of the insulin that was initially added to the vesicle solution could not be accounted for. It was probably diluted in the dialysis solution at a concentration that was not detectable with the method used. The determination of the insulin concentration in the vesicle solution after dialysis was highly inaccurate. Firstly, the O.D.s measured for vesicles and insulin (Table 4.12) were off scale of the standard curve. Secondly, the choline in the egg yolk PC vesicles may also interact with the Folin-Ciocalteau phenol reagent. Hence, the concentration of 1.7 mg/ml of insulin measured in the vesicle solution is most likely too low. The results of the protein determination are therefore unreliable, and the experiment should be repeated using a better suited method.

By an FTIR study, binding of insulin to dodecylphosphocholine-d_{38} micelles, sodium dodecyl-d_{25} sulfate micelles, and to vesicles of different classes of phospholipids may be detected by conformational changes of the peptide. To a constant concentration of vesicles, increasing amounts of insulin would have to be added. The results would have to be compared with spectra of dimeric insulin with vesicles and of insulin in solution,

respectively. This study has to take into account the sensitivity of the spectrometer and interference from lipids. To this end a more sensitive detector has recently been installed on the IFS 85 spectrometer.

Two-dimensional NMR studies of insulin bound to dodecylphosphocholine-d_{38} or sodium dodecyl-d_{25} sulfate micelles with a diameter of 5 nm should be carried out on a 500 MHz spectrometer.

REFERENCES

Adams, M.J., Blundell, T.L., Dodson, E.J., Dodson, G.G., Vijayan, M., Baker, E.N., Harding, M.M., Hodgkin, D.C., Rimmer, B., Sheat, S. (1969), *Nature* **224**, 491

Alpert, N.A., Keiser, W.E., Szymanski, H.A. (1970), *Theory and Practice of Infra-Red Spectroscopy*, Plenum Press

Anfinson, C.B. (1973), *Science* **181**, 223

Arrondo, J.L.R., Mantsch, H.H., Mullner, N., Pikula, S., Martonosi, A. (1987), *J. Biol. Chem.* **262**, 9037

Aue, W.P., Bartholdi, E., Ernst, R.R. (1976), *J. Chem. Phys.* **64**, 2229

Bachmann, P., Aue, W.P., Müller, L., Ernst, R.R. (1977), *J. Magn. Reson.* **28**, 29

Bandekar, J., Krimm, S. (1980), *Biopolymers* **19**, 31

Banwell, C.N. (1983), *Fundamentals of Molecular Spectroscopy*, **3rd ed.**, McGraw-Hill, London, 72-123

Barnes, A.J., Orville-Thomas, W.J. (eds.) (1977), *Vibrational Spectroscopy - Modern Trends*, Elsevier, 1977

Bartholdi, E., Ernst, R.R. (1973), *J. Magn. Reson.* **11**, 9

Bates (1962), *J. Res. Natl. Bur. Stand.* **66A**, 179

Bax, A. (1982), *Two-Dimensional Nuclear Magnetic Resonance in Liquids*, Reidel, London

Berne, B.J., Pecora, R. (1976), *Dynamic Light Scattering*, Wiley, New York

Billeter, M., Braun, W., Wüthrich, K. (1982), *J. Mol. Biol.* **155**, 321

Birktoft, J., Blow, D.M. (1972), *J. Mol. Biol.* **68**, 167

Blake, C.C.F., Geisow, M.J., Swan, I.D.A., Rerat, C., Rerat, B. (1974), *J. Mol. Biol.* **88**, 1

Blundell, T.L. et al. (1972), *Adv. Protein Chem.* **26**, 279

Blundell, T.L., Johnson, L.N. (1976), *Protein Crystallography*, Academic Press, London

Bodenhausen, G., Freeman, R., Turner, D.L. (1977), *J. Magn. Reson.* **27**, 511

Bodenhausen, G., Vold, L., Vold, R.R. (1980), *J. Magn. Reson.* **37**, 93

Bösch, Ch., Brown, L.R., Wüthrich, K. (1980), *Biochim. Biophys. Acta* **603**, 298

Braiman, M.S., Rothschild K.J. (1988), *Ann. Rev. Biophys. Biophys. Chem.* **17**, 541

Braunschweiler, L., Bodenhausen, G., Ernst, R.R. (1983), *Mol. Phys.* **48**, 535

Braunschweiler, L., Ernst, R.R. (1983), *J. Magn. Reson.* **53**, 521

Byler, D.M., Susi, H. (1986), *Biopolymers* **25**, 469

Cantor, C.R., Schimmel, P.R. (1980), *Biophysical Chemistry*, **Part II**, W.H. Freeman & Co., San Francisco, 433-465

Cheshnovsky, D., Neuringer, L.J., Williamson, K.L. (1983), *J. Protein Chem.* **2** (4), 335

Chothia, C. (1976), *J. Mol. Biol.* **105**, 1

Creighton, T.E. (1984), *Proteins*, W.H. Freeman & Co., New York, 160, 17

Crick, C., Rich, A. (1955), *Nature* **176**, 780

Davis, D.G., Bax, A. (1985), *J. Am. Chem. Soc.* **107**, 2820

DeLisi, Ch., Berzofsky, J.A. (1985), *Proc. Natl. Acad. Sci. USA* **82**, 7048

DeMarco, A., Wüthrich, K. (1976), *J. Magn. Reson.* **24**, 201

Dickerson, R. (1964), in *The Proteins*, **2nd ed., Vol. 2** (Neurath, H., ed.), Academic Press, New York, 603

Dodson, E.J., Dodson, G.G., Hodgkin, D.C., Reynolds, C.D., (1979), *Can. J. Biochem.* **57**, 469

Dwivedi, A.M., Krimm, S. (1984), *J. Phys. Chem.* **88**, 620

Eisenberg, D. (1970), in *The Enzymes*, **3rd ed., Vol. 1** (Boyer, P.D., ed.), Academic Press, New York, 1

Eisenberg, D., Weiss, R.M., Terwilliger, T.C. (1984), *Proc. Natl. Acad. Sci. USA* **81**, 140

Elliot, A., Ambrose, E.J. (1950), *Nature* **165**, 921

Ernst, R.R., Bodenhausen, G., Wokaun, A. (1987), *Principles of Nuclear Magnetic Resonance in One and Two Dimensions*, Oxford Science Publ.

Farias, R.N. (1987), *Biochim. Biophys. Acta* **906**, 459

Ferraro, J.R., Basile, L.J. (eds.) (1978), *Fourier Transform Infrared Spectroscopy*, **Vol. 1**, Academic Press, London

Fesik, S.W. (1988), *Nature* **332**, 865

Fischer, W.H., Saunders, D., Brandenburg, D., Wollmer, A., Zahn, H. (1985), *Hoppe-Seyler's Z. Biol. Chem.* **366**, 521

Forrest, J.B. (1977), *Ph.D. Thesis SFU*, 53

Fredericq, E. (1957), *J. Am. Chem. Soc.* **79**, 599

Fredericq, E., Neurath, H. (1950), *J. Am. Chem. Soc.* **72**, 2684

Glusker, J.P., Trueblood, K.N. (1972), *Crystal Structure Analysis: A Primer*, Oxford University Press, London

Goldman, J., Carpenter, F.H. (1974), *Biochemistry* **13**, 4567

Green, D.W., Reedy, G.T. (1978), in *Fourier Transform Infrared Spectroscopy*, **Vol. 1** (Ferraro, J.R., Basile, L.J., eds.), Academic Press, London, 1-59

Guéron, M. (1978), *J. Magn. Reson.* **30**, 515

Haasnoot, C.A.G. (1983), *J. Magn. Reson.* **52**, 153

Haris, P.I., Chapman, D. (1988a), *Biochim. Biophys. Acta* **943**, 375

Haris, P.I., Chapman, D. (1988b), *Biochem. Soc. Trans.* **17**, 161

Haris, P.I., Lee, D.C., Chapman, D. (1986), *Biochim. Biophys. Acta* **874**, 255

Harris, R.K. (1983), *Nuclear Magnetic Resonance Spectroscopy*, Longman Scientific & Technical, Essex

Heidenreich, K.A., Olefsky, J.M. (1985), in *Molecular Basis of Insulin Action* (Czech, P.M., ed.), Plenum Press, London, 45-66

Hiroyuki, S., Kemmler, W., Rubenstein, A.H., Steiner, D.F. (1971), in *Insulin Action* (Fritz, I.B. ed.), Academic Press, New York, 77

Holloway, P.W., Mantsch, H.H. (1989), *Biochemistry* **28**, 931

Hoult, D.I., Richards, R.E. (1975), *Proc. Roy. Soc. London Ser. A*, **344**, 311

Hua, Q.-X., Weiss, M.A. (1991), *Biochim. Biophys. Acta* **1078**, 101

Jacobs, S. (1985), in *Molecular Basis of Insulin Action* (Czech, P.M., ed.), Plenum Press, London, 31-44

Jakobsen, R.J., Brown, L.L., Hutson, T.B., Fink, D.J., Veis, A. (1983), *Science* **220**, 1288

Jeffrey, P.D., Coates, J.H. (1965), *Biochim. Biophys. Acta* **109**, 551

Jeffrey, P.D., Coates, J.H. (1966), *Biochemistry* **5**, 489

Kauppinen, J.K., Moffatt, D.J., Mantsch, H.H., Cameron, D.G. (1981), *Appl. Spectrosc.* **35**, 271

Kessler, H., Gehrke, M., Griesinger, Ch. (1988), *Angew. Chemie Int. Ed. Engl.* **27**, 490

Klevit, R.E. (1985), *J. Magn. Reson.* **62**, 551

Kline, A.D., Justice, R.M. jr. (1990), *Biochemistry* **29**, 2906

Koenig, J.L., Tabb, D.L. (1980), in *Analytical Applications of FT-IR to Molecular and Biological Systems* (Durig, J.R., ed.), Reidel, Dordrecht, 241

Krimm, S. (1962), *J. Mol. Biol.* **4**, 528

Krimm, S., Abe Y. (1972), *Proc. Natl. Acad. Sci. USA* **69**, 2788

Krimm, S., Bandekar, J. (1980), *Biopolymers* **19**, 1

Krimm, S., Bandekar, J. (1986), *Adv. Protein Chem.* **38**, 181

Kumar, A., Wagner, G., Ernst, R.R., Wüthrich, K. (1980a), *Biochem. Biophys. Res. Comm.* **96**, 1156

Kumar, A., Ernst, R.R., Wüthrich, K. (1980b), *Biochem. Biophys. Res. Comm.* **95**, 1

LeMaster, D.M., Richards, F.M. (1988), *Biochemistry* **27**, 142

Lord, R.S., Gubensek, F., Rupley, J.A. (1973), *Biochemistry* **12**, 4385

Lowry, D.F., Redfield, A.G., McIntosh, L.P., Dahlquis, F.W. (1988), *J. Am. Chem. Soc.* **110**, 6885

Marion, D., Wüthrich, K. (1983), *Biochem. Biophys. Res. Comm.* **113**, 967

Marshall, A.G., Verdun, F.R. (1990), *Fourier-Transforms in NMR, Optical, and Mass Spectrometry*, Elsevier, 49-51

Miyazawa, T. (1960), *J. Chem. Phys.* **32**, 1647

Neuhaus, D., Wagner, G., Vasák, M., Kägi, J.H.R., Wüthrich, K. (1985), *Eur. J. Biochem.* **151**, 257

Noggle, J.H., Schirmer, R.E. (1971), *The Nuclear Overhauser Effect*, Academic Press, New York

Oomen, R.P., Kaplan, H. (1987), *Biochemistry* **26**, 303

Oschkinat, H., Cieslar, Ch., Holak, T.A., Clore, G.M., Gronenborn, A.M. (1989), *J. Magn. Reson.* **83**, 450

Oschkinat, H., Griesinger, Ch., Kraulis, P.J., Sorenson, O.W., Ernst, R.R., Gronenborn, A.M., Clore, G.M. (1988), *Nature* **332** (24), 374

Parker, F.S. (1983), *Applications of Infrared, Raman, and Resonance Raman Spectroscopy in Biochemistry*, Plenum Press, New York

Pauling, L. (1960), *The Nature of the Chemical Bond*, **3rd ed.**, Cornell University Press, Ithaka, N.Y.

Pekar, A.H., Frank, B.H. (1972), *Biochemistry* **11**, 4013

Pessin, J.E., Mottola, C., Yu, K.-T., Czech, P.M. (1985), in *Molecular Basis of Insulin Action* (Czech, P.M., ed.), Plenum Press, London, 3-30

Peterson, G.L. (1979), *Anal. Biochem.* **100**, 201

Pocker, Y., Biswas, S.B. (1981), *Biochemistry* **20**, 4354

Purcell, J.M., Susi, H. (1984), *J. Biochem. Biophys. Methods* **9**, 193

Rabold, J.F., Moore, W.H., Krimm, S. (1977), *Macromolecules* **5**, 1065

Ramachandran, G.N., Kolaskev, A.S. (1974), *Biochim. Biophys. Acta* **359**, 298

Ramachandran, G.N., Mitra, A.K. (1976), *J. Mol. Biol.* **107**, 85

Ramachandran, G.N., Sasisekharan, V. (1968), *Adv. Protein Chem.* **23**, 283

Rance, M., Sorensen, O.W., Bodenhausen, G., Wagner, G., Ernst, R.R., Wüthrich, K. (1983), *Biochem. Biophys. Res. Comm.* **117**, 479

Redfield, A.G., Gupta, R.K. (1971), *Cold Spring Harbor Symp. Quant. Biol.* **36**, 405

Redfield, A.G., Kunz, S.D. (1975), *J. Magn. Reson.* **19**, 250

Redfield, A.G., Kunz, S.D., Ralph, E.K. (1975), *J. Magn. Reson.* **19**, 114

Rüegg, M., Metzger, V., Susi, H. (1975), *Biopolymers* **14**, 1465

Sasisekharan, V. (1959), *Acta Crystallog.* **12**, 897

Schoenborn, B.P., Nunes, A.C. (1972), *Ann. Rev. Biophys. Bioeng.* **1**, 529

Schroeder, W.A. (1968), *The Primary Structure of Proteins*, Harper & Row, New York

Segrest, J.P., De Loof, H., Dohlman, J.G., Brouillette, C.G., Anantharamaiah, G.M. (1990), *Proteins: Struct. Funct. Genet.* **8**, 103

Segrest, J.P., Jackson, R.L., Morrisett, J.D., Gotto, A.M. (1974), *FEBS Lett.* **38**, 247

Solomon, I. (1955), *Phys. Rev.* **99**, 559

Sorensen, O.W., Eich, G.W., Levitt, M.H., Bodenhausen, G., Ernst, R.R. (1983), *Progr. Nucl. Magn. Reson. Spectrosc.* **16**, 163

States, D.J., Haberkorn, R.A., Ruben, D.J. (1982), *J. Magn. Reson.* **48**, 286

Steiner, D.F., Clark, J.L., Nolan, C., Rubenstein, A.H., Margoliash, E., Melani, F., Oyer, P.E. (1970), in *The Pathogenesis of Diabetes Mellitus, Proceedings of the 13th Nobel Symposium* (Cerasi, E., Luft, R., eds.), Almqvist & Wiksell, Stockholm, 123

Steiner, D.F., Duiguid, J.R., Patzelt, C., Chan, S.J., Quinn, P., Labrecque, A., Hastings, R. (1978), in *Proinsulin, Insulin, C-Peptide* (Baba, S., Kaneko, T., Yanaihara, N., eds.), Exerpta Medica, Amsterdam-Oxford, 9

Stryer, L., Haugland, R.P. (1967), *Proc. Natl. Acad. Sci. USA* **98**, 719

Surewicz, W.K., Mantsch, H.H. (1988), *Biochim. Biophys. Acta* **952**, 115

Surewicz, W.K., Mantsch, H.H., Stahl, G.L., Epand, R.M. (1987a), *Proc. Natl. Acad. Sci. USA* **84**, 7028

Surewicz, W.K., Moscarello, M.A., Mantsch, H.H. (1987b), *Biochemistry* **26**, 3881

Surewicz, W.K., Szabo, A., Mantsch, H.H. (1987c), *Eur. J. Biochem.* **167**, 519

Susi, H. (1969), in *Structure and Stability of Biological Macromolecules* (Timasheff, S.N., Fasmann, G.D., eds.), Marcel Dekker, New York, 575

Susi, H., Byler, M. (1986), *Methods Enzymol.* **130**, 290

Susi, H., Timasheff, S.N., Stevens, L. (1967) *J. Biol. Chem.* **242**, 5460

Swank, R.T., Munkres, K.D. (1971), *Anal. Biochem.* **39**, 462

Tanford, C. (1973), *The Hydrophobic Effect*, Wiley Interscience, New York

Timasheff, S.N., Susi, H., Stevens, L. (1967), *J. Biol. Chem.* **242**, 5467

Torchia, D.A., Sparks, S.W., Bax, A. (1988), *Biochemistry* **27**, 5135

Traub, W., Piez, K.A. (1971), *Adv. Protein Chem.* **25**, 243

Wagner, G. (1983), *Quart. Rev. Biophys.* **16 (1)**, 1

Wagner, G., Kumar, A., Wüthrich, K. (1981), *Eur. J. Biochem.* **114**, 375

Wagner, G., Wüthrich, K. (1982), *J. Mol. Biol.* **155**, 347

Wagner, G., Wüthrich, K., Tschesche, H. (1978), *Eur. J. Biochem.* **86**, 67

Weber, G. (1972), *Ann. Rev. Biophys. Bioeng.* **1**, 553

Weiss, M.A., Nguyen, D.T., Khait, I., Inouye, K., Frank, B.H., Beckage, M., O'Shea, E., Shoelson, S.E., Karplus, M., Neuringer, L.J. (1989), *Biochemistry* **28**, 9855

Westler, W.M., Kainosho, M., Nagao, H., Tomonaga, N., Markley, J.L. (1988), *J. Am. Chem. Soc.* **110**, 4093

Wider, G., Hosur, R.V., Wüthrich, K. (1983), *J. Magn. Reson.* **52**, 130

Wider, G., Lee, K.H., Wüthrich, K. (1982), *J. Mol. Biol.* **155**, 367

Wüthrich, K. (1986), *NMR of Proteins and Nucleic Acids*, J. Wiley & Sons, New York

Wüthrich, K., Wider, G., Wagner, G., Braun, W. (1982), *J. Mol. Biol.* **155**, 311

Yang, P.W., Mantsch, H.H., Arrondo, J.L.R., Saint-Girons, I., Guillon, Y., Cohen, G.N., Barzu, O. (1987), *Biochemistry* **26**, 2706

Zubay, G. (1983), *Biochemistry*, **1st ed.**, Addison-Wesley Publishing Co., Inc., 25